Title
Photodissociation Studies of the Chlorotoluenes at 193 nm and 248 nm

Author
Helfand, M.S.

Publication Date
1989-11-01

LBL-28127

Lawrence Berkeley Laboratory
UNIVERSITY OF CALIFORNIA

Materials & Chemical Sciences Division

Photodissociation Studies of the Chlorotoluenes at 193 nm and 248 nm

M.S. Helfand
(Ph.D. Thesis)

November 1989

Prepared for the U.S. Department of Energy under Contract Number DE-AC03-76SF00098.

DISCLAIMER

LBL-28127

Photodissociation Studies of the Chlorotoluenes at 193 nm and 248 nm

Marion Skalweit Helfand
Ph.D. Thesis

Materials and Chemical Sciences Division
Lawrence Berkeley Laboratory
University of California
Berkeley, CA 94720

November 1989

This work was supported by the U.S. Department of Energy under
Contract No. DE-AC03-76SF00098.

PHOTODISSOCIATION STUDIES OF THE CHLOROTOLUENES AT 193 nm AND 248 nm

Marion Skalweit Helfand

ABSTRACT

The photodissociation reactions of o-, m-, and p-chlorotoluene have been investigated at 193 nm and 248 nm in a crossed molecular beam-laser beam apparatus with a rotatable molecular beam source. Chapter 2 describes the studies at 193 nm. It is found that all three isomers have three primary reaction channels, each involving loss of the chlorine atom albeit with differing amounts of the excess available energy, 51 kcal/mole, in the translational degree of freedom of the products. The most likely explanation for the existence of three channels with identical products is that dissociation is occurring from different electronic states, especially triplet states, due to the presence of the Cl substituent. The branching ratios between the three primary channels and the average translational released in the three dissociation channels are also similar for the three isomers. Secondary dissociation of the tolyl radical product is observed, and this allows one to estimate the CH_3-C_6H_4 bond energy in the radicals.

Chapter 3 continues with the photodissociation reactions of these molecules at 248 nm. At 248 nm, each isomer has two primary dissociation channels, again both involving loss of Cl. Because there are fewer electronic states in this region of the spectrum, an

assignment of the electronic states giving rise to the two channels is possible. The fast channel is tenatively assigned as coming from molecules in the first excited triplet state, T_1, while the slow peak is thought to result from ground state dissociation. The branching ratio between these two channels is different for the three isomers however, and this is attributed to differences in the rates of dissociation for the three isomers from T_1.

Chapter 4 discusses a first attempt at development of a sensitive means of detecting Cl atoms using a resonant ionization method involving a VUV photon at 118.877 nm plus a UV photon at 356.6 nm. Some sort of Cl atom transition is detected but it does not coincide precisely with the transition at 118.877 nm. Detecting Cl ions from this resonant process is complicated by the fact that Cl_2 is the source of Cl atoms through photodissociation. The Cl_2 happens to possess ion pair states in the region of the VUV where this work occurred. Suggestions for improvement are given.

TABLE OF CONTENTS

ACKNOWLEDGMENTS

I wish to thank Yuan Lee for his guidance and encouragement over the past few years. Professor Lee took me as a student near the end of my second year, and I want to express my gratitude for this. He and his research group made my transition into the group as smooth as possible.

I would also like to thank the many people with whom I have had the opportunity to work. Professor John Clark and his students, Howard Nathel, Laura Philips, Steve Webb, Sheila Yeh, Doug Anthon, Ward Brown, and Cindy Buhse, as well as post-doctoral fellow, Dennis Guthals, were my first colleagues at Berkeley. Howard and Dennis certainly possessed a unique teaching style, and it is to them that I owe what little I know about picosecond laser systems. Office mates Laura and Steve took a young first year student under their wing.

My transition into the Lee group was assisted in part by Tim Minton, who taught me the molecular beam ropes on the MPI machine. Tim's practical expertise about everything from vacuum fittings to pump oil was nicely complemented by the more theoretical leanings of post-doc Gil Nathanson who joined the group in 1985. I never felt uncomfortable, even when asking the "dumbest" of questions of these two. After the big move of '86, I had the pleasure of working in parallel with Jim Myers. It's still a miracle that neither of us zapped the other with our respective short-pulse lasers in that cosy room! Post-doctoral fellow Peter Weber joined us in the MPI room and divided his time efficiently

between the nanosecond and picosecond world. Ralph Page and Andy Kung generously shared their physicists' point of view.

Near the very end of my tenure in Berkeley, I had the distinct pleasure of working with Eric Hintsa on the rotating source machine. Eric was a patient and capable teacher, having nursed many a student, post-doc and visiting scientist through their first encounters with the RSM. Xinsheng Zhao, creator of the legendary CMLAB2 program, also provided experimental advice and good humor and friendship.

However, the nicest part of being in a group is the friendships that one develops, within the lab environment. Office mates like Gary Robinson, Eric Hintsa, and later, Jim Myers, John Allman, Floyd Davis, Dr. Atsushi Yokoyama, and Prof. Walter Miller were good sources of advice and stimulating conversation on a variety of topics. Bob Continetti, who not only single-handedly managed the group move and made life easier for all of us, was always ready to discuss new data, or just about anything. Barbara Balko and Pam Chu were also enjoyable lab mates. If you want me to gather your signatures for you, Pam, let me know! Finally, I must acknowledge my very good friend, Anne-Marie Schmoltner--sounding board, political enthusiast, confidant. You have opened my eyes to many new things!

Ann Weightman, group administrator, has provided a pathway through the bureaucratic maze for which I am deeply indebted. I have also enjoyed just sitting in her office to let off steam. Thanks for everything Ann!

Of course, without the excellent technical support of an institution like Berkeley, none of these experiments would be possible. I am indebted to Fred Wolf and Andy Anderson, as well as the countless machinists and welders in the campus shop for their patience and friendly service. I learned a lot of drafting and good design practice during the informal lessons offered there. "Harry" Chilidakis and his merry band of electricians and welders and handy men kept our lab running smoothly.

Outside of lab, and indeed outside of California, there were many friends who, though busy in their own academic pursuits, kept in touch and inspired me. Steve Finkel kept me laughing from day 1 in Chem 1 through the worst moments in my graduate career. Liz Bolinger, Giulia Bonaminio, and Jesse and Diane Frankel encouraged me with their long distance, and then short distance support. Thanks for resuscitating my Mac's internal drive at the last minute, Jess'! Teachers and professors, Ben Cotton, Arthur Benade and Henry Sable pointed me in the right direction in high school and college.

Finally, I must thank my loving and supportive family. I could never have accomplished any of this without their unspoken confidence in me, and without their baby-sitting efforts. I look forward to spending more time with my daughter in the near future.

This work was supported by the Director, Office of Energy Research, Office of Basic Energy Sciences, Chemical Sciences Division of the U.S. Department of Energy under Contract No. DE-AC03-76SF00098.

To Bob and Abby

CHAPTER 1
INTRODUCTION

To quote a recent doctoral candidate[1] from our laboratory, "Though we have performed some completely original experiments in (the area of photodissociation). . . many of our experiments involve previous work by other researchers." This is certainly the case with the experimental work described in Chapters 2 and 3 of this dissertation, although the motivation for these studies was not merely to clarify and correct previous work, but also to expand upon the original experiments.

As will be described in Chapters 2 and 3 respectively, a variety of photodissociation experiments in molecular beams have been performed at both 193 nm and 248 nm on the isomers of chlorotoluenes. These experiments have identified primary and secondary photodissociation pathways, have determined the branching ratios for the primary pathways, have looked into the nature of the state initially excited at 193 nm, and the states from which dissociation occurs at 248 nm, and have allowed us to estimate the CH_3-C_6H_4 bond energies in the o-, m- and p-tolyl radical products.

Other photodissociation experiments have been performed on the isomers of chlorotoluene[2], and other chlorinated aromatics such as benzyl chloride[3], chlorobenzene[4], and the isomers of dichlorobenzene[5] over a number of years by Ichimura and others. These experiments were carried out in the gas phase, in cells and in molecular beams, over a wide range of excitation wavelengths. With

the chlorotoluenes in the 250 to 280 nm range, the primary products, Cl and tolyl radical, were identified via indirect means, and an attempt was made to identify the electronic state(s) involved in the dissociation, and to estimate dissociation rate constants. Fluorescence studies of these compounds were also performed in order to determine non-radiative lifetimes, and the dependence of these lifetimes on the excitation of specific vibrations, and on the vibrational energy in general. Because the dichlorobenzenes exhibited slightly different non-radiative lifetimes, and because this effect was attributed to the different symmetries of the compounds, the fluorescence data for the chlorotoluenes were also expected to show such differences, which they did not.

At 266 nm, it was also determined that the ortho isomer of chlorotoluene dissociates to yield Cl and the benzyl radical, rather than the o-tolyl radical[6]. The other isomers did not form the more stable benzyl radical, presumably because they do not have their methyl groups sufficiently close to the position on the aromatic ring where the hydrogen can be transferred from the methyl group. Photodissociation experiments have been performed previously on meta- chlorotoluene, chlorobenzene[7] and para-dichlorobenzene[8] at 193 nm in a molecular beam apparatus. However in this case, the laser, the molecular beam and the detector are mutually orthogonal and fixed in position, unlike the rotating molecular beam apparatus[9] used in the experiments to be described here. The former configuration poses difficulties in experiments where there are heavy, slow fragments to be detected. In addition, there was some question as to the nature of the state initially excited at 193 nm in

these molecules, whether it was an alkyl halide type, purely dissociative state, or whether the initial transition was localized to the ring.

Finally, Chapter 4 discusses the detection of Cl atom using a multiphoton ionization (MPI) technique in vacuum ultraviolet (VUV). A highly sensitive means of detecting Cl atoms, as well as other halogen atoms and H atom, was desired for a series of experiments aimed at measuring the rates of intramolecular vibrational energy redistribution (IVR) in molecules[10]. One particular case involves IVR in 2-chloroethyl radical. Briefly, the overtones of the various C-H stretches in the radical are pumped with one laser. What is important to note is that the third overtone is already sufficient to break the weak C-Cl bond, which has a bond strength of ~20 kcal/mole[11]. A second laser, poised to detect the nascent Cl atoms, is delayed with respect to the pumping laser, in order to measure the time required between excitation and dissociation. Of interest is whether IVR or dissociation will be rate-limiting. RRKM calculations indicate that the lifetime of the radical may be in the 10 picosecond range[12].

Development of a sensitive detection scheme is necessary because of the difficulty in producing intense beams of radicals[1,13], and because of the low cross-sections of the overtone transitions. Chapter 4 describes the earliest attempts in that direction, and offers several suggestions for improving upon this initial effort.

REFERENCES

1. E. J. Hintsa, Ph. D. Thesis, University of California, Berkeley, 1989.

2. A. Shimoda, T. Hikida, T. Ichimura, and Y. Mori, Chem. Lett., 265 (1979).

3. T. Ichimura and Y. Mori, J. Chem. Phys., 82, 4723 (1985).

4. T. Ichimura, T. Hikida, and Y. Mori, J. Chem. Phys., 63, 1445 (1975).

5. A. Shimoda, T. Hikida, and Y. Mori, J. Phys. Chem., 83, 1309 (1979).

6. T. Ichimura, Y. Mori, M. Sumitani, and K. Yoshihara, J. Chem. Phys., 84, 1943 (1986).

7. T. Ichimura, Y. Mori, H. Shinohara, and N. Nishi, Chem. Phys. Lett., 122, 51 (1985).

8. ibid, 55.

9. A. M. Wodtke and Y. T. Lee, J. Phys. Chem., 89, 4744 (1985).

10. J. D. Myers, Ph. D. Thesis, University of California, Berkeley.

11. T. K. Minton, P. Felder, R. J. Brudzynski, and Y. T. Lee, J. Chem. Phys., 81, 1759 (1984).

12. T. K. Minton and M. Côté, private communication.

13. D. E. Powers, J. B. Hopkins, and R. E. Smalley, J. Chem. Phys., 85, 2711 (1981); A. D. Sappey and J. C. Weisshaar, J. Phys. Chem., 91, 3731 (1987).

CHAPTER 2
PHOTODISSOCIATION STUDIES OF THE CHLOROTOLUENES AT 193 nm

I. INTRODUCTION

The considerable interest in photodissociation of aryl halides has been spurred by the vast amount of experimental and theoretical work performed on radiationless transition processes in molecules[1]. Molecules such as benzene[2], various deuterated benzenes[3], and fluorinated benzenes[4] have been studied extensively using fluorescence methods. However, compounds with poor fluorescence quantum yields such as the aryl halides are not attractive candidates for such methods. In addition, the flourescence of all molecules excited to higher singlet levels decreases dramatically. It is at such levels of excitation that non-radiative processes dominate the photophysics of the molecule, and that photodissociation studies prove useful in the understanding of the initial non-radiative decay processes, as well as what follows.

Photodissociation studies of various aryl halides, including chlorobenzene[5,6], meta-chlorotoluene[6] and para-dichlorobenzene[7] have been previously performed at 193 nm, using a crossed molecular beam-laser beam apparatus in which the products are detected at 90° with respect to the plane formed by the laser and molecular beams. These experiments tried to identify the primary products, the states initially excited, and those from which dissociation occurs. Unfortunately, the fixed detector configuration

with respect to the molecular beam did not allow them to collect all the data needed to elucidate the various process involved. Our experiments were performed on a crossed molecular beam-laser beam apparatus in which the molecular beam source can be rotated with respect to the detector[8]. In the investigation of o-, m-, and p-chlorotoluene at 193 nm, we have identified an additional primary dissociation channel, as well as a secondary channel. Such secondary channels are caused by the decomposition of highly internally excited primary products.

In addition to identifying the primary and secondary products of photodissociation at 193 nm, we were interested in looking for different features in the dissociation dynamics of the three isomers of chlorotoluene that could be attributed to structural differences. For example, in the case of the ortho compound, a previous experiment[9] has demonstrated that at 266 nm, benzyl radical is formed following Cl bond fission when hydrogen migration from the methyl group to the ring occurs. This is not observed for the other isomers. As benzyl radical is approximately 20 kcal/mole more stable than tolyl radical[10], it was of interest to see whether this could be observed at 193 nm in the measurements of product velocity distributions, particularly when monitored at mass to charge ratio (m/e) 91.

Polarization studies were also carried out in order to determine the nature of the state initially excited at 193 nm. Previous workers had raised the question of whether the excited state is of a more localized nature, centered on the carbon-halogen bond analogous to the alkyl halides[6], or whether it mainly involves the benzene ring.

II. EXPERIMENTAL

The rotatable molecular beam source apparatus used in these experiments has been previously described[8]. Briefly, a seeded, diferentially pumped molecular beam was crossed at right angles by a laser in a vacuum chamber. Dissociation products entered an ultra-high vacuum (UHV) detector chamber containing a mass spectrometer, and were detected as a function of their mass, velocity, and angle. The mass spectrometer consisted of an electron bombardment ionizer, a quadrupole mass filter, and a Daly-type[11] ion counter. A multichannel scaler CAMAC-interfaced with an LSI-11 microcomputer recorded the time-of-flight (TOF) spectra of products relative to when the laser was fired. A schematic of the beam apparatus is shown in Figure 1.

A continuous beam of the chlorotoluene isomer was formed by bubbling N_2 gas through a liquid sample held at 50° C, and expanding the mixture through a 0.13 mm diameter nozzle. The total pressure was maintained at approximately 300 torr. The stainless steel inlet line to the machine was maintained at approximately 70-80 °C to prevent condensation, and the nozzle was heated to between 138 and 140 °C to prevent formation of dimers. The nozzle temperature varied slightly from experiment to experiment, but this could not account for more than a fraction of a kcal/mole difference in the total energy available to the parent molecules. The resultant beam was collimated by passing through two skimmers,

differentially pumped in between, before entering the interaction region.

The ortho- and para-chlorotoluene (o-CT and p-CT) were obtained from MCB, and the meta-chlorotoluene (m-CT) was obtained from Aldrich. These compounds were degassed at liquid nitrogen temperature prior to use, but otherwise, were used without additional purification. A minor para-bromotoluene impurity had been previously noted[12] with the p-CT, but was not detected in this experiment.

A Lambda Physik MSC-103 excimer laser was used for the 193 nm photodissociation, operating on the ArF transition. The beam was focussed to a 1 mm × 3 mm spot size at the interaction region. The laser polarization dependence was studied using a rotatable "pile-of - plates" transmission polarizer, with 10 quartz plates set at Brewster's angle with respect to the incoming laser beam. It is estimated that the light was 97% polarized in this way. It is important to note that the polarization data were taken with the lowest possible laser energies (~2 to 3 mJ) since a crude energy dependence study showed that the signal is highly saturated from 3 mJ to 55 mJ. Saturation can reduce the apparent anisotropy of a transition. Figure 2 shows the TOF spectra of m/e 91 for o-CT taken at 20° with respect to the detector, at both these laser energies. These data indicate that no multiphoton absorption is taking place, by the fact that they appear identical, and by the fact that no products are formed with translational energies greater than the excess available after C-Cl bond fission. Figure 3 is a plot of signal intensity versus laser energy derived from these data.

RESULTS AND ANALYSIS

ortho-chlorotoluene

Time-of-flight (TOF) spectra were obtained at several mass-to-charge ratios (m/e) and laboratory angles. These data do not necessarily represent all mass-to-charge ratios at which signal can be detected, but are the most important in establishing the nature of primary and secondary reaction channels, and for obtaining product branching ratios.

CHLORINE LOSS CHANNELS: As has been previously shown[5-7], primary reaction channels involving Cl loss are important for compounds like ortho-chlorotoluene when excited in the ultraviolet region of the spectrum. Accordingly, TOF spectra were taken at m/e 35 and m/e 91, at 20°, 40°, and 60°. These spectra and the simulated spectra, generated by the CMLAB2 program[13], are shown in Figures 4 and 5. The CMLAB2 program will be discussed briefly below. So-called "Newton" diagrams, which illustrate the relationships between the laboratory and center-of-mass product velocities, and the laboratory and center-of-mass angles for these dissociation reactions, are shown in Figure 6.

The data are analyzed using the CMLAB2 data analysis program, presented and thoroughly discussed in reference 13. Essentially, the program accepts an assumed center-of-mass frame translational energy distribution, referred to as a "P(E)", and together

with parameters about the molecular beam and the experimental conditions performs a forward convolution to obtain the laboratory-frame time-of-flight spectrum which is then compared to the observed spectrum. The distribution is varied until a good fit to the spectrum is achieved.

The TOF spectrum at m/e 35 contains at least two, if not three, easily identifiable TOF distributions. The first of these is narrow and fast, while the latter are broad and slow. The TOF spectrum at m/e 91 contains only two readily noticeable TOF distributions: one that is also narrow and fast, and a second that is relatively broader and slow. The first feature in each of these spectra can be simulated using the same translational energy distribution (P(E)), shown in Figure 7, and by assuming that reaction 1 is occurring:

$$C_7H_7Cl \rightarrow C_7H_7 + Cl \qquad (1)$$

This indicates that these products result from the same reaction channel, and have an average translational energy release of 33 kcal/mole. The second, broader feature in each of the spectra can also be simulated by assuming that reaction 1 is responsible, but slightly different translational energy distributions are required for each mass. These distributions are shown in Figure 8. One notes that while the fast side of these functions are identical, the slower side extends out much further in the case of the function used to fit the Cl spectrum. It is as if some of the translationally slower o-tolyl or benzyl[9] radical product (mass 91) is missing, as indicated in Figure 9, which shows the m/e 91 TOF spectrum and a simulated spectrum

using the translational energy distributions and weightings used to fit the m/e 35 spectrum. The possibility of spontaneous secondary dissociation, in which primary products with sufficient energy from the initial dissociation process undergo subsequent dissociation, or of secondary photodissociation, where primary photoproducts absorb another photon and undergo decomposition, exists. Some likely products of such secondary dissociation are given in reactions 2a and 2b.

$$C_7H_7 \rightarrow C_6H_4 + CH_3 \qquad (2a)$$

$$C_7H_7 \rightarrow C_7H_6 + H \qquad (2b)$$

In order to determine whether secondary decomposition processes are important in this case, it is necessary to obtain TOF spectra at the various mass-to-charge ratios of the products in reactions 2a and 2b. TOF spectra taken at m/e 73, m/e 15, and m/e 90, together with their CMLAB2 simulations, are shown in Figures 10 through 12 respectively. The m/e 73 TOF spectrum is shown because the signal-to-noise ratio is better at this mass than at m/e 76. However, m/e 76,75, 74 and 73 spectra are identical, indicating that the lower masses are due to cracking of the m/e 76 ion in the ionizer. These spectra also contain features that suggest that the m/e 91 ion is "cracking" in the ionizer to yield m/e 76 and m/e 15. In addition to simple cracking of the m/e 91 ion, there are slower and faster components to these otherwise featureless TOF distributions. By assuming that the o-tolyl or benzyl radical undergoes spontaneous secondary dissociation according to reaction 2a, the slow

side of the m/e 73 spectrum can simulated. In order to do this, a primary translational energy distribution, or P(E), that describes how the dissociating m/e 91 product is initially formed, is used. It is derived by taking the difference between the appropriately weighted P(E)s used to fit the m/e 35 and m/e 91 TOF spectra. In addition, a secondary translational energy distribution is needed. These distributions are shown in Figures 13 and 14. In the secondary dissociation of tolyl radical, an average translational energy release of 11 kcal/mole is observed. One must also note that the same translational energy distributions are used to fit the m/e 15 data, indicating that the small amount of m/e 15 detected in the experiment is probably due to secondary decomposition alone. This will be discussed again shortly. Finally, the TOF spectrum at m/e 90 is identical to the one observed at m/e 91, demonstrating that the m/e 90 fragment is due to cracking of the tolyl radical. It is thus possible to rule out secondary dissociation according to reaction 2b.

The existence of a third primary reaction channel involving loss of Cl, according to reaction 1, is postulated. The translational energy distribution which is used to simulate the slow tail of the m/e 35 spectrum is shown in Figure 15, together with a distribution which is the sum of the two slower P(E)s used in fitting the Cl spectrum. While it is possible that only two Cl loss channels are present in the case of the ortho isomer, it will become more evident that a third channel may exist when the Cl TOF spectra of the other compounds are examined.

In addition to the primary and secondary dissociation processes already discussed, one must consider the possibility of a

primary channel involving loss of HCl, analogous to H_2 loss in benzene[14], and a primary channel involving loss of CH_3[15], as briefly mentioned above.

HCl ELIMINATION CHANNEL: No evidence for an HCl elimination channel has been found. Several independent means of verifying the absence of this channel were utilized. First, TOF spectra were taken at m/e 35, 36, 37 and 38 to see whether parent HCl is formed in the ionizer. All four spectra can be simulated by assuming that the two (or three) primary Cl loss channels account for the signal. One difficulty arises however: there is a large peak at m/e 39 in the mass spectrum of the molecule, arising from cracking of the six-membered ring. This is demonstrated by overlaying the m/e 39 and m/e 73 TOF spectra. Signal due to "leaking" of the strong signal at m/e 39 through the quadrupole and cracking of this ion in the ionizer appears in the TOF spectra at m/e 36, 37 and 38 too. Thus, the spectra at m/e 36 through 38 are really composites of the TOF spectra at m/e 35(37) and 39 as shown in Figure 16. A second, independent means of ruling out this channel is to look at m/e 91 and m/e 90; again, these TOF spectra are identical, that is m/e 90 results from cracking of the m/e 91 in the ionizer as shown in Figure 12 rather than from a channel involving loss of HCl. Finally, as Figure 17 reveals, the TOF spectra at masses 76 through 73 are identical to one and other also. Presumably if all the mass 90 resulting from HCl elimination were to undergo secondary dissociation, and were therefore undetectable, one would still be able to look for the products of secondary decomposition in the m/e 73 to

76 range. As these spectra are all identical, and their slow components (see Discussion) are composed of contributions from the various channels described above, it is reasonable to assume that an HCl elimination channel does not occur.

METHYL ELIMINATION: It is known that in the photodissociation of toluene at 193 nm, loss of H and CH_3 are the main dissociation channels[15]. Therefore, it was of interest to see whether a methyl elimination channel could be observed in the case of the chlorotoluenes. As has already been stated above, the signal at m/e 15 is very weak, and because the TOF spectrum is readily simulated by assuming that all of the methyl radicals observed are due to secondary dissociation of tolyl radical, one concludes that a primary methyl loss channel does not exist for chlorotoluenes, or is of such minor importance as not to be detectable.

In summary, two, and possibly three, primary dissociation channels were detected for ortho-chlorotoluene at 193 nm. These channels involve loss of chlorine atom, but differ in the amount of translational energy released in the dissociation. There may be other primary channels involving loss of hydrogen atom or molecule, but these products could not be easily detected in our experiment. These channels are not expected to be important. No evidence for the loss of HCl molecule or CH_3 was found.

In addition to these primary dissociation channels, secondary dissociation of the highly internally excited tolyl radical occurs. The secondary products are methyl radical and mass 76, benzyne. It appears that the tolyl or benzyl radical formed in the slower of the

two (or three) chlorine loss channels undergoes secondary dissociation. The reaction channels and the amount of translational energy released in each are summarized in Table 1.

POLARIZATION STUDIES: Polarization studies revealed no dramatic anisotropy, confirming the notion that the transition is to a (π, π^*) state which undergoes predissociation. These ideas are explored further in the Discussion. The polarization data are presented in Figures 18,19 and 37.

meta-chlorotoluene

Three dissociation channels were detected for meta-chlorotoluene at 193 nm. Again, these channels involve loss of chlorine atom according to reaction 1, and differ in the amount of translational energy released in the dissociation. The same approach used in fitting the primary data for ortho-chlorotoluene was used in fitting the primary data for meta-chlorotoluene.

The meta-tolyl radical also undergoes secondary decomposition to yield the same secondary products, namely methyl radical (m/e 15) and benzyne (m/e 76). These data were fit as for the ortho compound. The TOF spectra and the P(E)s used to fit both the primary and secondary dissociation are shown in Figures 20 through 27.

The average translational energy released for these primary and secondary decomposition channels is also given in Table 1, together with the values for the other compounds.

para-chlorotoluene

Essentially the same story may be told for para-chlorotoluene: three primary dissociation channels, each involving loss of Cl. As is evident from the TOF spectra and the P(E)s derived from them, this compound behaves much like its isomeric sisters at 193 nm. These data are displayed in Figures 28 through 35.

BRANCHING RATIOS: Branching ratios for the three primary reaction channels for all three compounds are sumarized in Table 1. They were calculated from the Cl TOF data using the following simplified version of the expression for the branching ratio described by Krajnovich[16]:

$$R(1/2) = [N'(1)/N'(2)] \times [(\int_0^\infty P_2(E_T)\ (v_2/u_2)\ dv_2)/(\int_0^\infty P_1(E_T)\ (v_1/u_1)\ dv_1)],$$

where N' is the total number of detected ion counts at mass 35, 20° from either the channel designated as 1 or 2, and the integrals are the calculated signal, evaluated numerically by the CMLAB2 program. Normally, the branching ratio expression contains additional factors to correct for the differences in the ionization cross sections of the fragments, and to correct for the relative abundance of the given mass-to-charge ratio detected in the the mass spectrum of the product fragment. These are needed when the branching ratios for channels which produce different products are to be

calculated, and when the ions of these products are capable of undergoing further decomposition, or "cracking", in the detector. In our case, the channels being compared form the same products, and so these factors cancel, leaving us with the expression above.

One should also note that the branching ratio calculations were performed using the Cl data because the Cl ion, formed in the detector, does not undergo further decomposition as does the tolyl or benzyl ion. If this "cracking" of the polyatomic ion in the detector were to occur to a greater extent for internally excited fragments, such as those produced in the slower Cl loss channels, the branching ratio determination involving the m/e 91 data would not be correct.

Lastly, it must be pointed out that, in this instance, the error in the branching ratio determinations is given simply by the extent to which the dynamically distinguishable channels overlap in time. This is given by the overlapping areas in the TOF spectra.

DISCUSSION

fast primary dissociation to yield Cl and m/e 91

The most reasonable assumption regarding the nature of the three primary chlorine atom loss channels is that they arise from dissociation on different electronic surfaces. An energy level diagram, outlining approximately where various electronic states in these molecules lie, as well as other relevant quantities, is presented in Figure 36. In that the fast dissociation process has a large fraction of the available energy in translation, one might suspect that a direct

dissociation is responsible. Although an early photodissociation experiment at 193 nm involving many aryl and alkyl-arylhalides did not show the existence of this fast channel[5], in more recent photodissociation studies of meta-chlorotoluene, chlorobenzene, and para-dichlorobenzene also at 193 nm[6,7] this fast channel was observed, and it is speculated that the transition giving rise to this channel is analogous to the one responsible for the direct dissociation process found in alkyl halides, namely a $\sigma^* \leftarrow np\pi$ transition. This could account for the leading edge of the TOF spectrum, with the remainder of the signal in the fast channel resulting from excitation to a (π, π^*) transition localized in the ring, followed by a pre-dissociation. Based on a comparison of the cross sections for the direct transition in alkyl chlorides and the transition localized on the ring, it is concluded[6] that such a direct transition in ortho-chlorotoluene would probably only contribute a few percent of the signal counts. Alternatively, all of the signal could arise from molecules which were excited to their singlet (π, π^*) transition and which then undergo a curve crossing with subsequent pre-dissociation on a repulsive triplet (σ, σ^*)[5] surface.

In order to determine whether a direct transition or pre-dissociation is more important in these molecules, polarization studies were performed, and the data, shown for the para isomer in figure 37, were analyzed particularly carefully at the fast edge of each TOF spectrum. The polarization data reveal no dramatic differences at the fast edge between the two polarizations used. Furthermore, in assuming the product angular distribution to be given by $2\pi(1 + \beta P_2(\cos(\theta))$ for a dipole allowed transition[16], it was

found that the β parameter varied between +0.05 and -0.15, with the transition moment at right angles to the Cl atom leaving direction. Note that only in the case of the para isomer is it possible to associate the transition moment direction with the inertial axes of the molecule. What is described would be more consistent with the pre-dissociation picture: a relatively isotropic angular distribution with perhaps a B-type transition moment in the case of the para isomer, and no differences in the TOF spectra taken with different polarizations, particularly at the leading edge of the spectra.

slow primary channels yielding Cl and m/e 91

The two slower primary channels, also previously observed[5-7], are assumed to result from dissociation from different electronic states. After the initial excitation, some molecules can dissociate via the rapid channel discussed above. However, non-radiative decay processes become competitive with the dissociation. The molecules dissociate on different electronic surfaces, and the tolyl fragments produced via these channels are left with an average internal energy of 13 and 6 kcal/mole, respectively. Some of these slower tolyl fragments undergo secondary decomposition to form methyl radical and m/e 76, benzyne. The fraction which do undergo spontaneous secondary dissociation may be estimated from the areas under the experimental and simulated spectra shown in Figure 10. In the case of o-CT, approximately 48 percent of the tolyl radicals dissociate due to their high internal excitation.

The average translational energy release of 13 kcal/mole for the faster of these two channels is similar to that of the fast channel in the 248 nm dissociation[17] which perhaps occurs from both the first excited singlet state, S_1, and the lowest triplet state, T_1, of the molecule. Freedman, et al.[5] speculate that the molecules undergo rapid internal conversion to S_1, followed by an intersystem crossing to the lowest triplet state, T_1 where dissociation ultimately occurs. However, they do not observe the fastest of the three possible channels, and conclude that all of the molecules internally convert to S_1. Ichimura, et al.[6] assign the second fastest channel to dissociation from T_1, produced directly via intersystem crossing from the initially excited singlet level, S_3, while the fast channel results from the S_1 state. They may also have observed the slowest chanel, as discussed below. The Cl atom, with its reasonably large spin-orbit splitting could certainly promote ISC[18]. Ichimura and coworkers have also claimed that this second primary channel has a non-statistical translational energy distribution[6], and that this indicates that dissociation takes place before the vibrational and rotational energy resulting from the internal conversion(IC) or intersystem crossing(ISC) process has time to distribute itself throughout the molecule. Unfortunately, the existence of the third component in the Cl TOF spectrum, and the fact that the tolyl radical TOF spectrum is affected by secondary decomposition of the tolyl radical precludes determining the exact shape of the P(E) for this particular primary channel. If one chooses one's deconvolution of the slow components to the spectrum appropriately, one can probably make the P(E) distribution more or less "non-statistical", at will. Furthermore, if

dissociation is occurring from an electronically excited state of the molecule, and not from S_0, the P(E) used to fit this channel will be inherently "non-statistical" since the number of vibrational levels in an excited electronic state will be less than the corresponding number in the ground state. Finally, since the detection efficiency for slower products is lower in their experimental apparatus, and since they do not state specifically whether they correct for this in the inversion of their data which is used to obtain their P(E)s, Ichimura et al. might have a P(E) skewed to faster average translational energies, making their P(E)s look even more "non-statistical".

Finally, the studies done by Ichimura, et al. all assumed that a slow primary channel was responsible for the slight slow tail in their Cl TOF spectra. They were limited to detecting Cl atoms with 3 kcal/mole or more translational energy so that it is difficult to see that a third channel even exists. Our data are somewhat more convincing as we are able to detect products with a minimum of 0.5 kcal/mole. Nonetheless, it would be more satisfying if there were not such a substantial amount of overlap between the two translational energy distributions used to fit the slower portion of the TOF spectra, particularly in the case of the ortho isomer. The exact shape of the P(E) used to fit the slowest channel is uncertain, making comparisons with theoretical energy distributions unjustified at this point.

Let us reiterate what is known. Clearly, two, and perhaps three, states are giving rise to products. Due to the presence of the Cl substituent, intersystem crossing is favored over internal conversion

in these molecules, implying that triplet states play an important role in their dissociation, but dissociation from the ground state can not be ruled out for the slowest channel. The fastest channel is certainly not due to a direct dissociation from the state initially excited, because there is no observed anisotropy of the product angular distribution. Photodissociation experiments at other wavelengths would be useful in determining the exact nature of the electronic states which give rise to the observed TOF spectra. A first step in this direction will be presented in Chapter 3.

secondary dissociation of tolyl radical to yield CH3 and C6H4

Figure 10 shows quite clearly the extent to which secondary decomposition of the tolyl radical occurs. In this way, the slow side of the m/e 73 TOF spectrum has been modelled, while nearly the entire m/e 15 TOF spectrum can be accounted for in this way. The structure observed in the difference spectra (Figures 14, 27, and 35) shows, in a relative fashion, which of the three primary Cl loss channels accounts for the secondary dissociation observed for each molecule. In the case of the ortho isomer, most of the secondary products result from the middle channel; for the meta isomer, the middle channel still plays a large role, but the slowest channel becomes more prominent; for the para case, the slowest channel dominates. This somewhat follows the trend observed in the medium:slow branching ratios, except for the meta and para isomers. Their ratios are the same, but there is apparently more secondary dissociation from the slow state in the para isomer.

Previously, it has been possible to estimate bond energies in radical products by looking at the energy threshold where secondary dissociation occurs[20]. Only those products with sufficiently slow recoil velocities, or conversely, only those primary products with sufficient internal energy to break a given bond, will yield secondary products. By examining the primary difference P(E)s, one notes in the case of the ortho isomer, for example, that the probability extends out to 45 kcal/mole, but it is no longer appreciable after, say, 32 kcal/mole. That might suggest that the tolyl radicals with less than 32 kcal/mole in translation, or more than 19 kcal/mole internal energy (excess available energy - maximum translational energy possible to yield secondary products), undergo secondary dissociation, i.e. one would approximate the CH_3-C_6H_4 bond energy in the o-tolyl radical to be roughly 19 kcal/mole. However, given that the difference P(E) does extend past 32 kcal/mole, this is only a rough estimate. Similarly, one can estimate the CH_3-C_6H_4 bond energies in the m- and p-tolyl radicals to be 21 and 30 kcal/mole respectively.

Also problematic is the fact that the m/e 73 TOF spectrum can not be completely simulated. There is a fast component to the spectrum that has not been accounted for at this time. It does not appear to be the result of a secondary process, e.g. secondary photodissociation of the tolyl radical, as the methyl radical spectrum would reflect this. It also cannot be the result of molecular elimination reactions, e.g. HCl or even CH_3Cl elimination, as such processes would necessarily result from strained intermediates (see below). This would probably leave a considerable amount of internal

excitation in the products. In addition, CH_3Cl elimination would only be a possibility in the case of the ortho isomer, and the fast component is present in the m/e 73 spectra of all of the molecules. Until the nature of the fast component is revealed, it is not possible to state that all primary and secondary reaction channels of these molecules have been identified.

Absence of HCl elimination channel

Several experiments have been performed on vinyl chloride and other chlorinated ethylenes[21,22] in which HCl elimination has been observed to be a major channel. The absorption spectra of these molecules[22] are very similar in appearance to those of the chlorinated benzenes, and it is reasonable to assume that similar states are responsible for the absorption features of both kinds of molecules. The HCl and acetylene or chloroacetylene products formed are found to be highly vibrationally excited[21,22], indicating that there is probably a great deal of strain on the molecule in bringing the H and Cl atoms close enough together. This may be one reason why the chlorotoluenes can not undergo this elimination reaction: the existence of the very stable ring to which the H and Cl atoms are attached prevents sufficient deformation to allow the HCl bonding to occur. Additionally, the H and Cl atoms are further separated in the chlorotoluenes as the C-C bond distance is somewhat longer in the benzene ring than in the ethylenes as is shown in Figure 38[23]. The activation barrier to HCl elimination was estimated to be 72 kcal/mole[22] in the case of vinylchloride, and from all

indications, should be higher than this in the case of the chlorotoluenes. Perhaps the barrier exceeds the available energy, or if the barrier is not so high, the HCl products may be quite slow and are buried in the tails of the m/e35 to m/e 38 TOF spectra.

Differences between the three isomers

All in all, the three isomers are remarkably similar in their dissociation behavior at 193 nm. The differences in branching ratios are within the experimental error, due to the overlap of the dynamically distinguishable channels. It appears however that dissociation via the slowest channel is much more important in the para isomer as this component to the TOF spectrum is more evident. As the para isomer is the most symmetric of the three, it seems reasonable that it should behave somewhat differently than the ortho and meta isomers. It does not show any more isotropy in its product angular distribution than the others do, which demonstrates that rapid curve crossing and predissociation are likely in these molecules.

V. CONCLUSIONS

Photodissociation studies of the isomers of chlorotoluene at 193 nm have been performed using a crossed molecular beam-laser beam apparatus in which products can be detected at various angles with respect to the molecular beam direction. This allows us to easily observe all of the products of photodissociation, and to

determine whether these products are the result of a primary photodissociation event, or whether they are the result of a primary product undergoing subsequent, secondary, decomposition.

For all three isomers, we have observed three primary channels, which all involve loss of the Cl atom. In addition to the three primary channels, there is one secondary decomposition channel which involves dissociation of the tolyl radical, formed in one of the Cl loss channels. Approximate branching ratios between the three channels, for the three molecules, have been determined and are given in Table 1, together with the average amount of energy released in translation. There is no evidence that HCl elimination occurs from these molecules, nor are there any obvious differences among the velocity distributions of the three isomers attributable to differences in their structure. There are differences however in the way that the tolyl products of the three undergo secondary dissociation. Secondary dissociation occurs mostly from the middle channel for the ortho isomer, from both the middle and slow channels for meta, and mostly from the slow channel for the para compound. Rough estimates for the CH_3-C_6H_4 bond energies have been made from these data, and appear in Table 1. There appears to be one unidentified dissociation channel, which manifests itself as a fast component in the m/e 73 through 76 TOF spectra.

Polarization studies indicate that the state initially excited at 193 nm is of a delocalized nature, probably a (π, π^*) state. There is no evidence that a transition involving a more localized, $\sigma^* \leftarrow$ n state, such as occurs in the alkyl chlorides is of importance here.

REFERENCES

1. Freed, K. F., "Energy Dependence of Electronic Relaxation Processes in Polyatomic Molecules" in Topics in Applied Physics, XV,: Radiationless Processes in Molecules and Condensed Phases, ed. F. K. Fong, Springer Verlag, Berlin (1976) is an excellent review with 143 references.

2. a) G. B. Kistiakowsky and C. S. Parmenter, J. Chem. Phys., 42, 2942 (1965); b) C. S. Parmenter and A. H. White, J. Chem. Phys., 50, 1631 (1969); c) W. R. Ware, B. K. Selinger, C. S. Parmenter, and M. W. Schuyler, Chem. Phys. Lett., 6, 342 (1970).

3. a) C. Guttman and S. A. Rice, J. Chem. Phys., 61, 651 (1974); b) C. S. Parmenter and M. W. Schuyler, J. Chem. Phys., 52, 5366 (1970).

4. a) M. G. Rockley and D. Phillips, Chem. Phys. Lett., 21, 181 (1973); b) C. Guttman and S. A. Rice, J. Chem. Phys., 61, 661 (1974); c) L. J. Volk and E. K.C. Lee, J. Chem. Phys., 67, 236 (1977).

5. A. Freedman, S. C. Yang, M. Kawasaki, and R. Bersohn, J. Chem. Phys., 72, 1028 (1980).

6. T. Ichimura, Y. Mori, H. Shinohara, and N. Nishi, Chem. Phys. Lett., 122, 51 (1985).

7. ibid, 55.

8. A. M. Wodtke and Y. T. Lee, J. Phys. Chem., 89, 4744, (1985).

9. T. Ichimura, Y. Mori, M. Sumitani, and K. Yoshihara, J. Chem. Phys., 84, 1943, (1986).

10. The heat of formation for tolyl radical was estimated from the following relationship: ΔH_f^o(tolyl radical) = $D_o(CH_3C_6H_4\text{-}H)$ - $\Delta H_f^o(H)$ + $\Delta H_f^o(CH_3C_6H_5)$; the heat of formation for benzyl radical, and the

values used in the calculation for tolyl radical were obtained from the CRC Handbook of Chemistry and Physics, 61st ed., CRC Press, Boca Raton (1980). The values are ΔH_f^o(tolyl), 66 ± 2 kcal/mole; $D_o(CH_3C_6H_4\text{-}H)$ = 110 ± 2 kcal/mole; ΔH_f^o(H), 52.103 ± 0.001 kcal/mole; ΔH_f^o(toluene), 11.950 kcal/mole; ΔH_f^o(benzyl), 45 ± 1 kcal/mole.

11. N. R. Daly, Rev. Sci. Instrum., 31, 264, (1960).

12. G. N. Robinson, Ph. D. Thesis, University of California, Berkeley, 1987.

13. X. Zhao, Ph. D. Thesis, University of California, Berkeley, 1988.

14. A. Yokoyama, X. Zhao, E. J. Hintsa, R. E. Continetti, and Y. T. Lee, to be published.

15. R. J. Brudzynski, Jr., Ph. D. Thesis, University of California, Berkeley, 1987.

16. D. J. Krajnovich, Ph. D. Thesis, University of California, Berkeley, 1983.

17. R. N. Zare, Mol. Photochem., 4, 1 (1972).

18. See Chapter 3.

19. D. McClure, J. Chem. Phys., 20, 682 (1951).

20. T. K. Minton, G. M. Nathanson, and Y. T. Lee, J. Chem. Phys., 86, 1991 (1987).

21. M. Umemoto, K. Seki, H. Shinohara, U. Nagashima, N. Nishi, M. Kinoshita, and R. Shimada, J. Chem. Phys., 83, 1657, (1985).

22. M. J. Berry, J. Chem. Phys., 61, 3114 (1974).

23. Bond lengths and angles were obtained from the CRC Handbook of Chemistry and Physics, op. cit.

TABLE 1

	ortho	meta	para
fast $\langle E_{trans} \rangle$ (kcal/mole)	33	33	31
medium $\langle E_{trans} \rangle$ (kcal/mole)	13	13	13
slow $\langle E_{trans} \rangle$ (kcal/mole)	7	7	7
branching ratios (fast : medium : slow)	1 : 2.0 : 0.4	1 : 1.5 : 0.5	1 : 1.8 : 0.6
$\langle E_{trans} \rangle$, secondary (kcal/mole)	11	13	11
$D_o(CH_3\text{-}C_6H_4)$ (approximate) (kcal/mole)	19	21	30

Figure 1: Schematic of rotating molecular beam source apparatus: **1**, source chamber; **2**, heater and thermocouple; **3**, cryocooled plate; **4**, entrance lens and exit window for excimer laser; **5**, interaction region where laser and molecular beams intersect; **6**, liquid nitrogen cooled panels; **7**, valve to open detector to main chamber; **8**, TOF wheel for beam velocity measurements. It can be moved into, and out of position without breaking vacuum; **9**, 5000 l/s diffusion pump for main chamber; **10**, 6" diffusion pump (one of two) for source chamber; **11**, ionizer; **12**, quadrupole mass filter; **13**, magnetically suspended turbomolecular pump; **14**, ion optics for steering ions to **15**; **15**, "doorknob" ion target; **16**, plastic scintillator; **17**, turbomolecular pump; **18**, photomultiplier tube; **19**, liquid N_2 reservoirs.

Figure 2: o-CT TOF spectrum monitored at m/e 91, 20°, 193 nm and at laser energies of 3 mJ and 55 mJ. No multiphoton absorption is noted. Dashed lines represent the CMLAB2 simulations of these data.

Figure 3: Laser energy dependence of the o-CT signal monitored at m/e 91, 20°, 193 nm.

Figure 4: o-CT TOF spectrum monitored at m/e 35, 193 nm at 20°, 40° and 60°. The dashed lines represent the CMLAB2 simulations of these data.

Figure 5: o-CT TOF spectra, m/ 91, 193 nm, 20°, 40° and 60°.

Figure 6: "Newton" diagrams for the photodissociation of chlorotoluene at 193 nm to yield tolyl radical (C_7H_7) and Cl. The circles represent the maximum velocities of the product fragments with an excess available energy of 51 kcal/mole. V_b represents the average molecular beam velocity, u_{C7H7} represents the maximum

allowed center-of-mass velocity of the tolyl fragment, and their resultant, vlab, represents a single laboratory velocity monitored at 40° with respect to the molecular beam.

Figure 7: Center-of-mass translational energy distribution, P(E), used to simulate the fast peak in the o-CT m/e 35 and 91 spectra at all angles.

Figure 8: P(E)s used to simulate the middle peak in the o-CT m/e 35 and 91 TOF spectra, respectively.

Figure 9: o-CT TOF spectrum monitored at m/e 91, 20°, 193 nm. The simulated spectrum was generated by using the P(E)s used to fit the m/e 35 spectra. The difference between the observed and simulated spectra represents tolyl radical which undergoes secondary dissociation.

Figure 10: o-CT TOF spectrum, m/e 73, 20°, 193 nm with CMLAB2 simulation.

Figure 11: o-CT TOF spectrum, m/e 15, 20°, 193 nm with CMLAB2 simulation.

Figure 12: o-CT TOF spectrum, m/e 90, 20°, 193 nm with CMLAB2 simulation.

Figure 13: Difference P(E), derived from the o-CT m/e 91 and 35 P(E)s, used to fit the m/e 73 and 15 data. This difference represents the primary translational energy distribution of those tolyl products which undergo secondary dissociation.

Figure 14: The secondary P(E) used to fit the o-CT m/e 73 and 15 data. This is the translational energy distribution of the products of tolyl radical dissociation. $\langle E_{trans} \rangle$ = 11 kcal/mole.

Figure 15: P(E) used to simulate the slow tail observed in the o-CT m/e 35 TOF spectra, together with a P(E) which is the sum of this slow P(E) and the m/e 35 P(E) shown in Figure 8.

Figure 16: o-CT TOF spectra monitored at m/e 36 through 38, 20°, 193 nm. The simulations indicate that these TOF spectra are composites of the spectra at m/e 35(37) and m/e 39, due to leaking of the signal through the quadrupole mass filter, and cracking of the m/e 39 ion in the ionizer.

Figure 17: o-CT TOF spectra monitored at m/e 76 through 73, 20°, 193 nm. These data are simulated by assuming that the spectra at the lower masses result from cracking of the m/e 76 ion in the ionizer.

Figure 18: o-CT TOF spectrum monitored at m/e 91, 20°, 193 nm. The laser was horizontally polarized and the simulation assumes an anisotropy parameter, β, of 0.08.

Figure 19: Here the laser was vertically polarized, and the simulation again assumes a β parameter of 0.08.

Figure 20: m-CT TOF spectra monitored at m/e 35, 193 nm, at 20° and 60°, together with the CMLAB2 simulations.

Figure 21: Appropriately weighted P(E)s used to simulate the TOF spectra shown in Figure 20.

Figure 22: m-CT TOF spectra monitored at m/e 91, 193 nm, 20° and 60°, with CMLAB2 simulations.

Figure 23: Appropriately weighted P(E)s used to simulate the TOF spectra shown in Figure 22. The fast P(E) is the same one used to simulate the fast peak in the m/e 35 TOF spectra.

Figure 24: m-CT TOF spectrum, m/e 73, 20°, 193 nm, with CMLAB2 simulation.

Figure 25: m-CT TOF spectrum, m/e 15, 20°, 193 nm, with CMLAB2 simulation.

Figure 26: Difference P(E), derived from the m-CT m/e 91 and 35 P(E)s, used to fit the m/e 73 and 15 data.

Figure 27: The secondary P(E) used to fit the m-CT m/e 73 and 15 data. $\langle E_{trans} \rangle$ = 13 kcal/mole.

Figure 28: p-CT TOF spectra monitored at m/e 35, 193 nm, at 20°, 40° and 60°, with CMLAB2 simulation.

Figure 29: Appropriately weighted P(E)s used to simulate the TOF spectra shown in Figure 28.

Figure 30: p-CT TOF spectra monitored at m/e 91, 193 nm, at 20° and 40°, with CMLAB2 simulation.

Figure 31: Appropriately weighted P(E)s used to simulate the spectra shown in Figure 30.

Figure 32: p-CT TOF spectrum monitored at m/e 73, 193 nm, 20°, with CMLAB2 simulation.

Figure 33: p-CT TOF spectrum, m/e 15, 193 nm, 20°, with CMLAB2 simulation.

Figure 34: Difference P(E), derived from the p-CT m/e 91 and 35 P(E)s, used to fit the m/e 73 and 15 data.

Figure 35: Secondary P(E) used to fit the p-CT m/e 73 and 15 data. $\langle Et_{rans} \rangle$ = 11 kcal/mole.

Figure 36: Approximate energy level diagram for o-CT.

Figure 37: Polarization data, p-CT TOF spectra, monitored at m/e 91, 20°, 193 nm. The laser was horizontally and vertically polarized,

as indicated. The CMLAB2 simulations assumed a B parameter of 0.05.

Figure 38: Equilibrium structures of o-CT and chloroethylene.

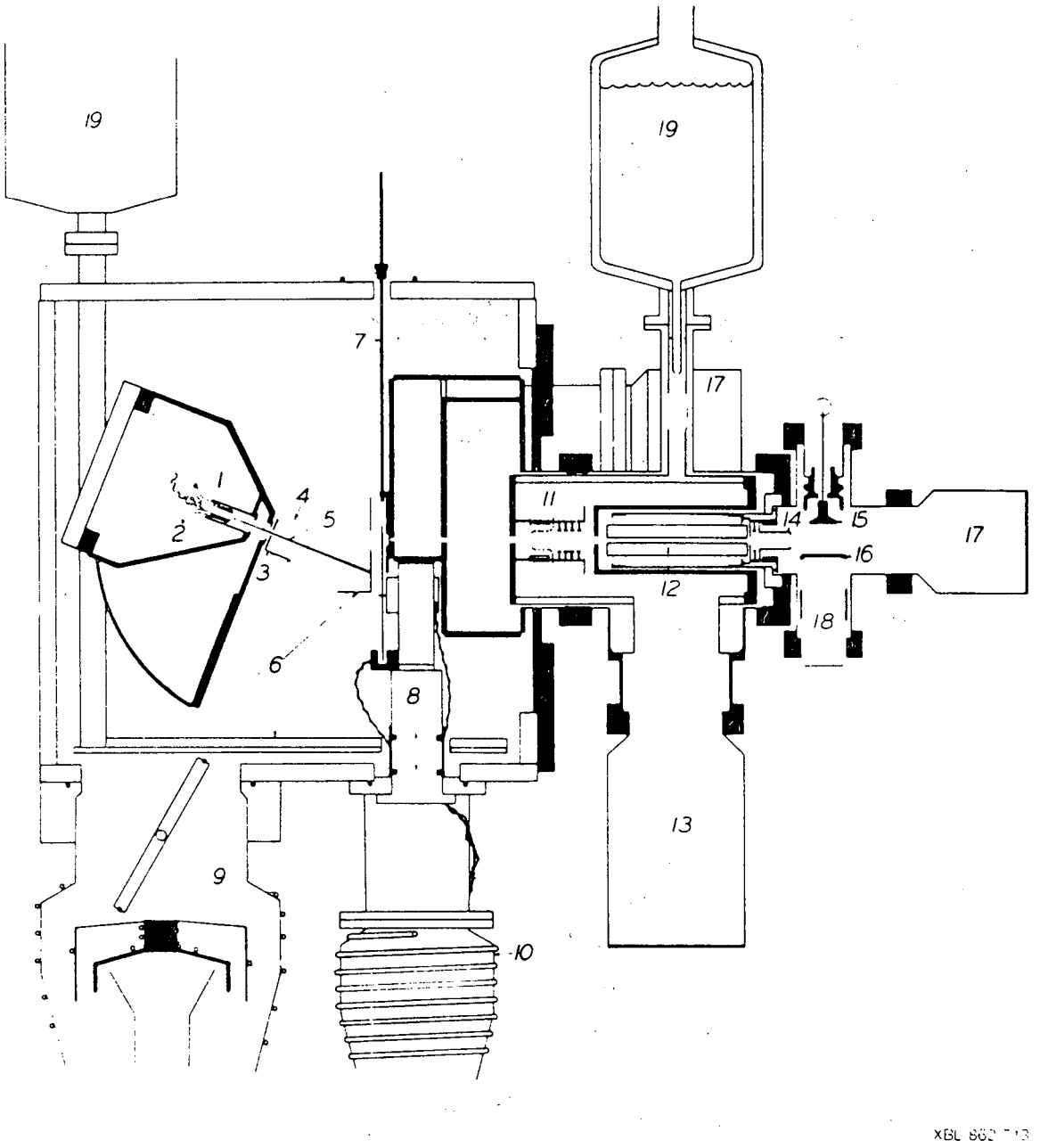

XBL 862-713

Figure 1

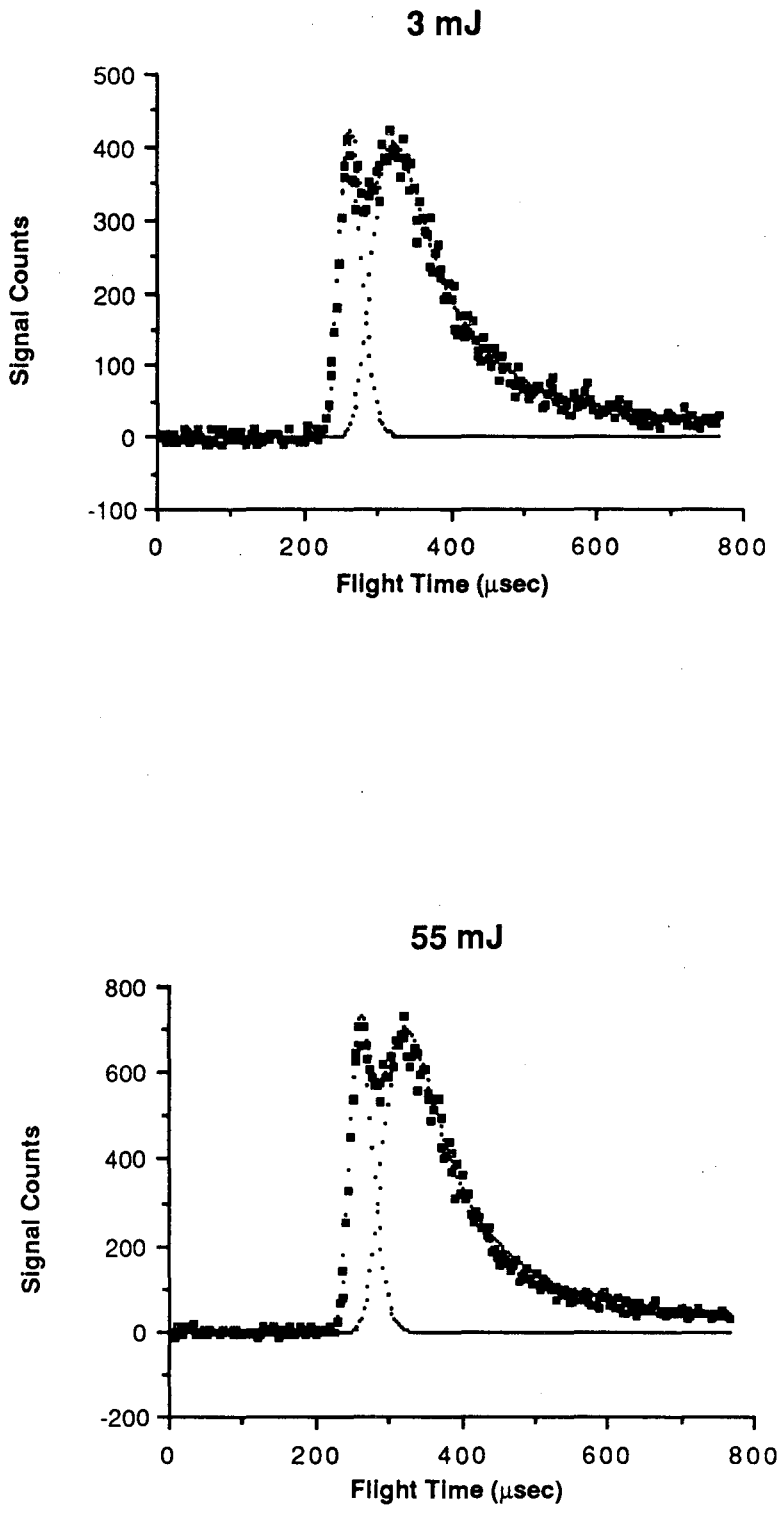
3 mJ
Signal Counts
500
400
300
200
100
0
-100
0
200
400
600
800
Flight Time (μsec)
55 mJ
Signal Counts
800
600
400
200
0
-200
0
200
400
600
800
Flight Time (μsec)

Figure 2

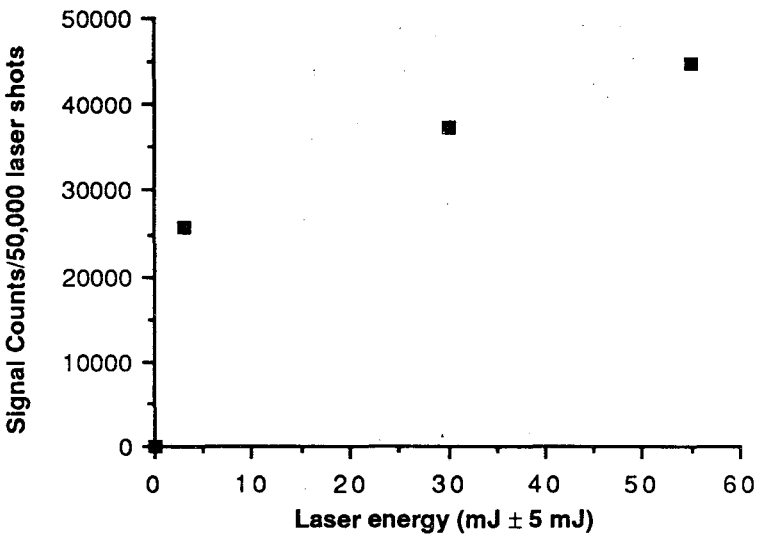
Signal Counts/50,000 laser shots
50000
40000
30000
20000
10000
0
0
10
20
30
40
50
60
Laser energy (mJ ± 5 mJ)

Figure 3

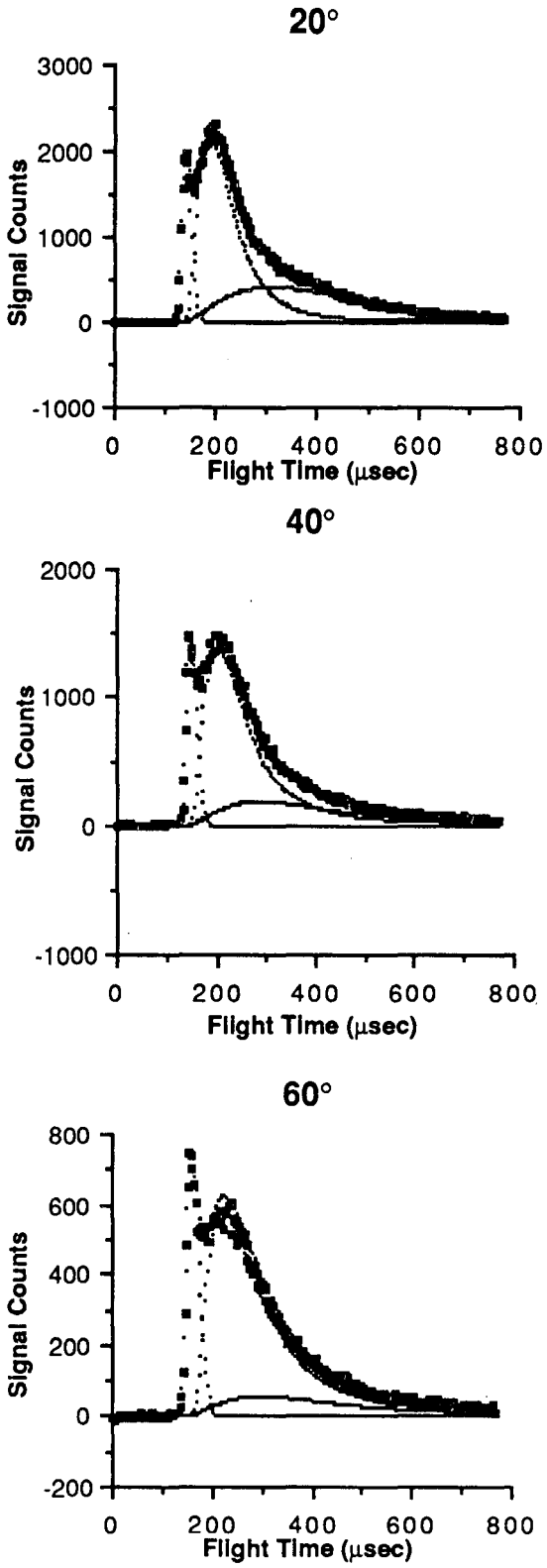
20°
3000
2000
1000
0
-1000
Signal Counts
0
200
400
600
800
Flight Time (μsec)
40°
2000
1000
0
-1000
Signal Counts
0
200
400
600
800
Flight Time (μsec)
60°
800
600
400
200
0
-200
Signal Counts
0
200
400
600
800
Flight Time (μsec)

Figure 4

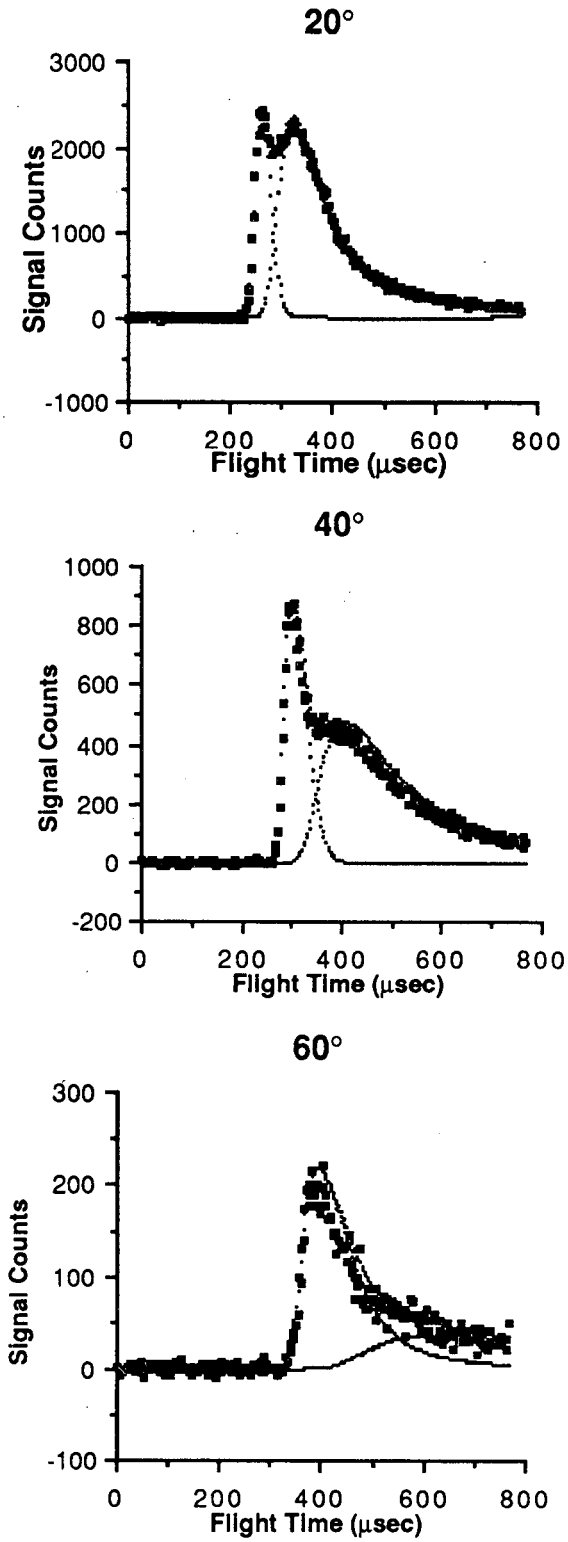
20°
Signal Counts
3000
2000
1000
0
-1000
0
200
400
600
800
Flight Time (μsec)
40°
Signal Counts
1000
800
600
400
200
0
-200
0
200
400
600
800
Flight Time (μsec)
60°
Signal Counts
300
200
100
0
-100
0
200
400
600
800
Flight Time (μsec)

Figure 5

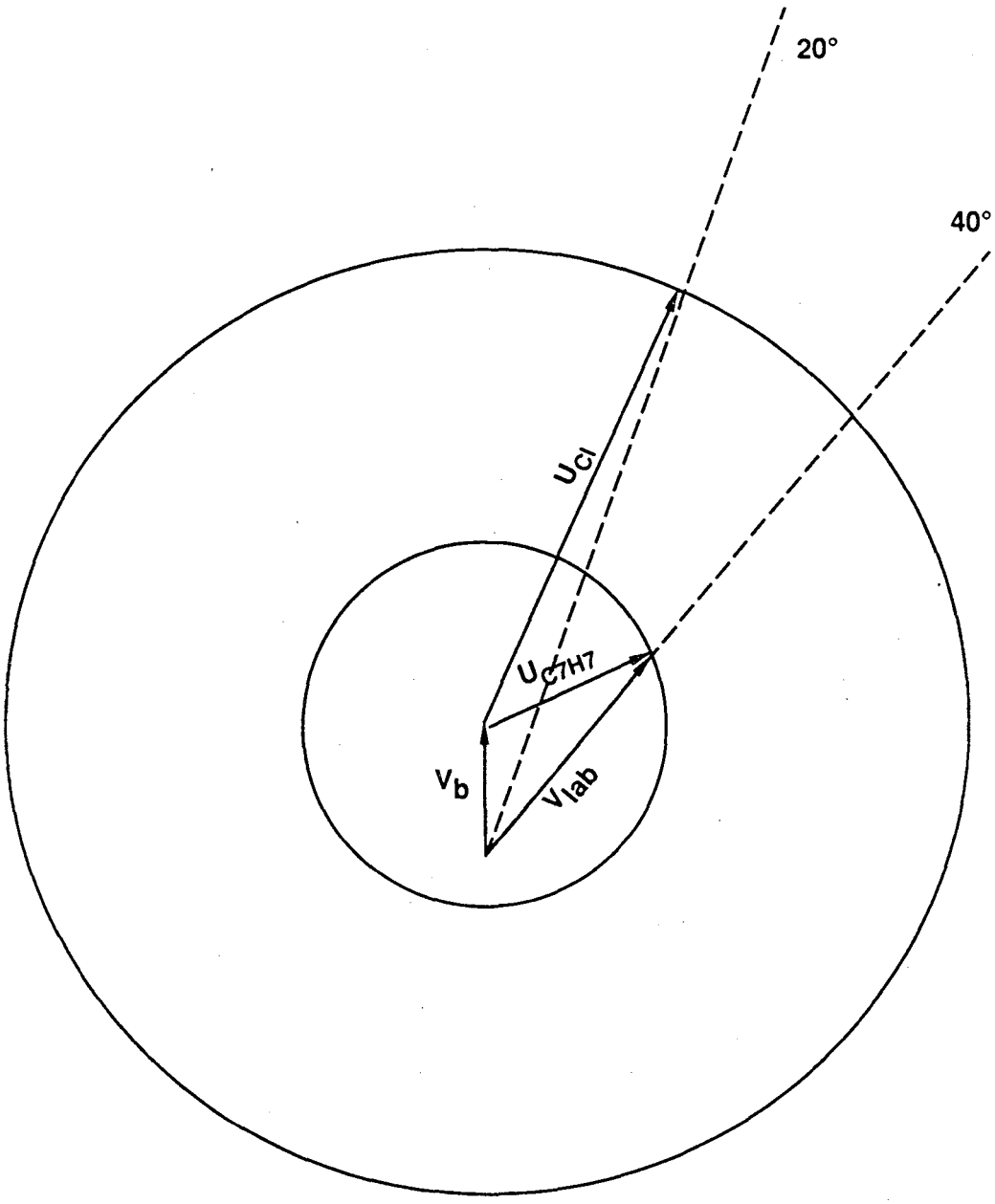

Figure 6

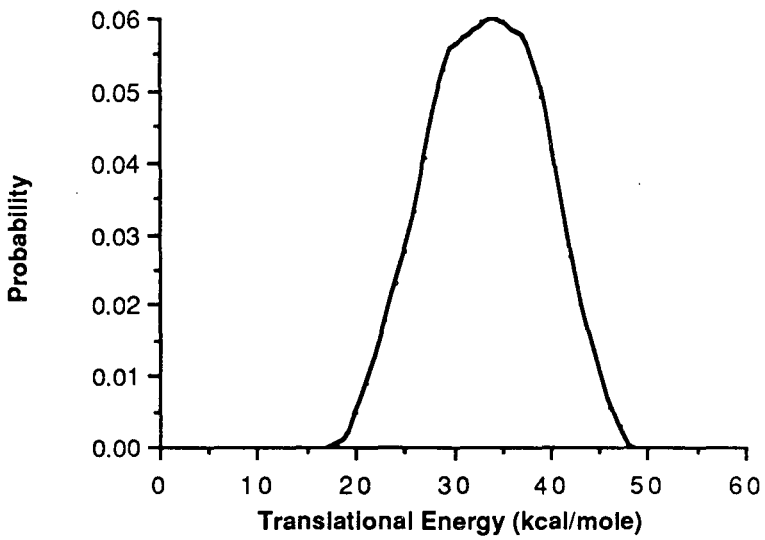
Probability
0.06
0.05
0.04
0.03
0.02
0.01
0.00
0
10
20
30
40
50
60
Translational Energy (kcal/mole)

Figure 7

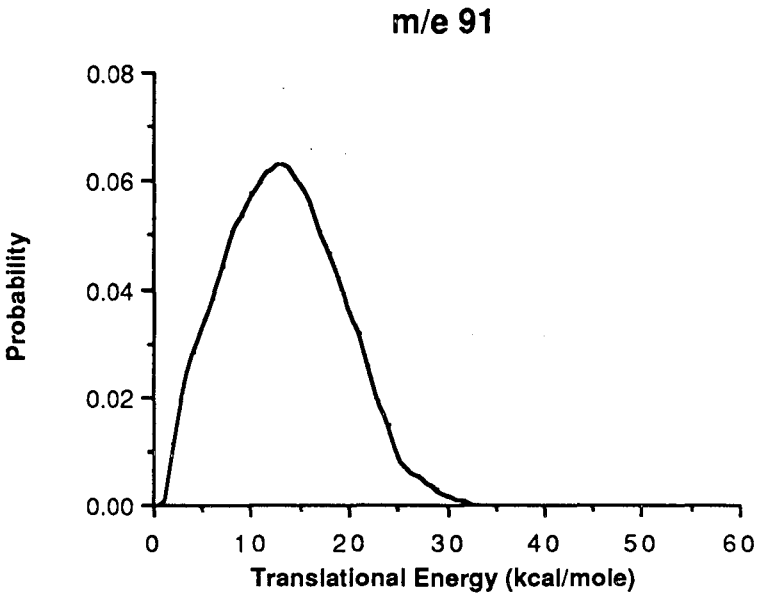
m/e 91
Probability
0.08
0.06
0.04
0.02
0.00
0
10
20
30
40
50
60
Translational Energy (kcal/mole)

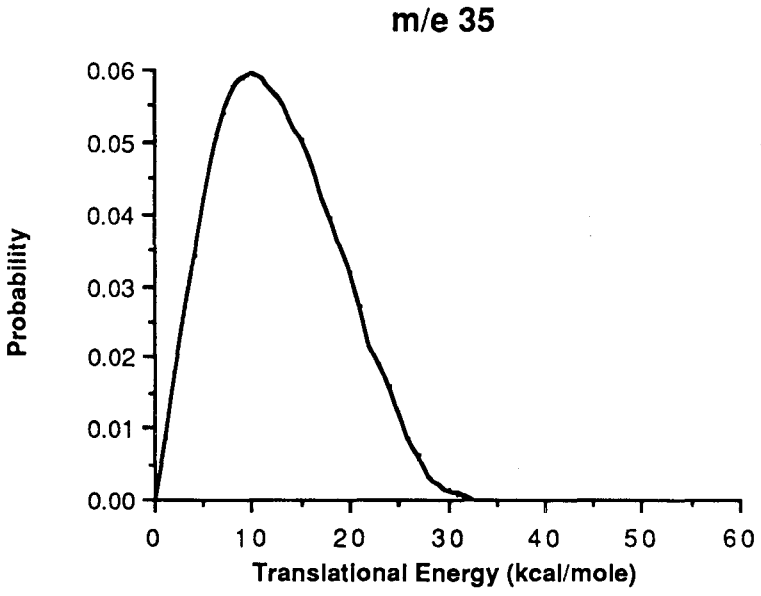
m/e 35
Probability
0.06
0.05
0.04
0.03
0.02
0.01
0.00
0
10
20
30
40
50
60
Translational Energy (kcal/mole)

Figure 8

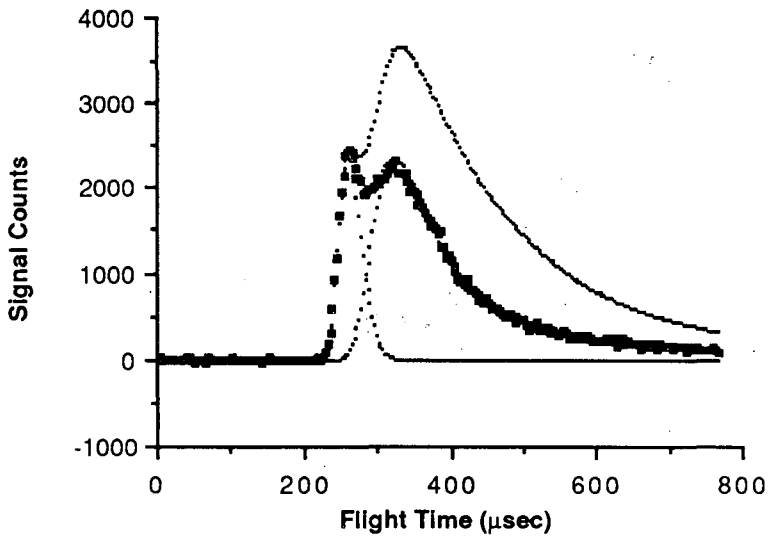
4000
3000
2000
1000
0
-1000
Signal Counts
0
200
400
600
800
Flight Time (μsec)

Figure 9

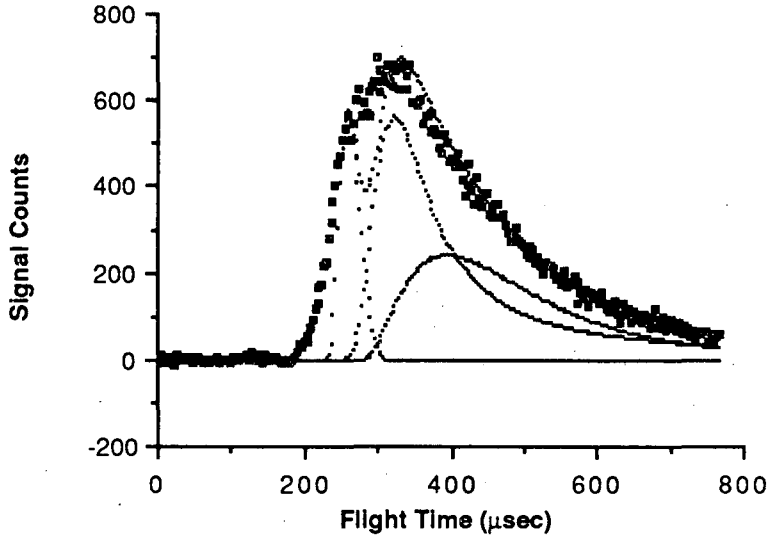
800
600
400
200
0
-200
Signal Counts
0
200
400
600
800
Flight Time (μsec)

Figure 10

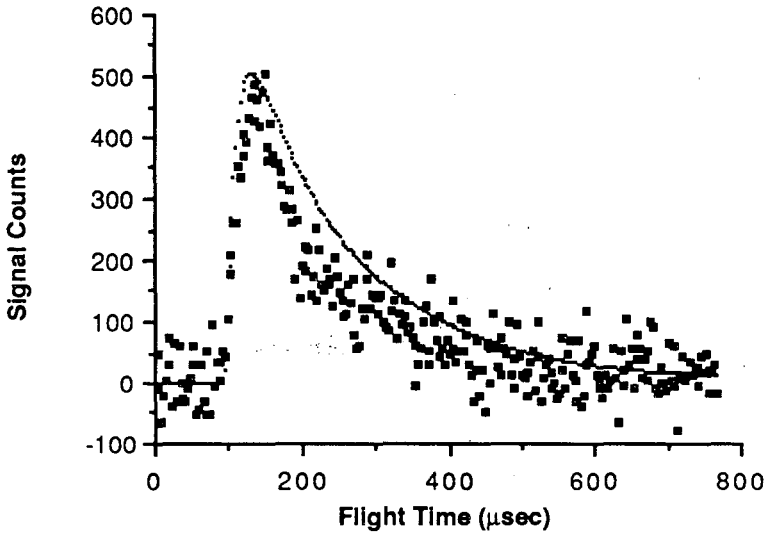
600
500
400
300
200
100
0
-100
Signal Counts
0
200
400
600
800
Flight Time (μsec)

Figure 11

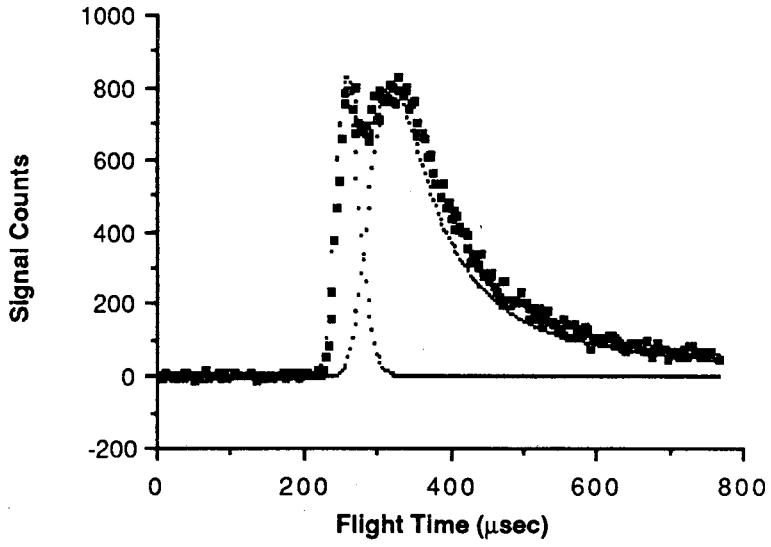
1000
800
600
400
200
0
-200
Signal Counts
0
200
400
600
800
Flight Time (μsec)

Figure 12

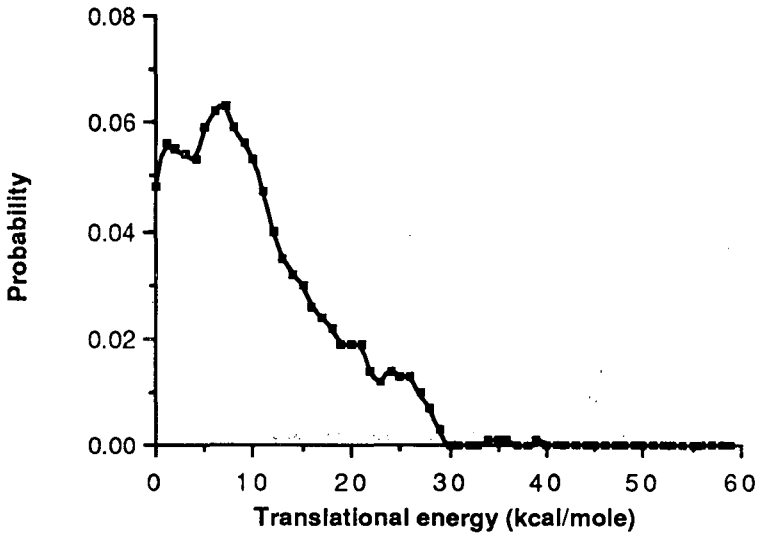
0.08
0.06
0.04
0.02
0.00
Probability
0
10
20
30
40
50
60
Translational energy (kcal/mole)

Figure 13

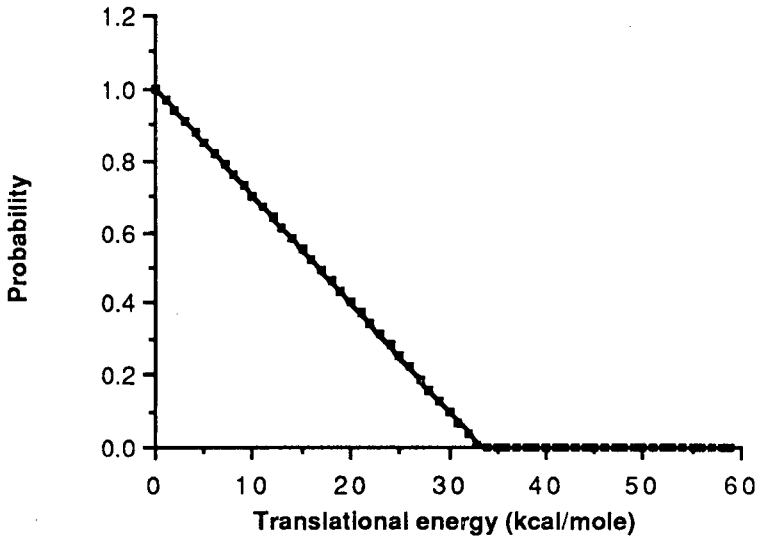
1.2
1.0
0.8
0.6
0.4
0.2
0.0
Probability
0
10
20
30
40
50
60
Translational energy (kcal/mole)

Figure 14

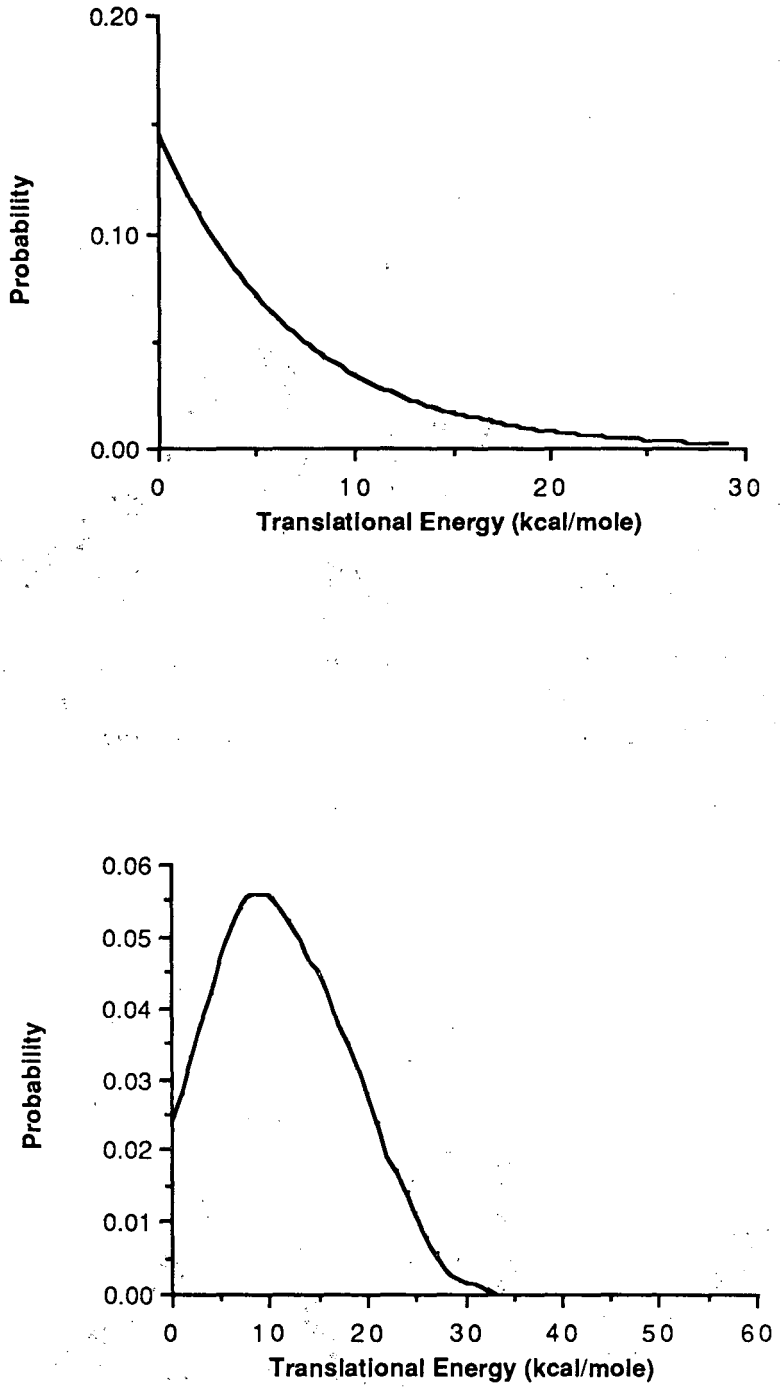
0.20
0.10
0.00
Probability
0
10
20
30
Translational Energy (kcal/mole)
0.06
0.05
0.04
0.03
0.02
0.01
0.00
Probability
0
10
20
30
40
50
60
Translational Energy (kcal/mole)

Figure 15

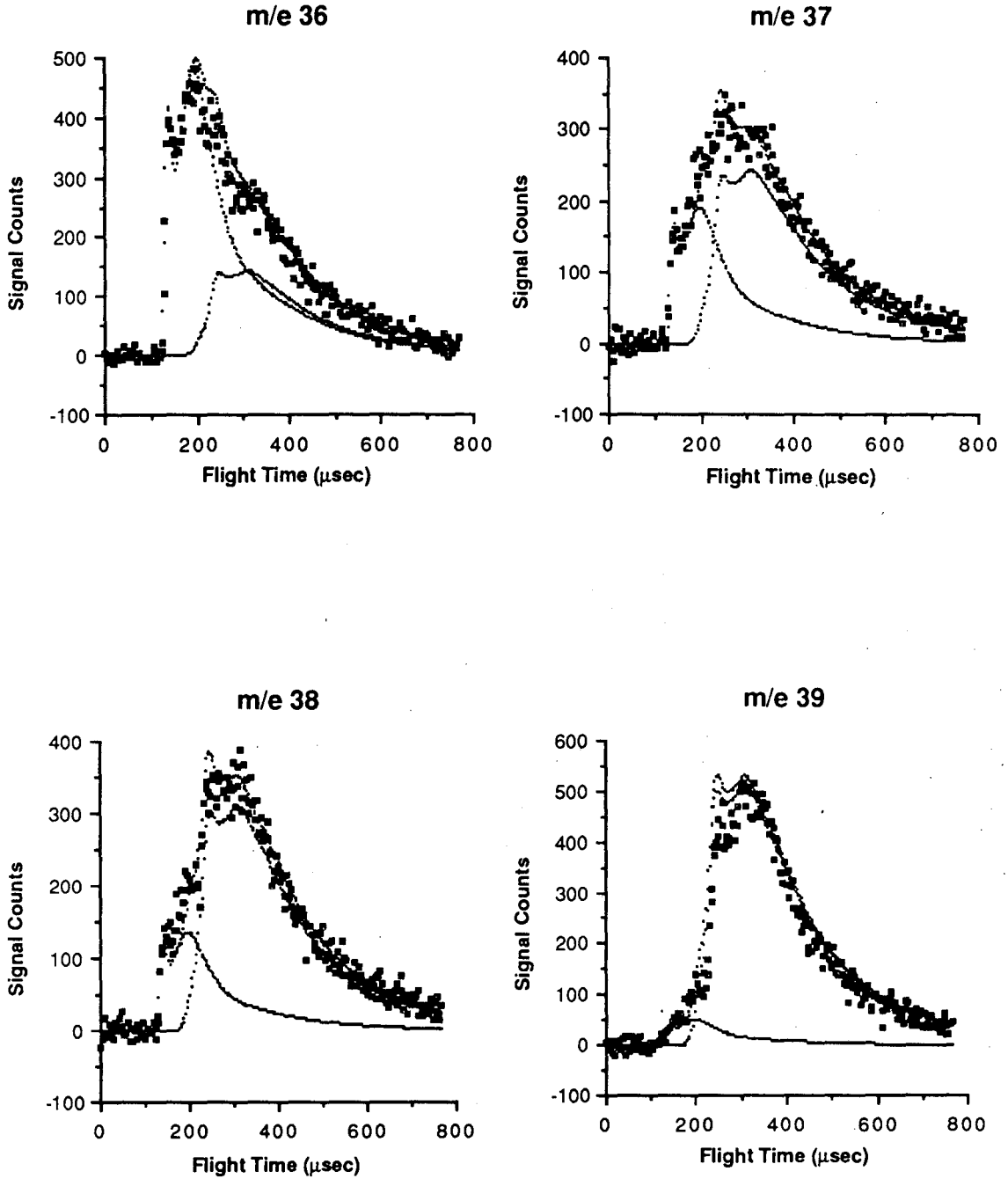
m/e 36
Signal Counts
500
400
300
200
100
0
-100
0
200
400
600
800
Flight Time (μsec)
m/e 37
Signal Counts
400
300
200
100
0
-100
0
200
400
600
800
Flight Time (μsec)
m/e 38
Signal Counts
400
300
200
100
0
-100
0
200
400
600
800
Flight Time (μsec)
m/e 39
Signal Counts
600
500
400
300
200
100
0
-100
0
200
400
600
800
Flight Time (μsec)

Figure 16

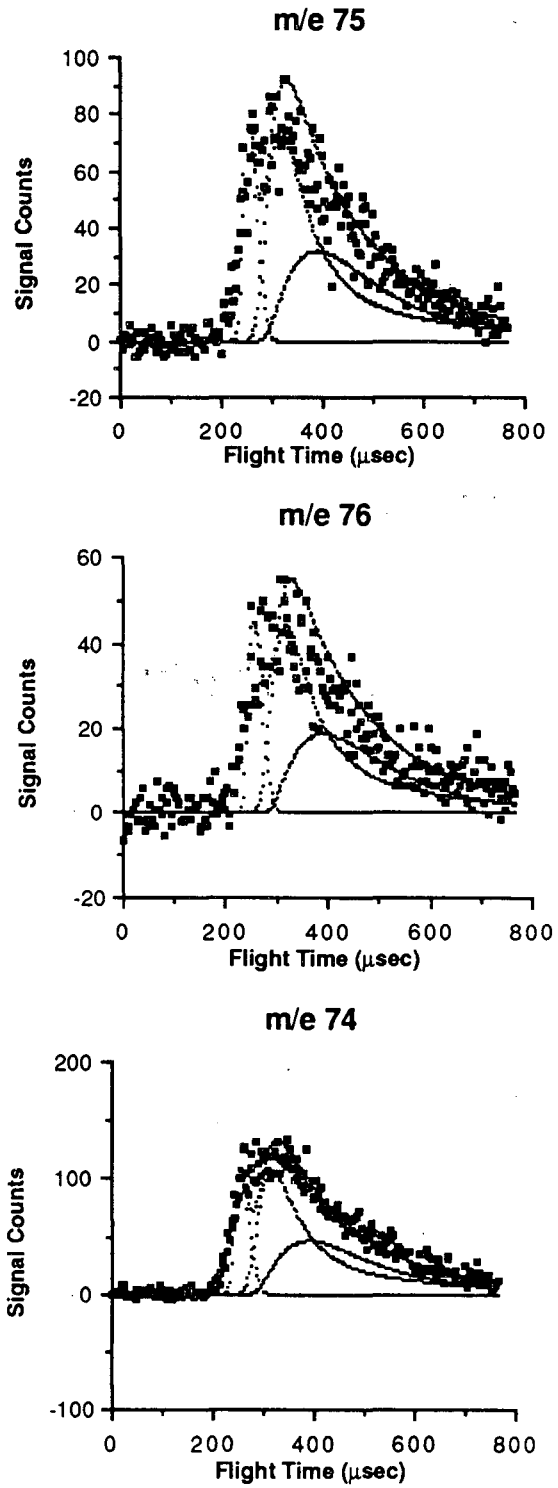
m/e 75
Signal Counts
100
80
60
40
20
0
-20
0
200
400
600
800
Flight Time (μsec)
m/e 76
Signal Counts
60
40
20
0
-20
0
200
400
600
800
Flight Time (μsec)
m/e 74
Signal Counts
200
100
0
-100
0
200
400
600
800
Flight Time (μsec)

Figure 17

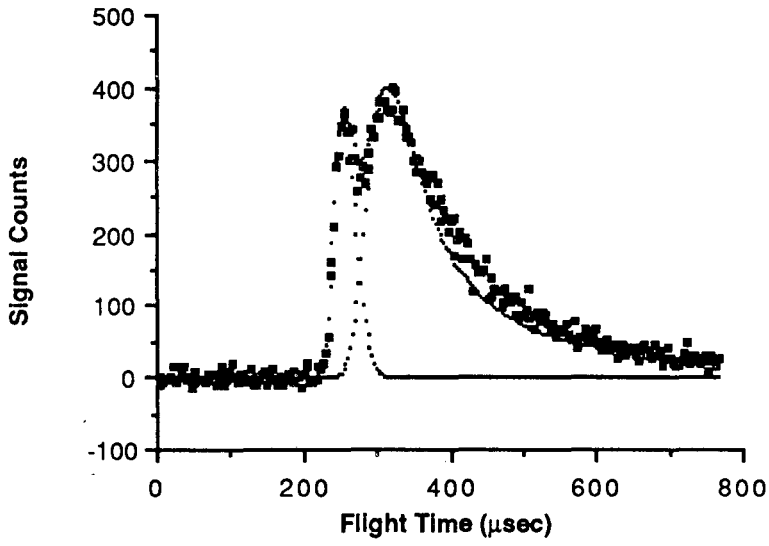
500
400
300
200
100
0
-100
Signal Counts
0
200
400
600
800
Flight Time (μsec)

Figure 18

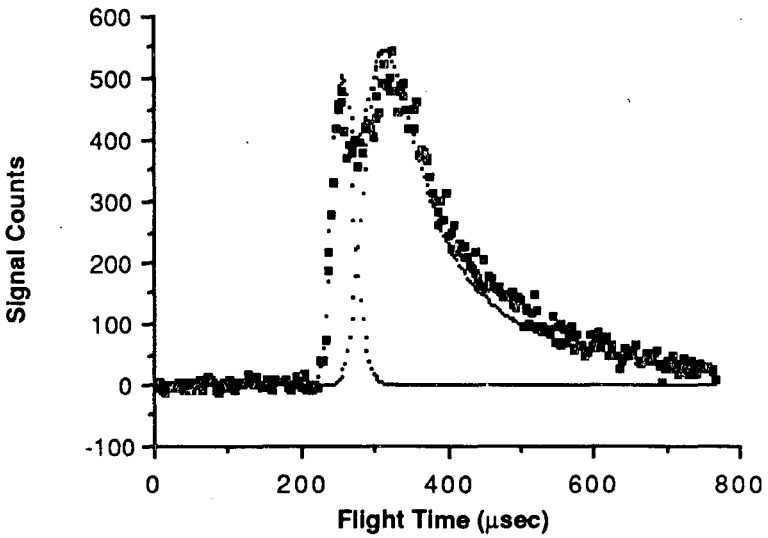
Signal Counts
600
500
400
300
200
100
0
-100
0
200
400
600
800
Flight Time (μsec)

Figure 19

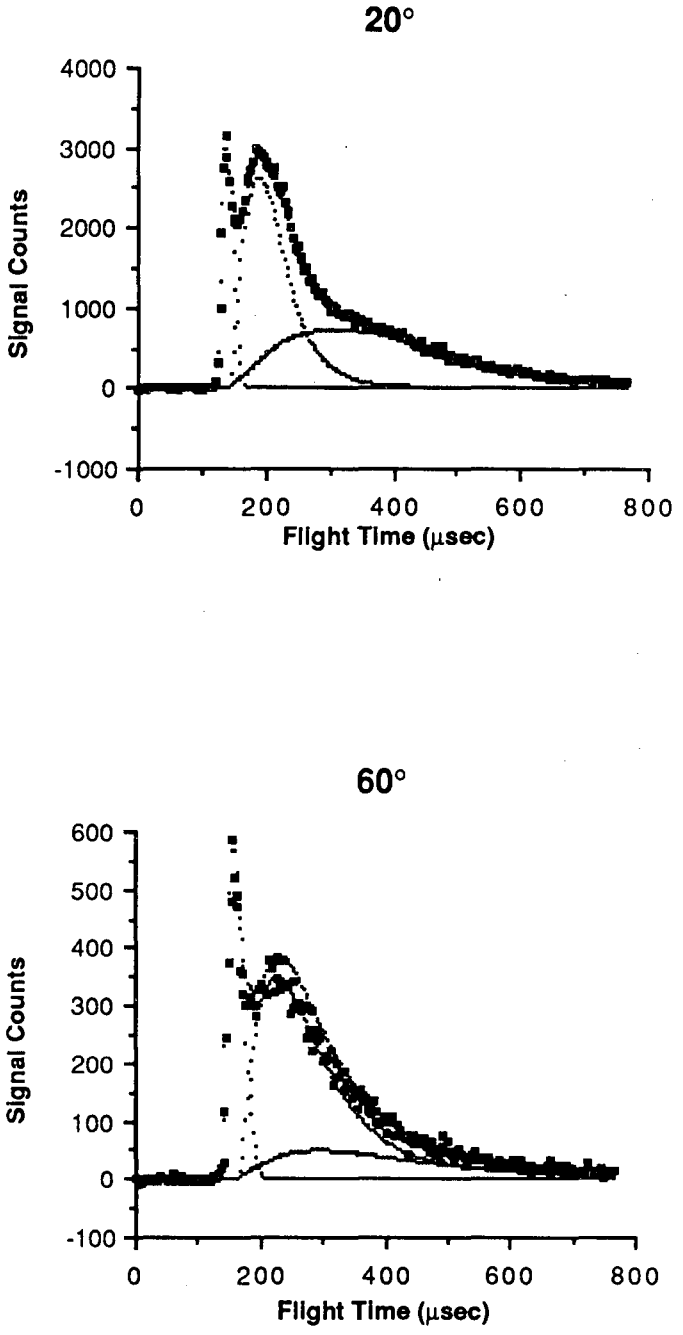
20°
4000
3000
2000
1000
0
-1000
Signal Counts
0
200
400
600
800
Flight Time (μsec)
60°
600
500
400
300
200
100
0
-100
Signal Counts
0
200
400
600
800
Flight Time (μsec)

Figure 20

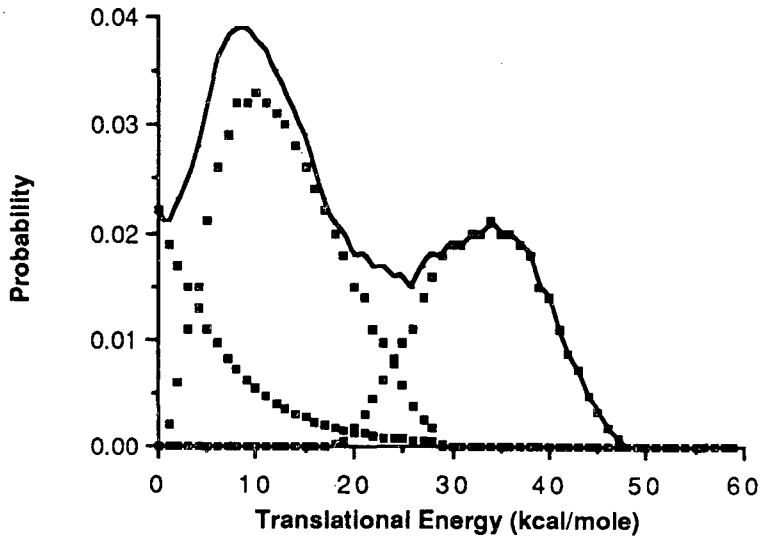
0.04
0.03
0.02
0.01
0.00
Probability
0
10
20
30
40
50
60
Translational Energy (kcal/mole)

Figure 21

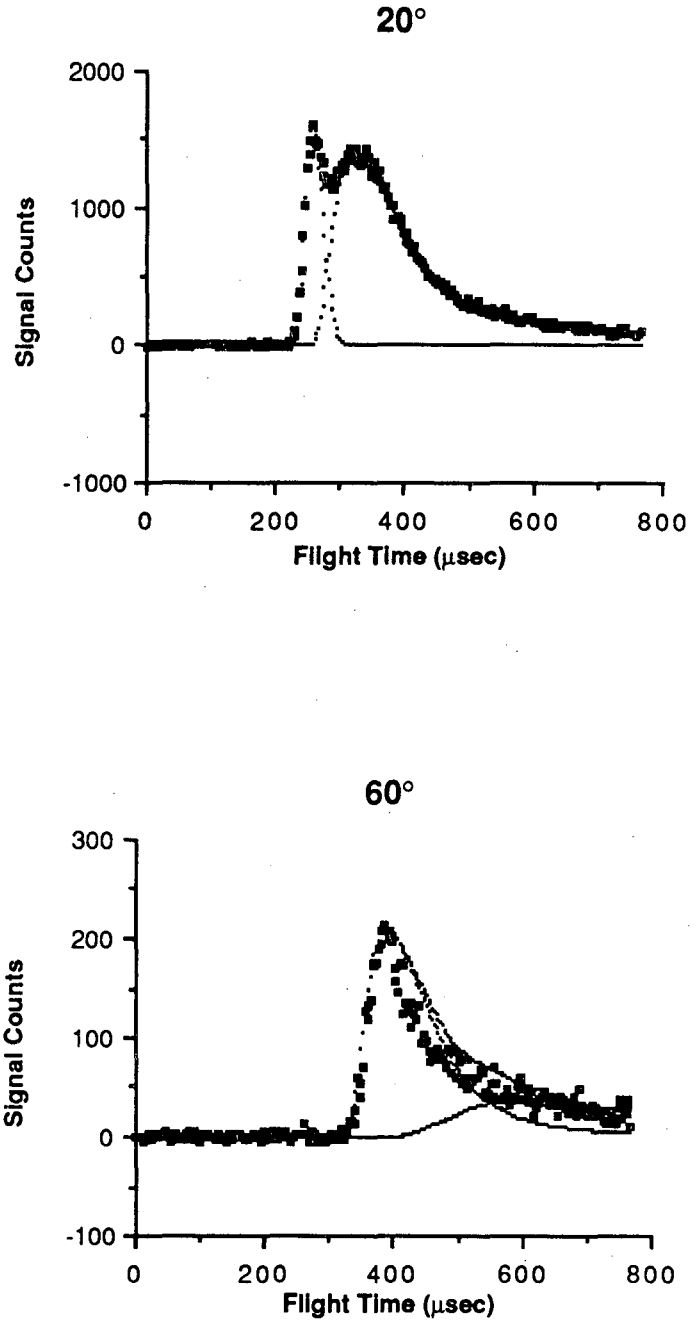
20°
2000
1000
0
-1000
Signal Counts
0
200
400
600
800
Flight Time (μsec)
60°
300
200
100
0
-100
Signal Counts
0
200
400
600
800
Flight Time (μsec)

Figure 22

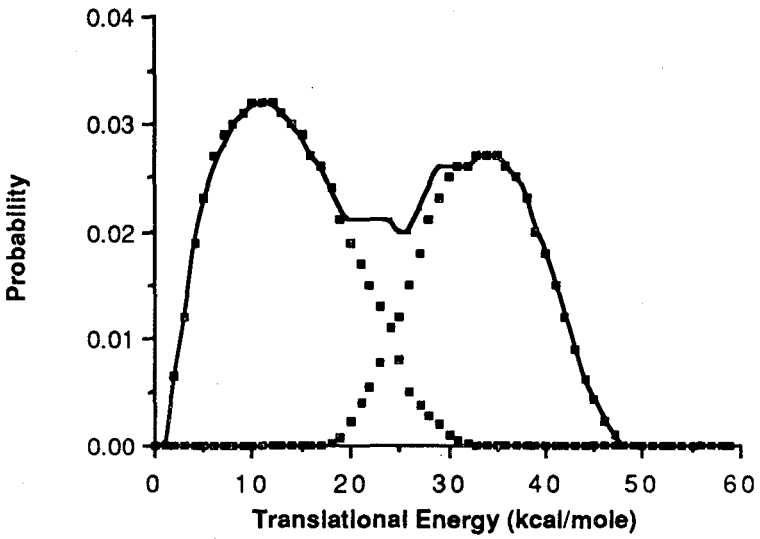
0.04
0.03
0.02
0.01
0.00
Probability
0
10
20
30
40
50
60
Translational Energy (kcal/mole)

Figure 23

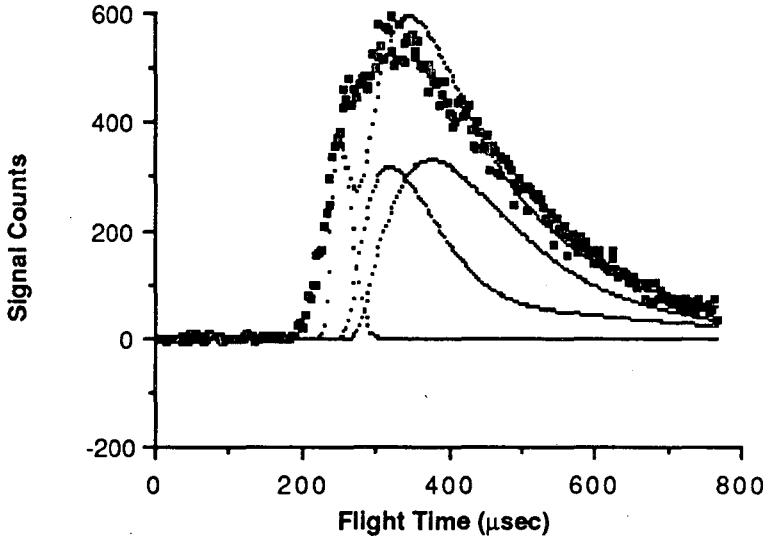
600
400
200
0
-200
Signal Counts
0
200
400
600
800
Flight Time (μsec)

Figure 24

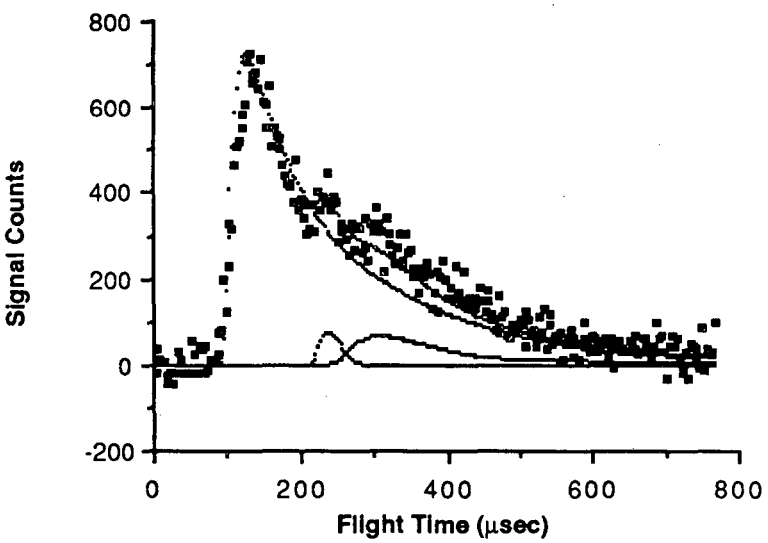
800
600
400
200
0
-200
Signal Counts
0
200
400
600
800
Flight Time (μsec)

Figure 25

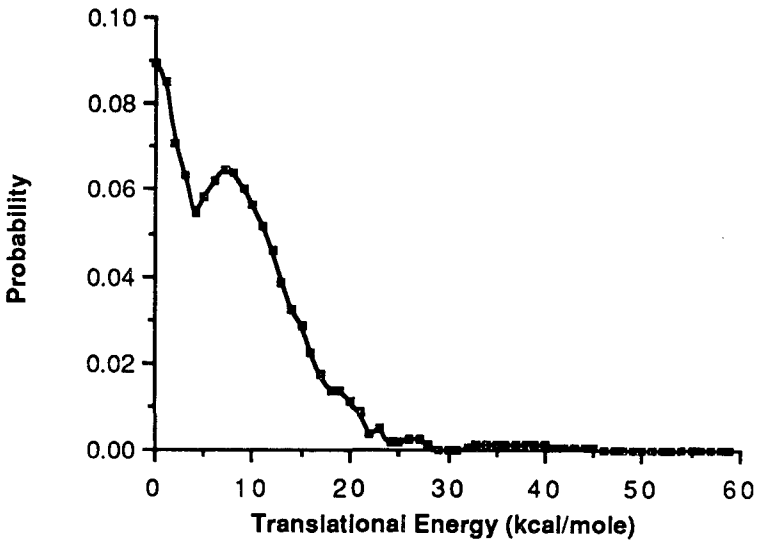
0.10
0.08
0.06
0.04
0.02
0.00
Probability
0
10
20
30
40
50
60
Translational Energy (kcal/mole)

Figure 26

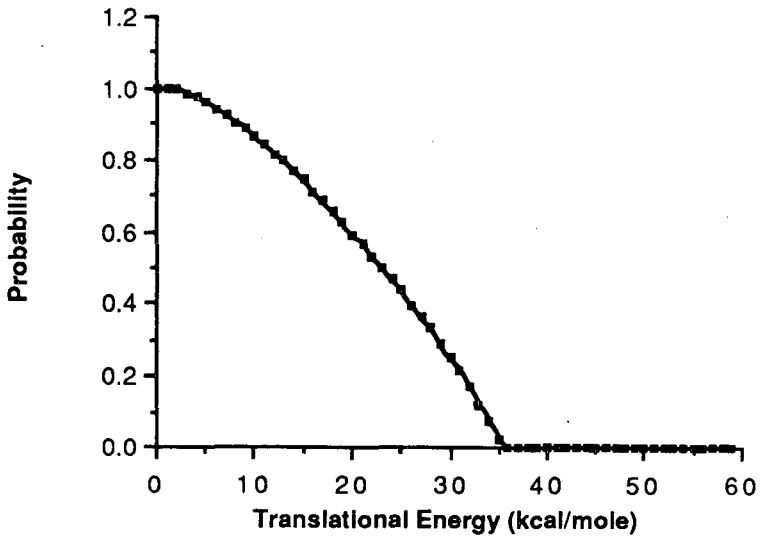
Probability
1.2
1.0
0.8
0.6
0.4
0.2
0.0
0
10
20
30
40
50
60
Translational Energy (kcal/mole)

Figure 27

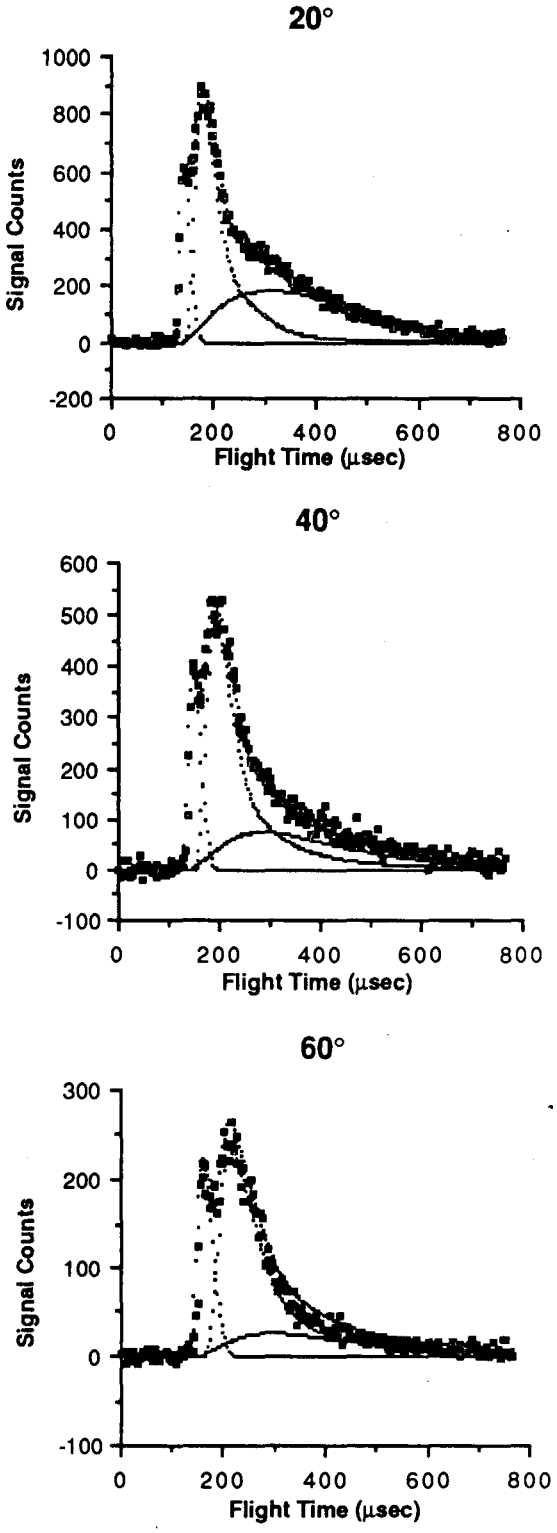
20°
Signal Counts
1000
800
600
400
200
0
-200
0
200
400
600
800
Flight Time (μsec)
40°
Signal Counts
600
500
400
300
200
100
0
-100
0
200
400
600
800
Flight Time (μsec)
60°
Signal Counts
300
200
100
0
-100
0
200
400
600
800
Flight Time (μsec)

Figure 28

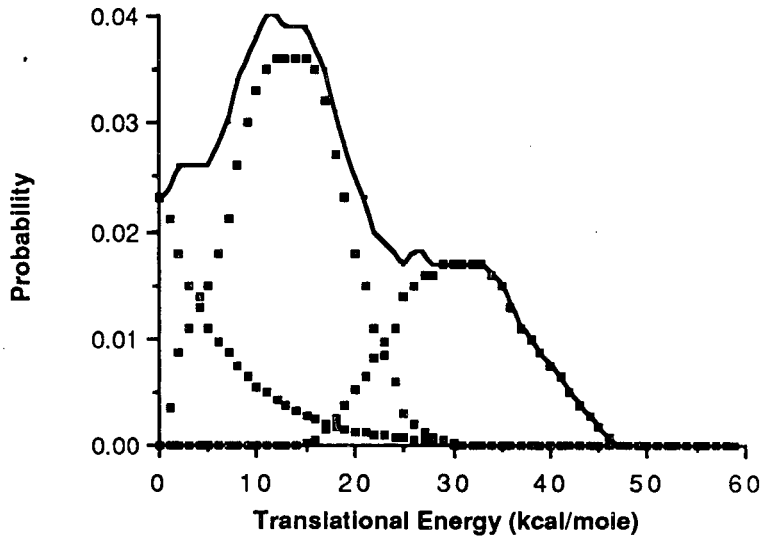
0.04
0.03
0.02
0.01
0.00
Probability
0
10
20
30
40
50
60
Translational Energy (kcal/mole)

Figure 29

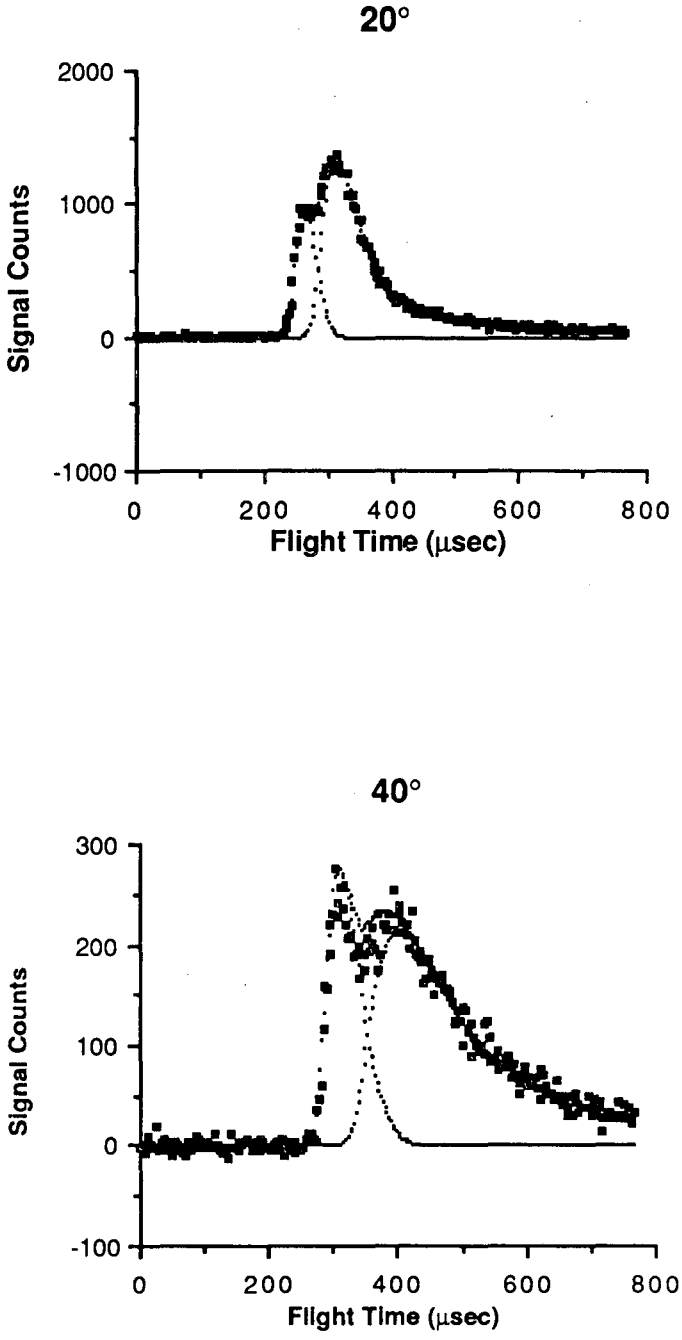
20°
2000
1000
0
-1000
Signal Counts
0
200
400
600
800
Flight Time (μsec)
40°
300
200
100
0
-100
Signal Counts
0
200
400
600
800
Flight Time (μsec)

Figure 30

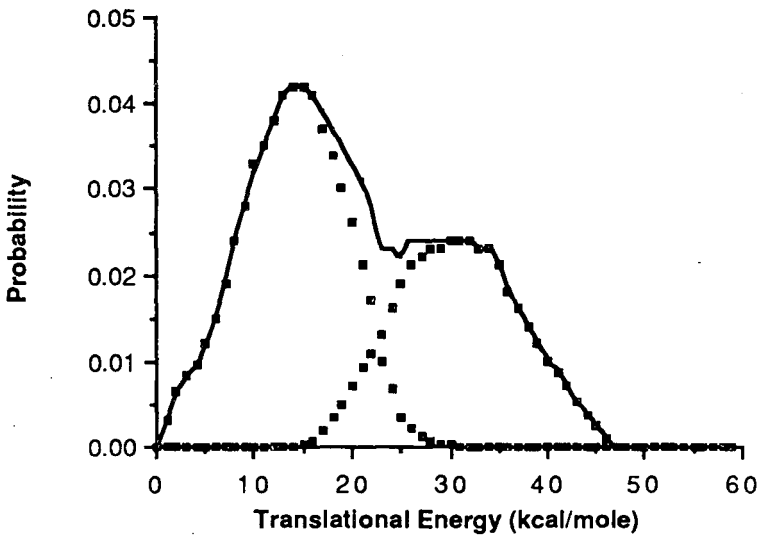
0.05
0.04
0.03
0.02
0.01
0.00
Probability
0
10
20
30
40
50
60
Translational Energy (kcal/mole)

Figure 31

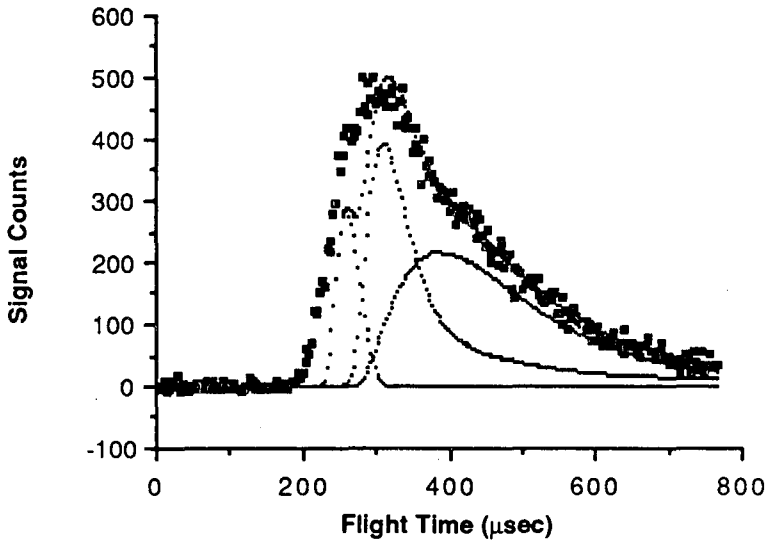
600
500
400
300
200
100
0
-100
Signal Counts
0
200
400
600
800
Flight Time (μsec)

Figure 32

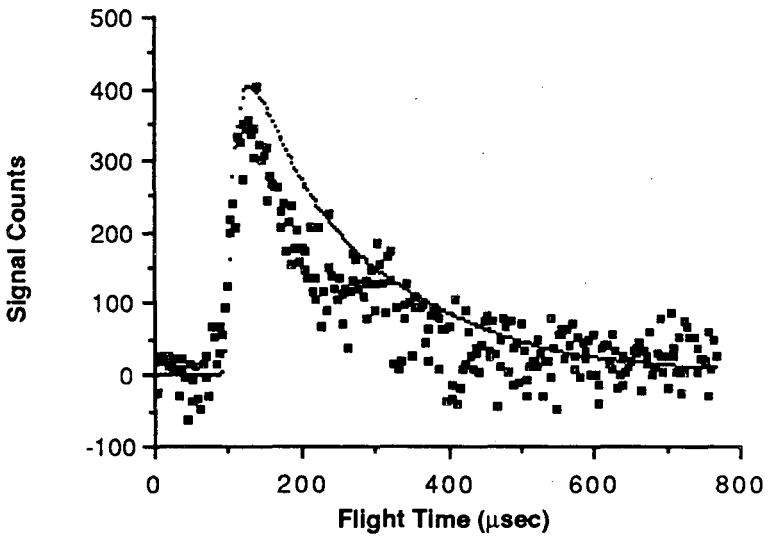
Signal Counts
500
400
300
200
100
0
-100
0
200
400
600
800
Flight Time (μsec)

Figure 33

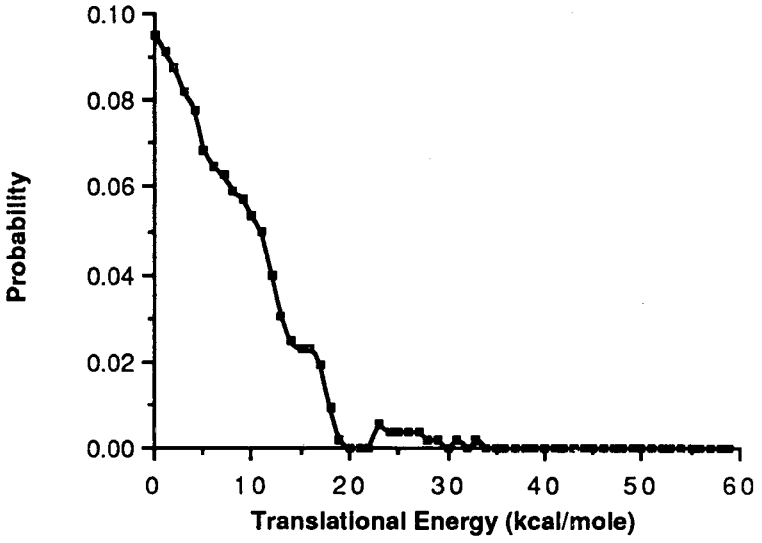
0.10
0.08
0.06
0.04
0.02
0.00
Probability
0
10
20
30
40
50
60
Translational Energy (kcal/mole)

Figure 34

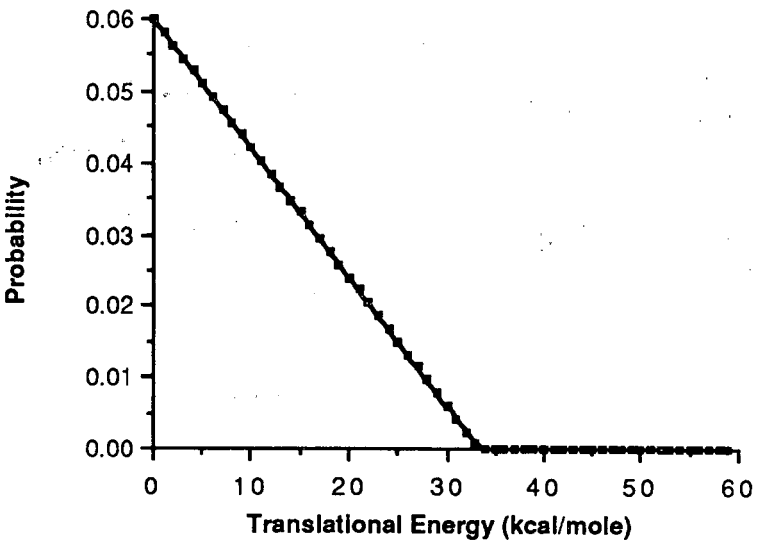
0.06
0.05
0.04
0.03
0.02
0.01
0.00
Probability
0
10
20
30
40
50
60
Translational Energy (kcal/mole)

Figure 35

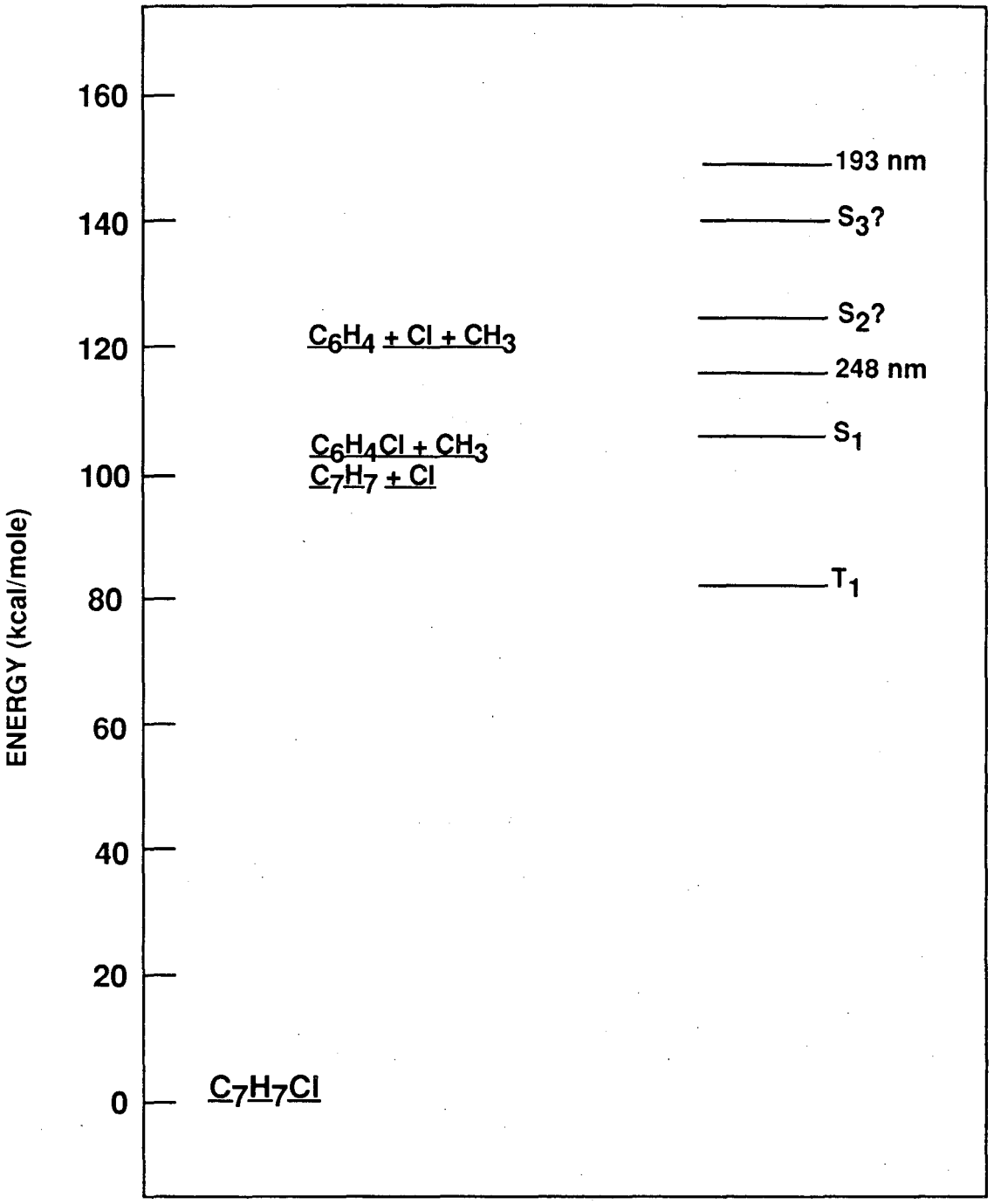
ENERGY (kcal/mole)
160
140
120
100
80
60
40
20
0
193 nm
S3?
S2?
248 nm
S1
T1
C6H4 + Cl + CH3
C6H4Cl + CH3
C7H7 + Cl
C7H7Cl

Figure 36

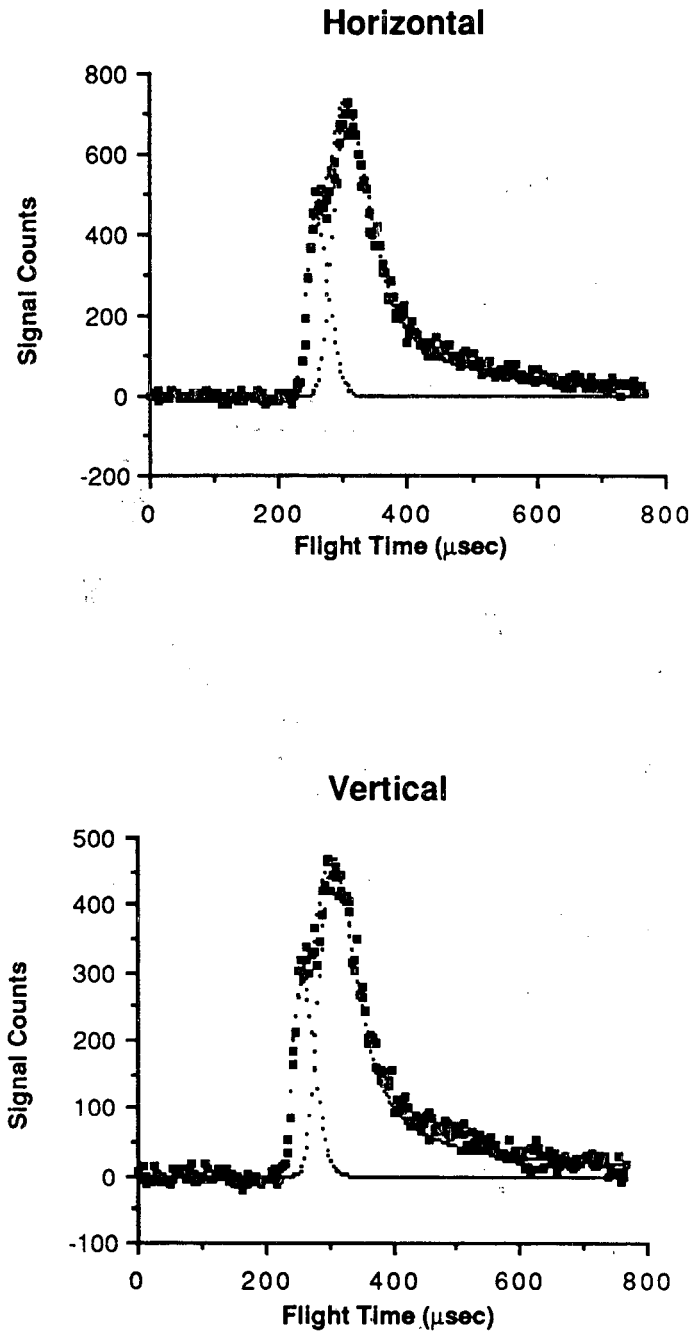
Horizontal
Signal Counts
800
600
400
200
0
-200
0
200
400
600
800
Flight Time (μsec)
Vertical
Signal Counts
500
400
300
200
100
0
-100
0
200
400
600
800
Flight Time (μsec)

Figure 37

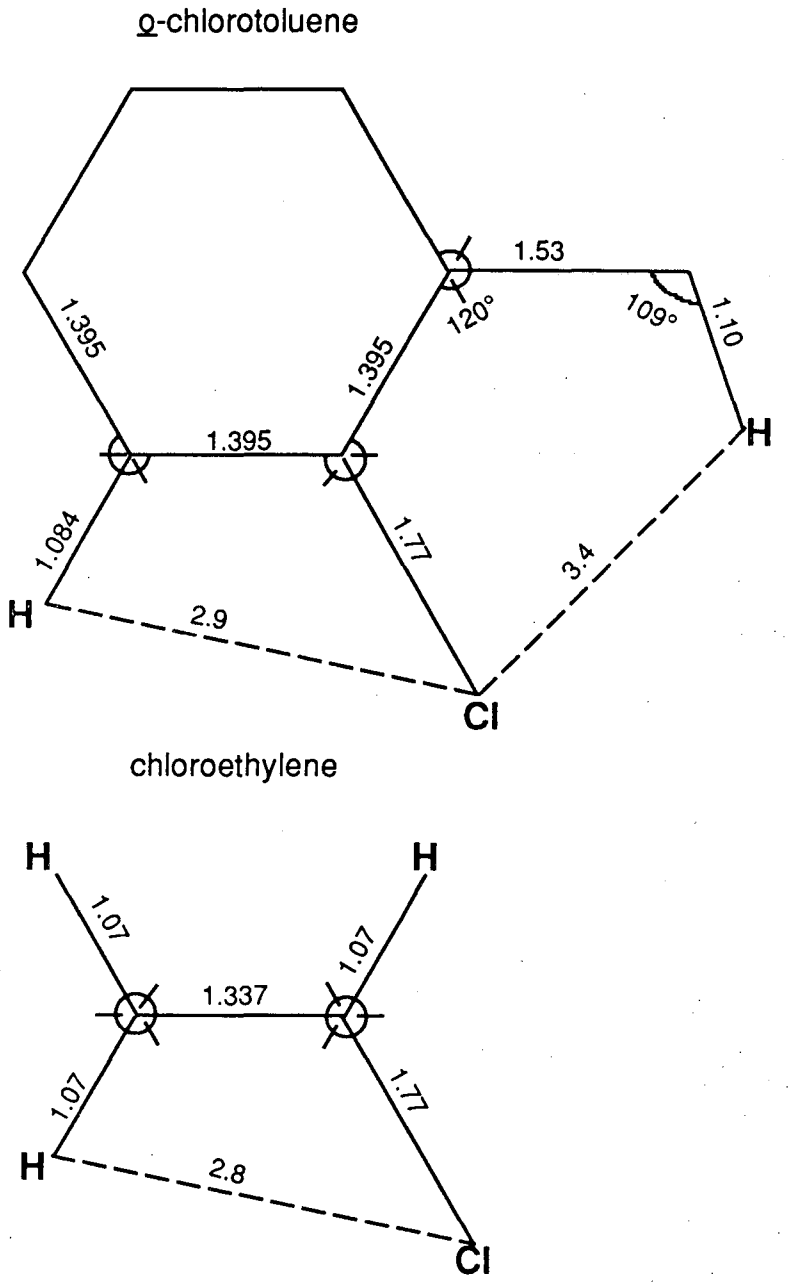
o-chlorotoluene
1.53
120°
109°
1.10
1.395
1.395
1.395
H
1.084
1.77
3.4
H
2.9
Cl
chloroethylene
H
H
1.07
1.07
1.337
1.07
1.77
H
2.8
Cl

Figure 38

CHAPTER 3
PHOTODISSOCIATION STUDIES OF THE CHLOROTOLUENES AT 248 nm

I. INTRODUCTION

In the previous chapter, photodissociation data for the chlorotoluenes at 193 nm have been presented. It was noted that the three isomers behave virtually identically at this wavelength, with identical primary and secondary dissociation channels, and similar branching ratios. Data at 248 nm were obtained to help in assigning which electronic states might be involved in the two Cl loss channels observed at 193 nm. While the 248 nm data by themselves are not sufficient to make these assignments, they are quite interesting in their own right.

The three isomers each have two primary Cl loss channels at 248 nm, but the branching ratios between these channels are different for the three isomers. These differences might be the result of the different symmetries of the molecules, as will be discussed in this chapter. Assignments of the electronic states giving rise to the two Cl loss channels are also made.

II. EXPERIMENTAL

The experimental setup was identical to that at 193 nm, with the exception of the laser wavelength and the spot size. The Lambda-Physik 103 MSC excimer laser was operated on the KrF

transition to produce the 248 nm radiation, and the beam was focussed to a 2 mm × 5 mm spot in the interaction region. Otherwise, molecular beam conditions and other experimental conditions were identical to those reported in the previous chapter.

III. RESULTS AND ANALYSIS

ortho-chlorotoluene

Time-of-flight spectra were obtained at m/e 91 and m/e 35, at 20° and 248 nm, in order to assist in the determination of which electronic states were involved in the Cl loss channels observed at 193 nm. These spectra both contain two easily identifiable TOF distributions, one narrow and fast, the other, broad and slow. These spectra are shown in Figure 1.

The fitting of the TOF data using the CMLAB2 program[1] has been described in the previous chapter. Both features in these spectra could be fit by assuming that reaction 1 is occurring, albeit with different amounts of the excess available energy in the translational degree of freedom:

$$CH_3\text{-}C_6H_4\text{-}Cl \rightarrow CH_3\text{-}C_6H_4 + Cl \qquad (1).$$

The translational energy distributions used to fit the TOF spectra taken at m/e 91 and 35, shown in Figure 2, are identical for each of these fragments, indicating that these fragments result from the same reaction channels. The fast distribution is observed to

extend to the total excess available energy of 18 kcal/mole, which means that some of the products are formed with all of the available energy in translation. These products have an average translational energy release of 10 kcal/mole. The slow P(E) peaks at 0 kcal/mole, and the average translational energy of fragments produced via this channel is 2 kcal/mole. These results are summarized in Table 1.

meta- and para-chlorotoluene

These isomers are virtually identical to the ortho compound in their dissociation behavior at 248 nm. Again, only two channels are observed, both yielding Cl atom and tolyl or benzyl radical, CH_3-C_6H_4, according to reaction (1). The TOF spectra, taken at m/e 35 and 91, and at 20° for the meta isomer, together with the P(E)s used to fit them are found in Figures 3 and 4. The TOF spectra and P(E)s for the para compound are shown in Figures 5 and 6. The average translational energy released is found in Table 1, and is summarized briefly here: fast primary Cl loss channel: m-CT, 9 kcal/mole, p-CT, 11 kcal/mole; slow primary Cl loss channel: m-CT, 2 kcal/mole, p-CT, 2 kcal/mole.

Branching ratio calculations

What is unusual about these TOF spectra at 248 nm is that the branching ratios for dissociation via the two channels are so different for the three compounds. These branching ratios are given in Table 1. They were calculated from the Cl TOF data using the following

simplified version[2] of the expression for the branching ratio described by Krajnovich[3]:

$$R(T_1/S_0) =$$

$$[N'(T_1)/N'(S_0)] \times [(\int_o^\infty P_{So}(E_T)\ (v_{So}/u_{So})\ dv_{So})/(\int_o^\infty P_{T1}(E_T)\ (v_T/u_T)\ dv_T)],$$

where N' is the total number of detected ion counts at mass 35, 20° from either the channel designated T_1 or S_0, as will be discussed next, and the integrals are the calculated signal, evaluated numerically by the CMLAB2 program[1].

IV. DISCUSSION

fast primary dissociation to yield Cl and m/e 91

As at 193 nm, it is most reasonable to assume that the two primary dissociation channels observed are the result of dissociation on two different electronic surfaces. Fortunately, more is known about the spectroscopy of these molecules in this region of the optical spectrum[4], and as the number of states from which the molecules can dissociate is limited to three, one can perhaps assign the states responsible.

At 248 nm, the available excess energy, as previously defined, is 19 kcal/mole. All three molecules have some products with the total available energy in translation. The three isomers have

slightly different fast P(E)s, as will be discussed later, and a slightly different average translational energy release in this channel.

The three isomers, ortho, meta, and para, are excited to 3530.8 cm^{-1}, 3732.8 cm^{-1}, and 4038.1 cm^{-1} respectively above their S_1 origins at 248 nm[4]. The fluorescence quantum yields at this wavelength are negligibly small, and it has been shown that the non-radiative lifetimes of the three molecules at this level of excitation are virtually the same. Even at 2000 cm^{-1} excess energy, the non-radiative lifetimes of the three molecules have already converged to a value of 1 ns. It is also known that these molecules undergo rapid intersystem crossing to T_1, within ca. 1 ns.[5].

Based on the above observations, the fast channel can be assigned to dissociation from either S_1 or T_1, or perhaps, from both. At 248 nm, there is just enough energy to allow dissociation from S_1, but it is also known that ISC to T_1 proceeds rapidly. Thus, the fast channel is assigned to dissociation largely from T_1, but one must remember that dissociation from S_1 is energetically allowed so that some of the fastest product may result from this electronic state.

slow primary channel yielding Cl and m/e 91

If dissociation were only to occur from S_1 to give the fast products, the slower channel could result from dissociation by triplet state molecules or ground state molecules. On the other hand, if dissociation from T_1 is responsible for most of the faster products, then only ground state molecules can give the slow products. The average translational energy released is quite small, 2 kcal/mole, for

each of the molecules. The TOF spectra of all three molecules are fit using the same "Boltzmann" $P(E_T)$, a $P(E_T)$ of the form $E_T^{1/2}\exp(-E_T/E)$, where in this case, E equals 2 kcal/mole. This P(E) peaks at zero kcal/mole translational energy, implying that disssociation is occurring from the ground state. Together with the evidence assigning T_1 to the fast channel, the second dissociation channel is identified as coming from the ground state. RRKM calculations to model ground state dissociation are underway, and will allow us to confirm our assignment of the electronic state which gives rise to the slow TOF distribution. Next, one should address what is the most likely pathway the molecule takes to reach the ground state. Because of the large energy gap between the electronic origins of the first excited triplet and ground states[6], ISC is expected to occur more slowly[7], but this is still a more likely process than internal conversion (IC) from S_1. The branching ratio differences observed between the three molecules will be discussed next.

branching ratio differences at 248 nm

At this level of excitation, it is known that the three molecules will have similar non-radiative lifetimes. However, the TOF spectra indicate that the amount of products coming from dissociation of the S_1 andT_1 states versus the amount of products coming from dissociation of the S_0 state is different among the three isomers. That is to say, the TOF spectra are measuring the relative amounts of dissociation from S_1 and T_1, and from S_0, and from this it can be said that the relative rates of dissociation from S_1 and T_1, and ISC to S_0

are being measured. Figure 7 provides a graphic description of the competing dissociation pathways. A measure of the non-radiative lifetime from fluorescence studies cannot distinguish among the various processes taking place.

What can give rise to these observed differences in the relative rates of dissociation and electronic relaxation among the three isomers? The major difference between the three isomers is their symmetry. The ortho and meta isomers are of low symmetry, belonging to the C_S class. The para isomer has higher symmetry, belonging to the class C_{2V}. How the symmetry of the molecules can affect the branching ratios as observed will be discussed next.

molecular symmetries and T_1/S_0 branching ratios

A large body of theory has been developed[7] to address the interesting phenomenon of electronic relaxation and non-radiative transitions generally. In principle, if the Franck-Condon factors and energy gaps between the states involved in the non-radiative transition are known, then the relative rates of non-radiative transitions may be calculated. In practice, however, the Franck-Condon factors are not known for molecules with negligible fluorescence yields like the chlorotoluenes.

The results of several experiments have been attributed to symmetry effects[8], but again, most of these involve measurements of non-radiative lifetimes from fluorescence data, rather than measurements of the rates of the "non-radiative" processes individually, e.g., dissociation and intersystem crossing. One study on

chlorotoluenes did seek to determine photodissociation and triplet quantum yields following excitation in the range of 250 nm to 280 nm[6], and dissociation rates were estimated from these data. It was concluded that the triplet state was responsible for some of the dissociation products, but further ISC to the ground state with subsequent dissociation could not be ruled out. This study also revealed that when excited to the 0-0 level in S1, o-CT dissociates somewhat faster than m-CT which, in turn, dissociates somewhat faster than p-CT following ISC to T_1. These differences were ascribed to the different symmetries of the molecules. It should also be pointed out that the 0-0 levels of the three molecules are at 271.5 nm for o-CT, 273.0 nm for m-CT, and 275.5 nm for p-CT. The small differences in dissociation rates could be merely the result of the slight excess of available energy from the different 0-0 energies. These slight excesses would not be very important in the dissociation of ground state molecules but might prove important in dissociation on the triplet surface and the excited singlet surface, with their relatively fewer vibrational levels.

The different Franck-Condon factors which result from the different shapes of these molecules can probably account for some differences in rates of electronic relaxation, ISC in this case. However, the rate is largely determined by the spin-orbit coupling of the Cl substituent alone[9].

Differences in the dissociation yields from two different electronic states have been observed. Since ISC rates are largely determined by the heavy atom substituent, let us assume that the T1 to So ISC rates are similar. Then, since the amounts of energy

available to each isomer are slightly different, it would seem that perhaps the differences in branching ratios can be ascribed to differences in the rate of dissociation from the upper electronic states. Our observations are consistent with the studies that estimated dissociation rate constants for the chlorotoluenes: the largest amount of dissociation from the triplet state occurs for o-CT, which has the largest triplet dissociation rate constant[5], and the smallest amount of dissociation from the triplet state occurs for p-CT, which has the smallest triplet dissociation rate constant. It certainly suggests that photodissociation experiments should be performed on other "families" of isomers, especially the isomers of difluorobenzene where fluorescence studies already indicate differences in the rates of non-radiative transitions[8]. All of the dihalobenzenes are attractive candidates because of their intersystem crossing abilities One could perhaps "tune" the ISC rate by using mixed dihalobenzenes, e.g. C_6H_4ClF, which should have a faster ISC rate than the chlorotoluenes, and in which the C-Cl bond is still weaker than the other C-X (X = halogen) bond, and thus will break preferentially. Then, the branching ratios obtained for these isomers could be compared with those obtained for the chlorotoluenes.

Finally, one must discuss the observed differences in the fast P(E)s used to fit these data. This is most likely due to the fact that the exit impact parameters (b) for dissociation are different. For the para isomer, b is 0; therefore, no rotational excitation of the departing fragments occurs, and energy is only partitioned between translational and vibrational degrees of freedom. By virtue of their geometry, the exit impact parameters for the ortho and meta isomers

are identical: 0.44 angstrom. A rigid radical impulsive model[10] of the dissociation process predicts that the amount of energy partitioned to translation, $E_{trans}/E_{available}$, is a function of b, namely $[1 + \mu b^2/I]^{-1}$, where μ is the reduced mass for the dissociation products, b is the exit impact parameter, and I is the moment of inertia about the axis perpendicular to the molecular plane. The quantities μ and I are 25.278 a.m.u. and 259.541 a.m.u.A^2, respectively. These are derived from the equilibrium structures of the molecules. For ortho and meta-chlorotoluene, the model predicts that 98% of the available energy appears in translation. This says that the ortho and meta isomers should have at most 18.6 kcal/mole in translation, versus 19 kcal/mole in translation for the para isomer, excluding the internal energy of the parent molecules. Such a small difference in the translational energies is beyond the resolution of these experiments. What is actually observed is that the ortho and para isomers apparently have products with translational energies slightly greater than the available energy as defined, 20 kcal/mole and 22 kcal/mole, respectively. As beam conditions were virtually identical for the three isomers, it is not possible to attribute the few extra kcals/mole to differences in the internal energies of the parent molecules. Such small shifts in the leading edge of the spectra may be the result of other experimental parameters, such as the ion flight time constant which is strongly affected by any fluctuations in the "doorknob" ion target voltage. However, it does appear that the three isomers yield products with all of the available energy in translation, so that the rigid radical model is probably appropriate here.

V. CONCLUSION

Photodissociation of the chlorotoluenes at 248 nm reveals that two dissociation pathways, both involving loss of the Cl atom, exist. These two channels have been assigned to dissociation from the T_1 state, and dissociation from the S_0 state, following intersystem crossing. It is known that the molecules are excited to approximately 3000 to 4000 cm-1 above the S_1 origin at 248 nm, and undergo rapid intersystem crossing to T_1 before dissociating. The average translational energy released is the same for each of the isomers, 9 kcal/mole for the triplet dissociation, and 2 kcal/mole for the ground state dissociation. However, the branching ratios for dissociation via these two channels are different for the three isomers: o-CT, T_1/S_0 = 3.3; m-CT, T_1/S_0 = 1.4; p-CT, T_1/S_0 = 0.3. The branching ratio differences are interpreted as being differences between the relative rates of dissociation from T_1, and intersystem crossing to and/or dissociation from S_0, and may result from the different shapes, and hence symmetries, of the molecules.

REFERENCES

1. X. Zhao, Ph. D. Thesis, University of California, Berkeley, 1988.

2. See Chapter 2, Results and Analysis.

3. D. Krajnovich, F. Huisken, Z. Zhang, Y. R. Shen, and Y. T. Lee, J. Chem. Phys., 77, 5977 (1982); D. Krajnovich, Ph.D. Thesis, University of California, Berkeley, 1983.

4. S. Nath Singh, R. Ammini Amma, S. N. Singh, Indian J. Pure Appl. Phys., 7, 768 (1969); A. Shimoda, T. Hikida, T. Ichimura, and Y. Mori, Chem. Lett., 265 (1979).

5. T. Ichimura, K. Nahara, R. Motoshige, and Y. Mori, Chem. Phys., 96, 453 (1985).

6. T. Ichimura, K. Nahara, Y. Mori, M. Sumitani, and K. Yoshihara, Chem. Phys., 95, 9 (1985).

7. D. F. Heller, K. F. Freed, and W. M. Gelbart, J. Chem. Phys., 56, 2309 (1972); C.-S. Huang and E. C. Lim, J. Chem. Phys., 62, 3826 (1975).

8. C. Guttman and S. A. Rice, J. Chem. Phys., 61, 661 (1974); L. J. Volk and E. K. C. Lee, J. Chem. Phys., 67, 236 (1977); A. Shimoda, T. Hikida, and Y. Mori, J. Phys. Chem., 83, 1309 (1979).

9. D. S. McClure, J. Chem. Phys., 20, 682 (1952).

10. S. Riley and K. R. Wilson, Discuss. Faraday Soc., 53, 132 (1972); L. J. Butler, Ph. D. Thesis, University of California, Berkeley, 1985.

TABLE 1

	ortho	meta	para
fast $\langle E_{trans} \rangle$ (kcal/mole)	10	9	11
slow $\langle E_{trans} \rangle$ (kcal/mole)	2	2	2
branching ratios (T_1/S_o)	3.3	1.4	0.3

Figure 1: o-CT TOF spectra, monitored at m/e 35 and 91, respectively, 20°, 248 nm, with CMLAB2 simulations.

Figure 2: Appropriately weighted translational energy distributions, P(E)s, used to fit the TOF spectra in Figure 1.

Figure 3: m-CT TOF spectra, monitored at m/e 35 and 91, 20°, 248 nm, with CMLAB2 simulations.

Figure 4: Appropriately weighted P(E)s used to fit the TOF spectra in Figure 3.

Figure 5: p-CT TOF spectra, monitored at m/e 35 and 91, 20°, 248 nm, with CMLAB2 simulations.

Figure 6: Appropriately weighted P(E)s used to fit the TOF spectra in Figure 5.

Figure 7: Schematic of the competing dissociation channels which give rise to the two observed TOF distributions in the case of each isomer.

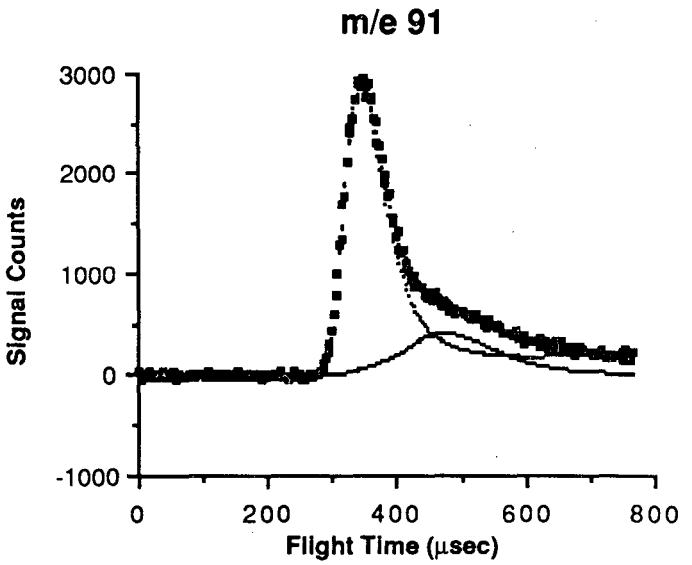
m/e 91
3000
2000
1000
0
-1000
Signal Counts
0
200
400
600
800
Flight Time (μsec)

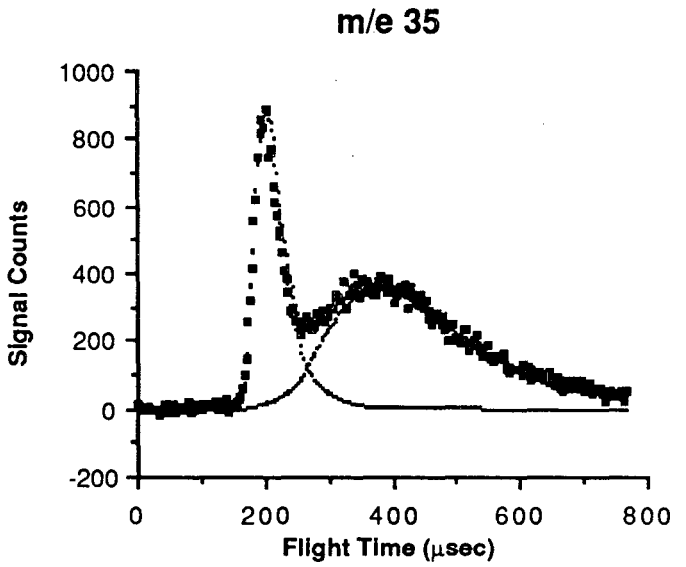
m/e 35
1000
800
600
400
200
0
-200
Signal Counts
0
200
400
600
800
Flight Time (μsec)

Figure 1

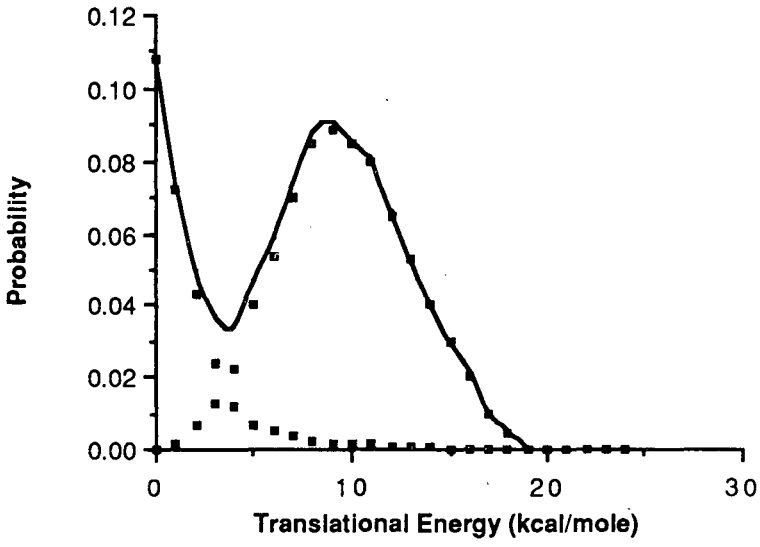
0.12
0.10
0.08
0.06
0.04
0.02
0.00
Probability
0
10
20
30
Translational Energy (kcal/mole)

Figure 2

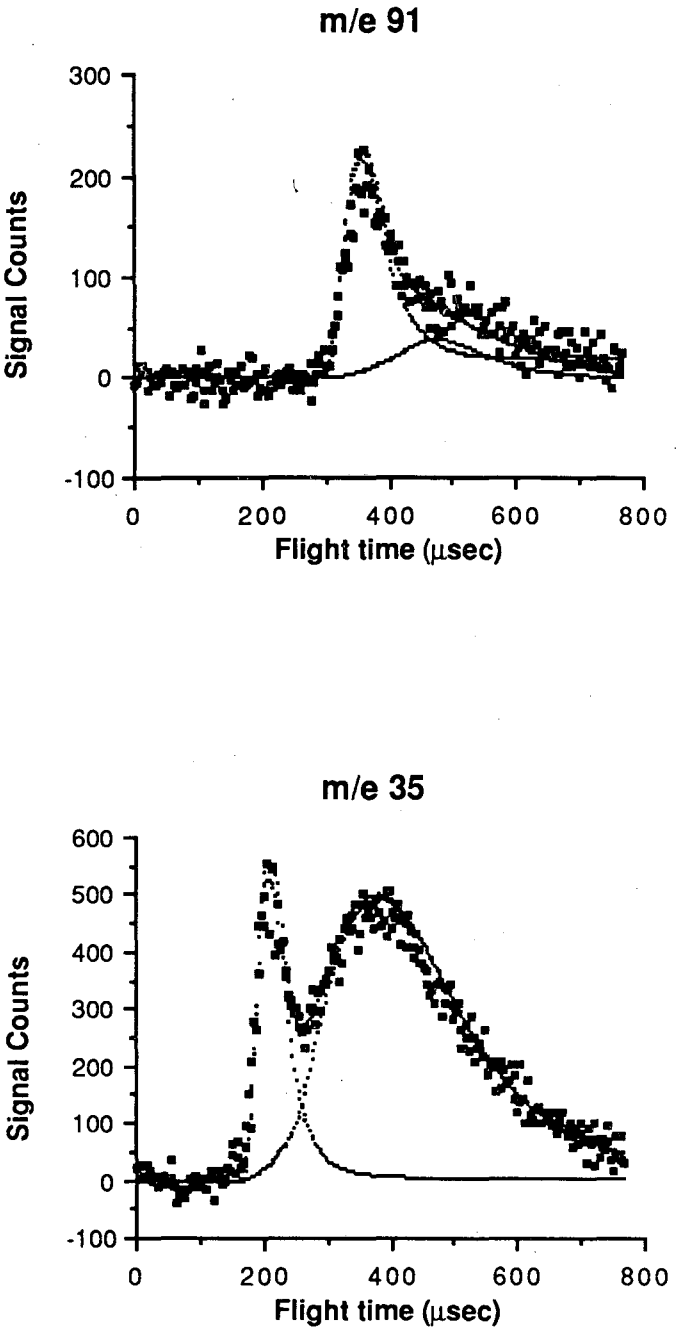
m/e 91
Signal Counts
300
200
100
0
-100
0
200
400
600
800
Flight time (μsec)
m/e 35
Signal Counts
600
500
400
300
200
100
0
-100
0
200
400
600
800
Flight time (μsec)

Figure 3

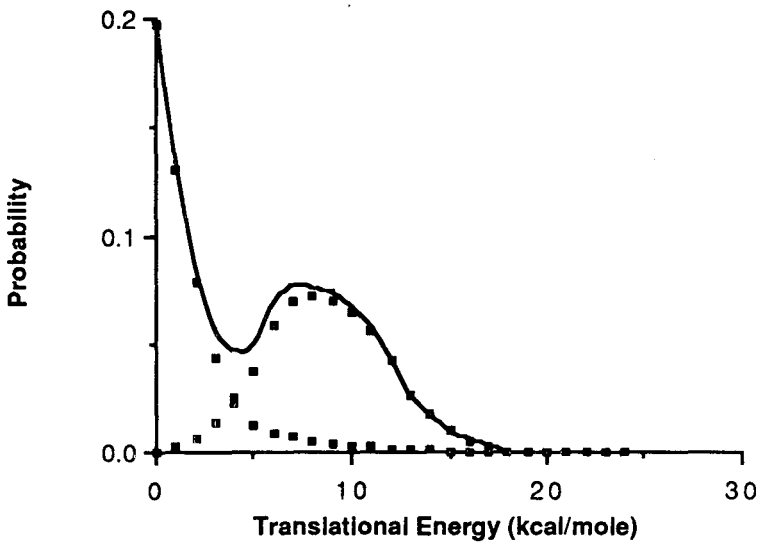
0.2
0.1
0.0
Probability
0
10
20
30
Translational Energy (kcal/mole)

Figure 4

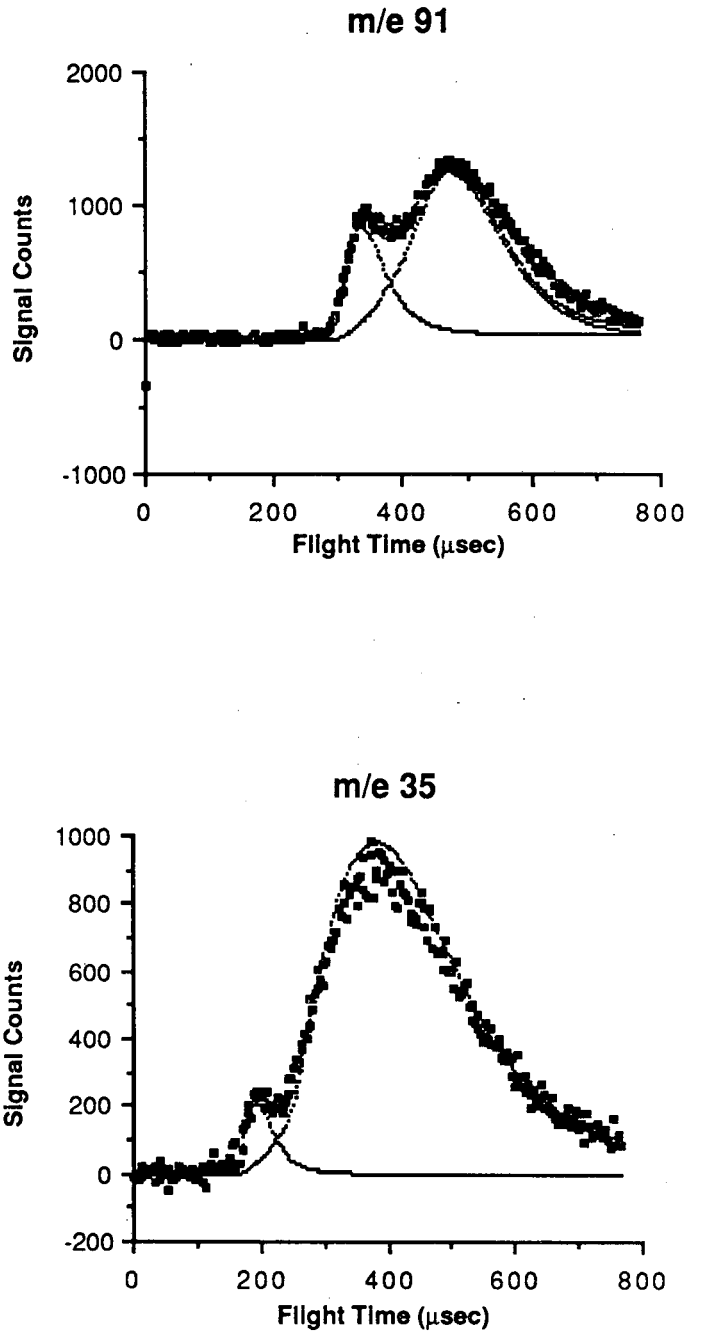
m/e 91
2000
1000
0
-1000
Signal Counts
0
200
400
600
800
Flight Time (μsec)
m/e 35
1000
800
600
400
200
0
-200
Signal Counts
0
200
400
600
800
Flight Time (μsec)

Figure 5

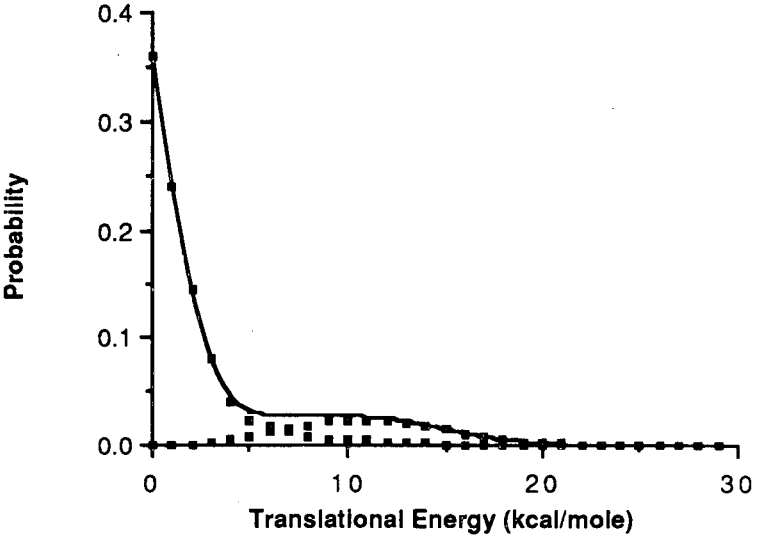
0.4
0.3
0.2
0.1
0.0
Probability
0
10
20
30
Translational Energy (kcal/mole)

Figure 6

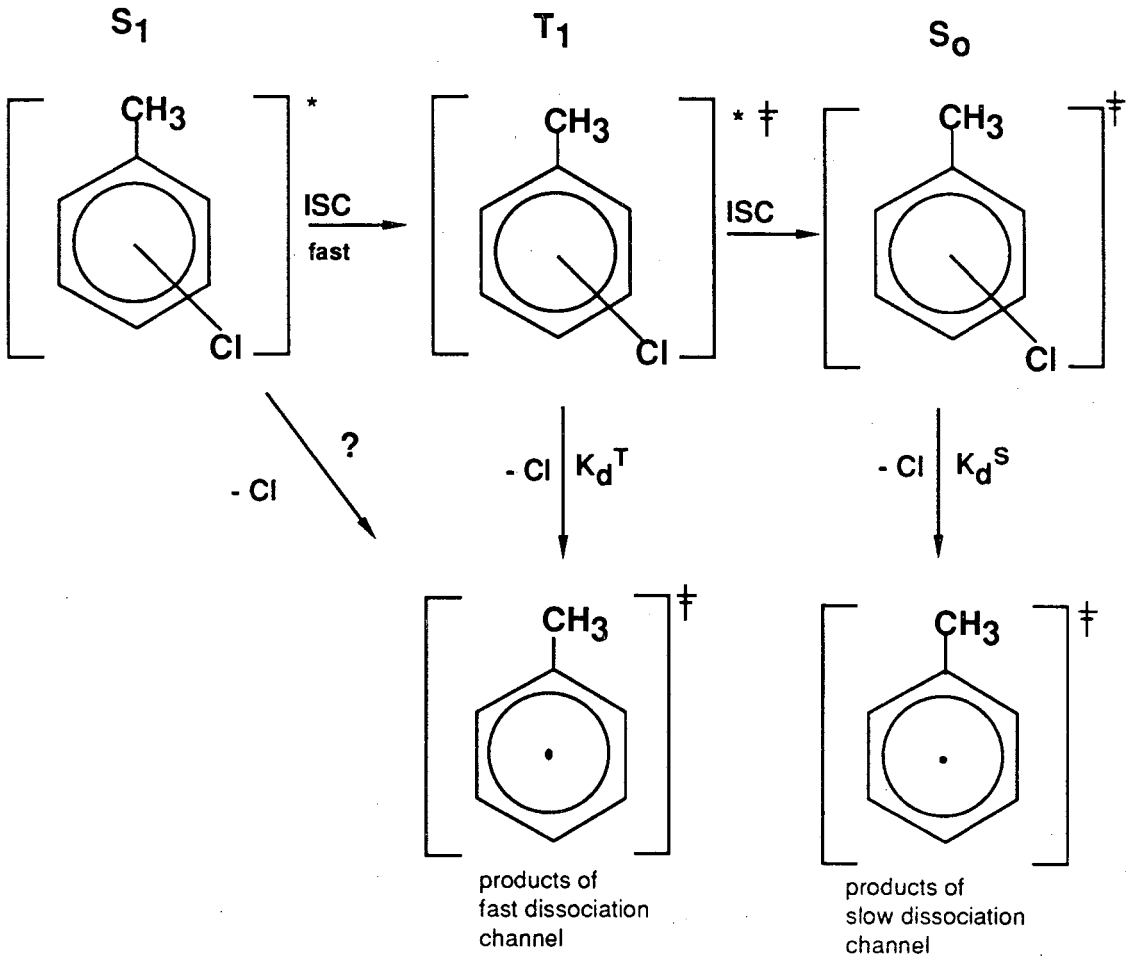
S1
T1
So
CH3
Cl
*
ISC
fast
* ‡
ISC
‡
?
- Cl
- Cl
K_d^T
- Cl
K_d^S
products of
fast dissociation
channel
products of
slow dissociation
channel

Figure 7

CHAPTER 4

1 + 1, VUV + UV, RESONANT IONIZATION OF Cl ATOM

I. INTRODUCTION

Resonantly enhanced multiphoton ionization (REMPI) is a highly sensitive and selective method of detecting molecules and atoms[1]. Detection limits as low as a single atom have been reported[2]. In our case, we were interested in detecting chlorine, hydrogen and bromine atoms resulting from secondary dissociation and overtone induced dissociation of such species as 2-chloroethyl radical[3], and 2-bromo-2,2-difluoroethyl radical[4]. Because of the difficulty in making large amounts of such radical species for investigation, and thus, in making the atoms to be detected, a sensitive technique such as REMPI is attractive.

Two photon resonances sufficiently close to the ionization threshold for the Br atom fall into the wavelength range easily accessible to the doubled output of a dye laser[5]. The same transitions for the Cl atom appear at somewhat shorter wavelengths, where mixing of the output of a doubled dye laser with the fundamental of a Nd:YAG laser would be necessary[6] to attain sufficient laser power. Strong single photon resonances close enough to the ionization theshold occur in the vacuum ultraviolet (VUV) for these halogen atoms, and for the hydrogen atom. In general, it appears that despite the lesser amount of laser power available in the VUV[7], the enhanced cross section for a one-photon versus a two-photon transition[8] warrants using a resonant ionization scheme in

which the first photon is in the VUV, and the second photon is energetic enough to ionize the electronically excited atom. Figure 1 depicts the important energy levels in the Cl atom, and the laser energies used to ionize the atom in our experiment.

The two simplest means by which VUV light of the desired frequency could be generated both rely on four-wave mixing in rare gases[7]. In the first method, to be described in this chapter, light at 118.877 nm, for exciting the single photon transition in Cl atom, was generated by tripling light at 356.6 nm in Xe. In the second method[8], currently being utilized, light at 594.4 nm and 297.2 nm is mixed in Kr to produce the desired 118.877 nm radiation. In the first case, residual UV radiation at 356.6 nm is sufficient to ionize the excited atoms, while in the second case, the residual 297.2 nm light ionizes the atoms.

The molecular beam apparatus used in these experiments was originally designed and constructed by Dr. Timothy K. Minton (TKM), and later modified. It is described in detail in the experimental section.

II. EXPERIMENTAL

The MPI Machine

The MPI machine, shown schematically in Figure 2, consists of a single source region where the sample molecule is introduced into the machine and a molecular beam is formed, a main chamber region where the molecular beam may be intersected at right angles by

laser beams during the course of an experiment, a time-of-flight (TOF) tube open to the main chamber region when ion products are to be detected, and a beam catcher region where the molecular beam is pumped away after leaving the main chamber.

Originally, the source was configured to produce a continuous molecular beam. The sample molecule, typically seeded in a rare gas carrier at a total pressure of 100 to 150 torr (13.3 to 20.0 kPa), is introduced through a 5 mil (.127 mm) nozzle and the resulting molecular beam is skimmed 0.22 inches (.559 cm) downstream by a 20mil (.508 mm) electroform skimmer. The tip of the nozzle can be heated up to several hundred degrees Celsius using thermal coaxial heating cable and a Variac. An iron-constantan thermocouple is used to measure the nozzle temperature. The sample inlet tube may also be heated when using low vapor pressure liquid samples or solid samples. The nozzle is at the end of a stainless steel inlet tube and is surrounded by a stainless cage which keys into the narrow end of a 14" reducer flange. The skimmer then fits neatly into the reducer flange and is bolted to the reducer and the nozzle cage. The background pressure in the source region is maintained at 10^{-4} torr ($\approx 10^{-2}$ Pa) by a water trapped 10" diffusion pump (Varian M10, 2200 l/s).

In TKM's original assembly, the reducer flange is separated from the main chamber housing by a 1" spacer. This is to prevent the reducer from approaching too closely to the ion optics which are located in the main chamber, directly below the time-of-flight tube. Thus the molecular beam is intersected by the laser beams 3.32 inches (8.43 cm) downstream from the nozzle. In 1987, the foreline

for the source was redesigned and a 0.5 inch spacer replaced the original 1" spacer. Now the intersection point between laser beams and the molecular beam is 2.81 inches (7.14 cm) downstream from the nozzle. This decreases the molecular beam diameter in the interaction region from approximately 0.30 inch (0.76 cm) to 0.26 inch (0.66 cm), based on a simple geometric calculation.

The main chamber region contains the ion optics which send ions produced by the laser beams up the time-of-flight (TOF) tube toward the detector. The detector will be described shortly. The ion optics, shown in Figure 3, were designed by Dr. Carl C. Hayden based on the ideas of Wiley and McLaren[9]. The assembly, from top to bottom, consists of the following electrostatic lenses: left and right beam steerers, front and rear top einzel lenses, a middle einzel lens, a bottom einzel lens, an accelerator lens, an extractor lens, the top and bottom plates which span the region where the ions are produced, referred to as the ion region lenses, and a spacer ring. The bottom ion region lens was originally used to mount an electron gun for electron impact ionization. However, the spacer ring was modified by TKM so that an electron gun was not required. The spacer now has two holes drilled through its sides to allow one to send a laser beam through the spacer, perpendicular to, but well below the molecular beam. In the center of the spacer ring, a small metal plate is mounted at a 45° angle with respect to the laser beam. By focussing a laser onto the metal plate, and by applying appropriate bias voltages to the plate and to the bottom ion region lens, photoelectrons are produced and sent through a 3/8" hole in the lens to ionize molecules in the beam. This photoelectron source was

used in the initial molecular beam diagnostics and in testing the TOF detector. Naturally, each of the other lenses also has a 3/8" hole in its center to allow passage of the ions to the TOF tube! In general, sufficient signal is obtained when only the ion region lenses and the extractor are used. Typically, this three lens assembly was used with the following voltages: ion region, bottom at 1300V and the top at 1100V; extractor voltage 1000 to 1050V. In order to increase the mass resolution, one must give the ions less kinetic energy or in other words, reduce the voltages applied to the ion region and extractor lenses. However, increased mass resolution brings about a decrease in the absolute signal magnitude and thus for most applications, resolution has been sacrificed to afford a higher count rate. The mass resolution is on the order of 5 to 10 a.m.u./e when the ion region and extractor lenses are used at the potentials given above.

The main chamber has two laser entry flanges, symmetrically disposed about the molecular beam axis. This allows one to align two laser beams, both orthogonal to the molecular beam, in an anti-collinear fashion through the center of the ion optics. One can then easily perform pump and probe experiments in which one often wishes to focus the laser beams independently, and in which the pump and probe wavelengths might be similar, making colinear laser beam recombination lossy or difficult. The laser entry flanges contain fused silica windows, 2" in diameter and 0.25" thick. The mating flanges on the main chamber housing have scribe marks to allow placement of crosshairs for accurate and reproducible alignment of the laser beams in the center of the ion optics.

The background pressure in the main chamber is typically at 10^{-6} torr ($\approx 10^{-4}$ Pa) or less. A Sargent Welch TurboTorr turbomolecular pump, (Model 3133,1500 l/s) provides the main pumping. A 6" liquid nitrogen (LN_2) trapped diffusion pump (Varian M6, untrapped 1500 l/s) is also available for pumping on the main chamber during the course of an experiment.

The time-of-flight (TOF) tube is connected to the main chamber region directly above the ion optics via a 3/8" hole, which is closed with a gate valve when the machine is not in use, or when the main chamber needs to be opened. The TOF tube is perpendicular to the plane formed by the molecular and laser beams, and is 40.75 inches (1.035 m) long. The distance from the region where the laser beams and molecular beam intersect is 7.00 inches, so that the ions must travel approximately 47.75 inches (1.213 m) before reaching the detector. The TOF spectrometer is calibrated using a simple molecule which does not give fragments differing by less than 5-10 a.m.u./e such as NO, which does not fragment under these mild photoionization conditions. Located at the top of the TOF tube is the detector. The detector consists of three parts: the ion target or"doorknob", a scintillator and a photomultiplier tube. The "doorknob" is a doorknob-shaped piece of stainless steel coated with aluminum, and biased at a potential of -30kV by a Hipotronics HVDC 0-50kV supply. The ions are rapidly accelerated toward the target and electrons are released by the target following ion impact. Each ion produces between 6 and 8 electrons depending on the size of the ion. These electrons then experience a large repulsive force and are acelerated away from the doorknob, toward the scintillator. The

scintillator is an aluminum coated piece of PILOT U or PILOT B, a plastic scintillator. The photons from the scintillator are detected by a photomultiplier tube (RCA 8850). The PMT is external to the vacuum, and is coupled to the quartz window behind which the scintillator sits with optical coupling grease. The ion pulses from the PMT are sent to a constant fraction discriminator, and the positive going pulses from the discriminator are used to trigger a level adaptor. The TTL pulses from the level adaptor are finally sent to a multichannel scalar, designed and built at Lawrence Berkeley Laboratory, with a resolution of 150 ns/ channel. The scalar is triggered by the laser to record these ion counts as a function of arrival time at the detector. Typically, thousands of the time-of-flight mass spectra obtained in this way are stored and averaged by a dedicated DEC LSI11/73 computer which is CAMAC interfaced to the scaler. Alternatively, in the case of large signals, the output from the PMT may be sent directly to a boxcar integrator. The TOF tube is maintained at a pressure of 10^{-7} torr ($\approx 10^{-5}$ Pa) by a Pfeiffer TPU-110 turbomolecular pump (110 l/s). In the event of a power failure, the TOF tube is automatically vented by a Pfeiffer TSF-010 automatic switch, on the low pressure side, to prevent oil from the turbo pump from contaminating the the surface of the "doorknob" and scintillator.

The last distinct section of the machine is the beam catcher region. The beam catcher region is separated from the main chamber by a steel wall with a 1" hole at its center. On the main chamber side of this wall is a very smooth, polished tube which approaches the ion optics to within 0.5 inch. Here the molecular beam begins to enter the beam catcher. This tube extends to the

other side of the wall. The beam catcher region is pumped by a 6" LN2 trapped diffusion pump (Varian M6) and is at a pressure of 10^{-7} torr ($\approx 10^{-5}$ Pa) during operation. The beam catcher serves to prevent molecules from colliding with the back wall of the machine and returning to the main chamber where collisions between these background molecules and the molecular beam could occur. Also, when using a pulsed molecular beam, one can detect time-dependent signals from pulses of molecules which re-enter the interaction region after having made the round trip to and from the back wall of the machine. The beam catcher wall prevents this from occurring. To cut down on spurious background of this nature even further, one could cool the beam catcher wall with LN_2 to condense the molecules.

The MPI machine is actually very flexible in its design. The source can be easily altered to install a pulsed nozzle and a skimmer. The source, continuous or pulsed, may also be attached to the beam catcher end of the machine. By removing the differential wall separating the beam catcher and the main chamber, the reducer may be brought to within approximately 0.5 inch of the interaction region. The beam catcher plate may be installed where the source reducer normally keys into the main chamber, and the extra 6" diffusion pump from the main chamber assumes the role of the beam catcher pump. Finally, two small flanges exist on the beam catcher end of the machine. The source can be reconfigured using a pulsed nozzle fitted with an extension that has a small transverse hole drilled through it[10]. A laser beam could enter the source region through a window in one of these flanges, and be made to intersect the molecular beam via the small hole. In this way, one may use the

machine to prepare cold free radicals by dissociating an appropriate precursor molecule in the nozzle, and allowing the stable radical species to be collisionally cooled.

VUV Generation

In order to generate the vacuum ultraviolet (VUV) radiation needed to detect Cl atom, the MPI machine has been fitted with a small gas cell at the entrance window for the laser. The cell has a Suprasil entrance window, and a LiF exit window. The transmission of LiF at 118.877 nm is estimated at 50% or better[11]. To generate the VUV light at 118.877 nm, a 356.6 nm beam is focussed at the center of the cell using a 10 cm Suprasil lens. The cell is evacuated, and then filled with an optimized pressure of Xe gas. The cell extends into the MPI machine in order to minimize the use of LiF optics required to refocus the UV and VUV light which diverges after exitting the cell. With this configuration, the UV spotsize is measured to be 0.3 cm at the interaction region of the laser with the sample. Figure 4 is a schematic of the machine and laser configuration used.

The UV light is generated by doubling the ouptut of a Quanta-Ray PDL pulsed dye laser, pumped by the second harmonic of a Quanta-Ray DCR1A Q-switched Nd:YAG laser. The dye laser is operated with Exciton LDS 698 dye, and its visible output is doubled in a Type I KDP crystal (INRAD). The visible and UV beams are separated using a Pellin Broca prism, and the UV radiation is directed into the cell and the machine with a pair of 45° 355 nm reflectors

(CVI Laser Corp.). The UV laser energy, as measured after the LiF output window of the gas cell, is typically 5 mJ in these experiments. The number of VUV photons produced is estimated by performing a one photon ionization on a known quantity of benzene molecules, and detecting the number of ions produced. Benzene was chosen for this measurement because it has a known photoionization cross-section, and because this cross-section is relatively insensitive to wavelength in the region of interest[12]. In this way, it is estimated that 10^6 VUV photons are produced in the interaction volume per laser shot. The spectral width of the dye laser light is measured to be about 0.5 cm^{-1} using a Fabry-Perot etalon. The UV wavelength is calibrated using a Ne optogalvanic cell[13] for each experiment to facilitate detection of the Cl signal.

Cl Atom Source

The Cl atoms to be detected are produced in situ by photodissociating Cl_2 with the residual 356.6 nm light. The absorption is to a state which correlates to two ground state Cl atoms[14]. It is estimated that 10^7-10^8 Cl atoms/laser shot are produced in an interaction volume of $\sim$ 0.1 cm^3. Thus, production and detection of the atoms is effected by a single laser pulse. Due to the corrosive nature of the Cl_2, a continuous source, constructed of stainless steel, is used. A Cl_2/Ar gas mixture is bled through the nozzle, and into the machine, through a Monel needle valve, and the background pressure in the source region, measured intermittantly

by a Bayert-Alpert ion gauge, is used to estimate the amount of Cl ultimately produced in the interaction region.

III. RESULTS AND ANALYSIS

The Xe pressure in the VUV gas cell is optimized by varying the gas pressure, and monitoring the amount of benzene ion produced in the one-photon ionization of this molecule. A plot of benzene ion signal versus Xe pressure is shown in Figure 5.

In searching for the Cl atom $^2D \leftarrow {}^2P$ transition, ion signals are monitored at both m/e 35 ± 5 a.m.u./e and 70 ± 5 a.m.u./e as a function of laser wavelength. The spectra for Cl and Cl_2 are shown in Figures 6 and 7. The spectral region of interest, i.e. where the $^2D \leftarrow {}^2P$ transition occurs, is shown in Figure 8 for both Cl_2 and Cl. Finally, the Cl spectrum is "normalized" by dividing it by the Cl_2 spectrum, and normalizing this ratio to 1. The normalized ratio is plotted versus wavelength in Figure 9, the peak coresponding to 84,103 ± 3 cm^{-1}, according to the optogalvanic calibration. The transition is reported at 118.877 nm, or 84121 cm^{-1} [15].

IV. DISCUSSION

The purpose for attempting to detect Cl atoms with VUV and UV light generated by a nanosecond laser was to begin to optimize the MPI machine for the task of detecting Cl and H atoms, produced in the overtone-induced decomposition of 2-chloroethyl radical for example, using a picosecond light source. In so far as VUV radiation

has been generated, and a transition in the Cl atom has been observed, the attempt has been successful. However, there are many areas of improvement. These will be outlined in the following discussion.

A. Cl Atom Source

At the time this experiment was conducted, a single laser was available for use, and so the "one laser generation-detection" scheme was born. It happens that the chlorine molecule has an abundance of states in the region of the VUV spectrum of interest to us, and at least one of those accessible is an ion pair state[16]. Thus, it is not unlikely that some portion of the Cl^+ generated in our experiment is the result of the dissociation of this ion-pair state. A worst case estimate of the number of Cl^+ formed via the ion-pair state is made by assuming that all Cl2 molecules which absorb a photon dissociate on this potential surface. This leads us to an estimate of 10 ions/shot in the interaction volume. This is roughly a factor of 3 more than the anticipated signal for the desired Cl atom ionization. Another source of Cl^+ in the experiment is from the cracking of Cl_2^+, produced by absorption of the VUV, and then the UV photon. Again, assuming that all of the Cl_2^+ crack to form Cl^+ and Cl, roughly 10 ions/shot are expected. Both these processes would create chlorine ions whose spectra are identical to that of the chlorine molecular ion, and as can be seen, this is very nearly the case. One way to get rid of the extraneous Cl^+ signal would be to use a thermal Cl atom source[17]. This source would also yield as many as 10^5 more Cl atoms than the dissociative source. This would give a more comfortable signal margin over the present detection limit of $\sim 10^6/cm^3$.

B. VUV Generation

It has been previously estimated[18] that by using a picosecond laser, a factor of 2×10^2 improvement in VUV laser energy will be realized. In practice[18], it is actually found that the picosecond VUV source produces roughly 10^2 times more ions per laser shot than the nanosecond source, in accordance with the estimate. It appears that the limiting factor in increasing the peak power in the non-linear medium (Kr in this case) is the four photon ionization of the gas. As stated above, the choice of tripling radiation at 356.6 nm was made in part because this wavelength could also be used to dissociate Cl_2 into two ground state atoms. Due to the limited tuning range of the picosecond dye laser, two photons at 297.2 nm will be "mixed" with a photon at 594.4 nm in Kr to generate the 118.877 nm photons required for Cl atom detection, rather than using the tripling process.

Recently the LiF exit window on the gas cell was replaced by a quartz capillary[18]. The UV and visible beams were tightly focussed through the tube and entered the machine. The conductance of the rare gas through the tube is negligible. This affords about a factor of 2 improvement of laser throughput into the vacuum chamber[11].

C. Wavelength Calibration

While the optogalvanic cell is a good means of calibrating the frequency of the visible and UV laser, it would also be helpful to generate a VUV spectrum, using the MPI machine, of some molecule, preferably with a known spectrum, with sharp features in the wavelength range of interest. This could be used as a standard for future calibration.

Obviously, a peak has been observed in the Cl atom spectrum, but it does not coincide precisely with the reported transition. Either the wavelength calibration is incorrect, or the $^2D \leftarrow {}^2P$ transition is not responsible for the observed peak. With the new picosecond laser, and an improved source of Cl atoms, the transition will be observed with fewer ambiguities.

V. CONCLUSION

A first effort has been made at detection of Cl atoms using a resonant ionization method which involves absorption of a VUV photon, followed by absorption of a second UV photon of an energy sufficient to ionize the atom. The atoms are detected in a TOF spectrometer.

In this particular experiment, there are other sources of Cl^+ background which make it necessary to extract the desired signal from the rather noisy data. This, coupled with a low Cl atom number density in the beam, and a low VUV photon flux make it difficult to assess whether the desired $^2D \leftarrow {}^2P$ transition at 118.877 nm (84,121) has been observed. A peak in the Cl atom spectrum is observed at 84,103 $\pm$ 3 cm^{-1}, 18 cm^{-1} lower in frequency than reported.

REFERENCES

1. V. S. Letokhov, Laser Photoionization Spectroscopy, Academic Press, Inc., Orlando (1987).

2. G. S. Hurst, M. G. Payne, S. D. Kramer, and J. P. Young, Rev. Mod. Phys., 51, 767 (1979).

3. J. D. Myers, Ph. D. Thesis, University of California, Berkeley

4. T. K. Minton, Ph. D. Thesis, University of California, Berkeley, 1986.

5. S. Arepalli, N. Presser, D. Robie, and R. J. Gordon, Chem. Phys. Lett., 117, 64 (1985).

6. ibid, 88.

7. R. Hilbig and R. Wallenstein, IEEE J. Quant. Electron., QE-19, 194 (1984); C. R. Vidal, "Four Wave Frequency Mixing in Gases", in Tunable Lasers, ed. L. F. Mollenauer and J. C. White, Springer Verlag, Heidelberg (1986).

8. J. D. Myers, A. H. Kung, Y. T. Lee (others?), unpublished results.

9. W. C. Wiley and I. H. McLaren, Rev. Sci. Instrum., 26, 1150 (1956).

10. E. J. Hintsa, Ph. D. Thesis, University of California, Berkeley (1989).

11. This was an estimate given by an engineer at Harschaw-Filtrol, where we purchase our LiF optics.

12. J. Berkowitz, Photoabsorption, Photoionization, and Photoelectron Spectroscopy, Academic Press, New York (1979).

13. J. R. Nestor, Appl. Opt., 21, 4154 (1982); R. H. Page, private communication.

14. K. R. Wilson, Symposium on Excited State Chemistry, ed. J. N. Pitts, Gordon and Breach, New York (1970).

15. Atomic Transition Probabilities, Vol. II, NBS, Washington, (1966).

16. Lee, Suto and Tang, J. Chem. Phys., 84, 5277, (1986).

17. J. J. Valentini, M. J. Coggiola, and Y. T. Lee, Rev. Sci. Intrum., 48, 58 (1977).

18. J. D. Myers, private communication.

Figure 1: Cl atom energy levels, and photon energies used in the resonant ionization scheme described.

Figure 2: Stylized schematic of the MPI machine: **1**, nozzle; **2**, skimmer; **3**, VUV cell; **4**, ion optics with intersecting laser and molecular beams; **5**, "doorknob" ion target; **6**, plastic scintillator; **7**, photomultiplier tube.

Figure 3: Ion optics: **1,9**, mounting plates; **2**, spacer ring; **3**, bottom ion region; **4**, top ion region; **5**, extractor; **6**, accelerator; **7**, einzel lenses; **8**, beam steerers.

Figure 4: Schematic of laser setup used: **SHG**, second harmonic generation; **PHS**, prism harmonic separator(Quanta Ray); **P**, quartz right-angle prism; **PB**, Pellin-Broca prism; **BS**, beam stop; **L**, lens; **C**, VUV cell; **VC**, vacuum chamber.

Figure 5: Plot of benzene ion signal observed versus Xe pressure in VUV cell.

Figure 6: Cl ion signal as function of VUV frequency.

Figure 7: Cl_2 ion signal as function of VUV frequency.

Figure 8: Blowup of spectral region where Cl transition is expected; Cl and Cl_2 ion signals as function of VUV frequency.

Figure 9: Cl ion signal, normalized by dividing by the Cl_2 ion signal. Error in signal level indicated by dots.

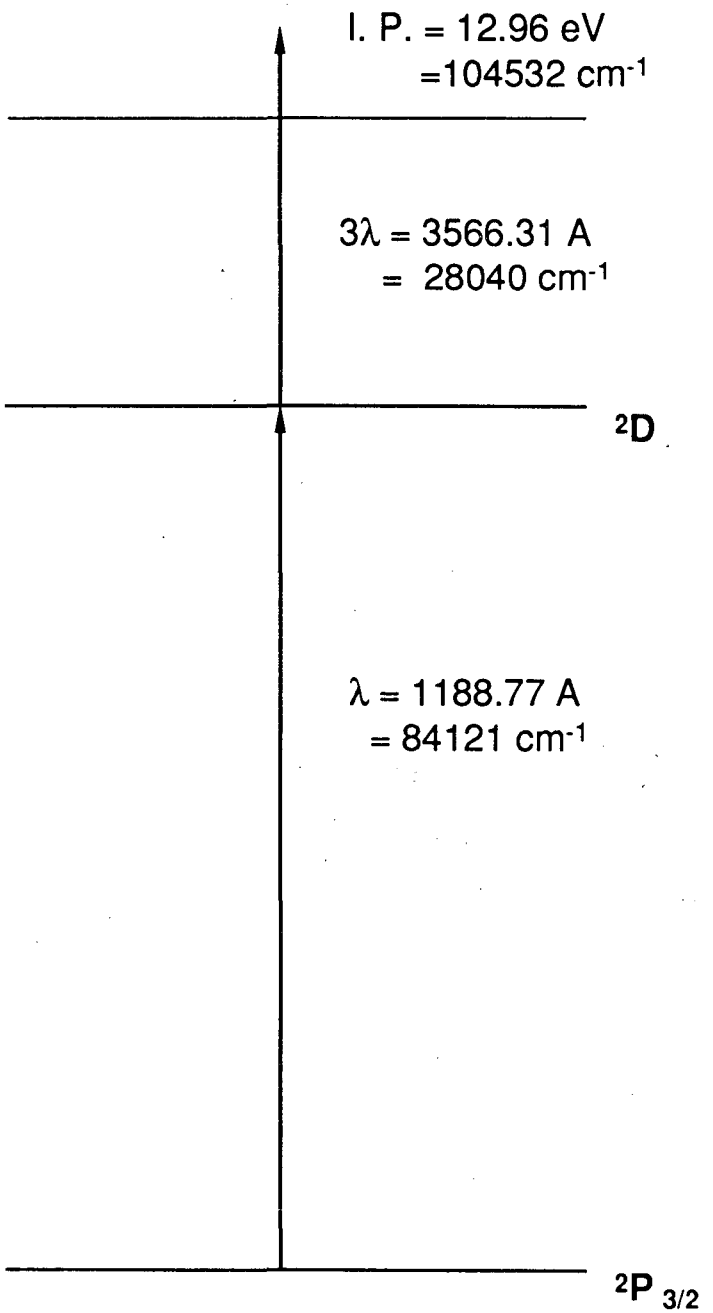
I. P. = 12.96 eV
=104532 cm-1
3λ = 3566.31 A
= 28040 cm-1
2D
λ = 1188.77 A
= 84121 cm-1
2P 3/2

Figure 1

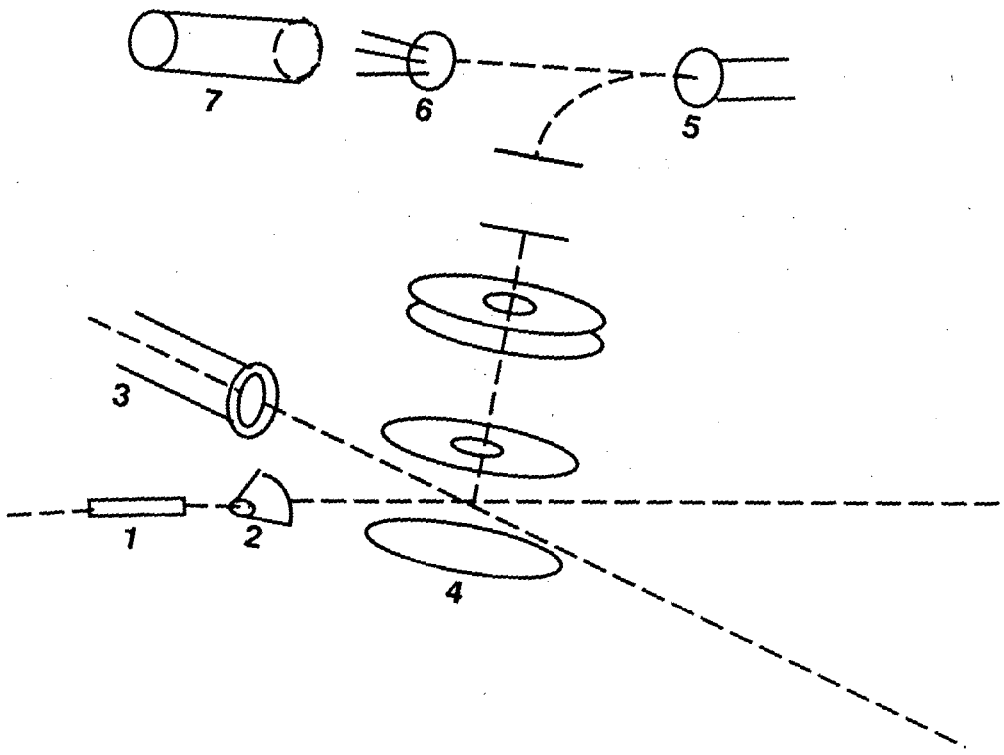

Figure 2

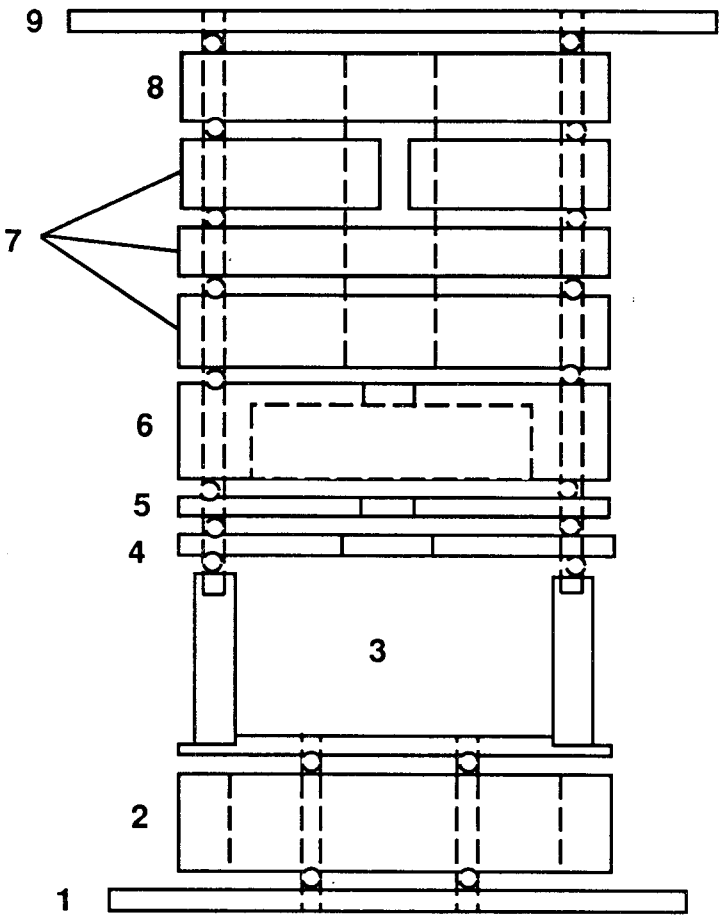

Figure 3

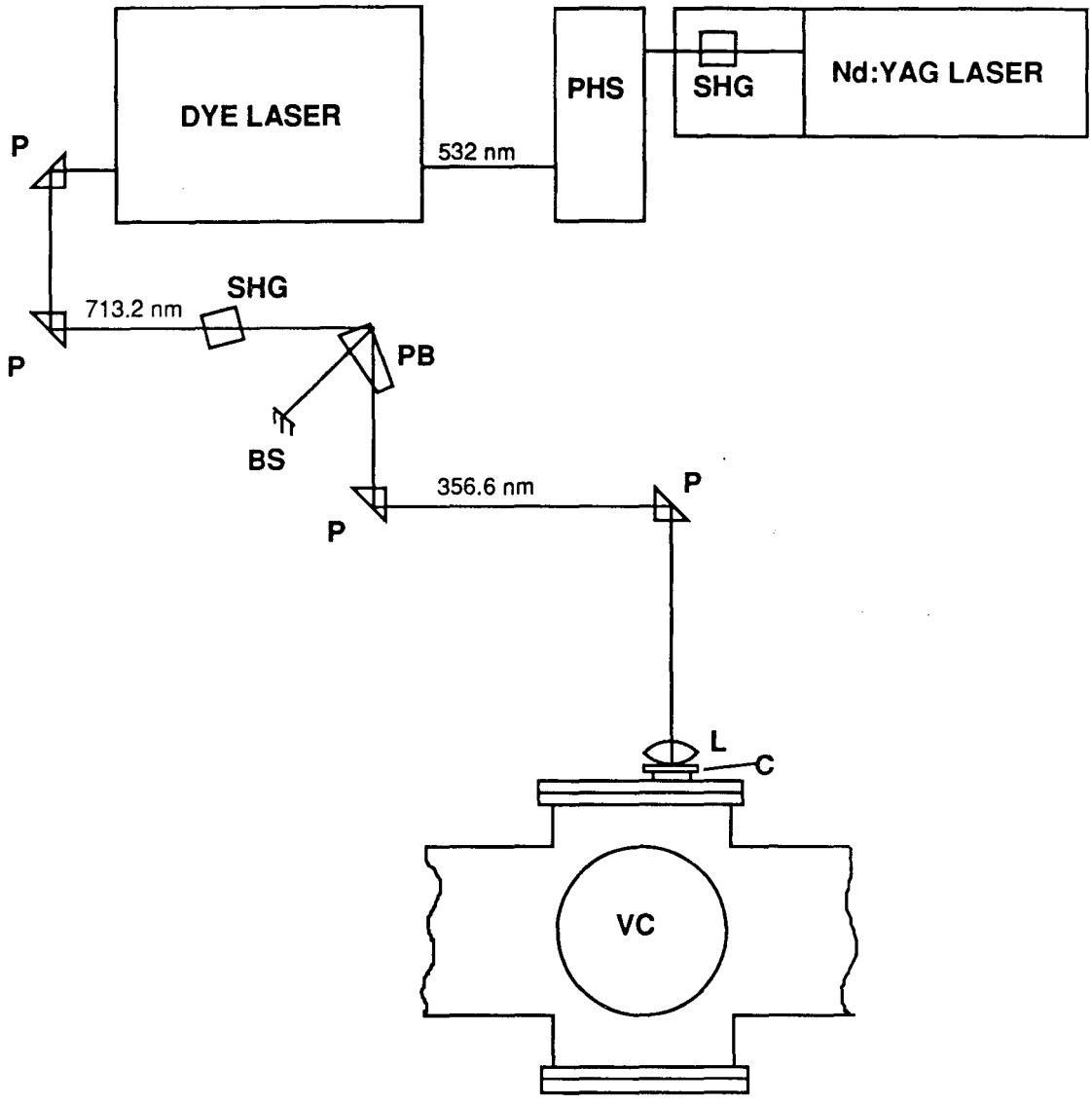
DYE LASER
PHS
SHG
Nd:YAG LASER
532 nm
P
713.2 nm
SHG
P
PB
BS
356.6 nm
P
P
L
C
VC

Figure 4

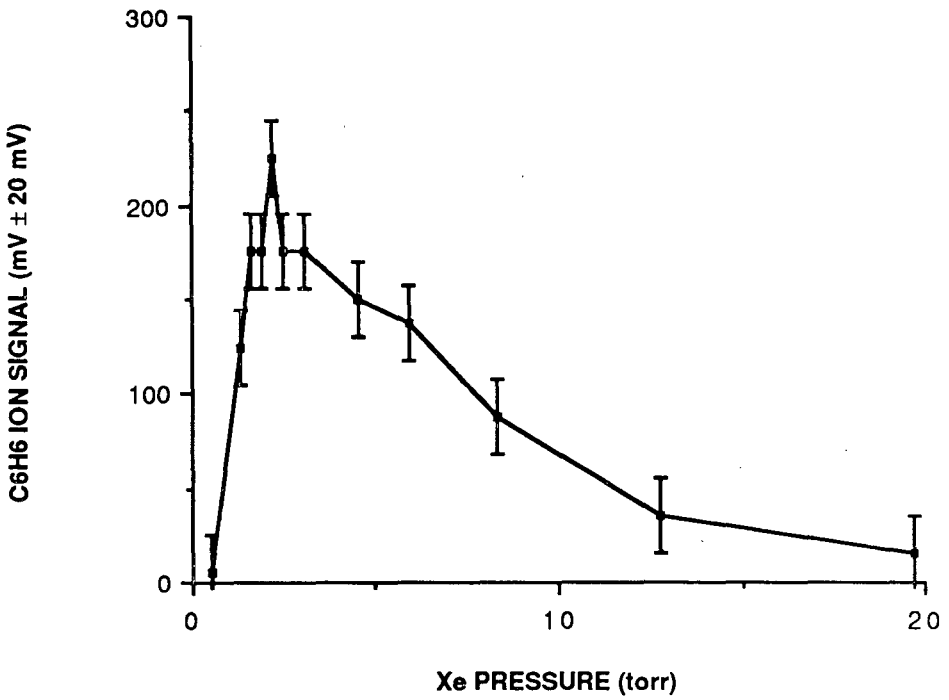

Figure 5

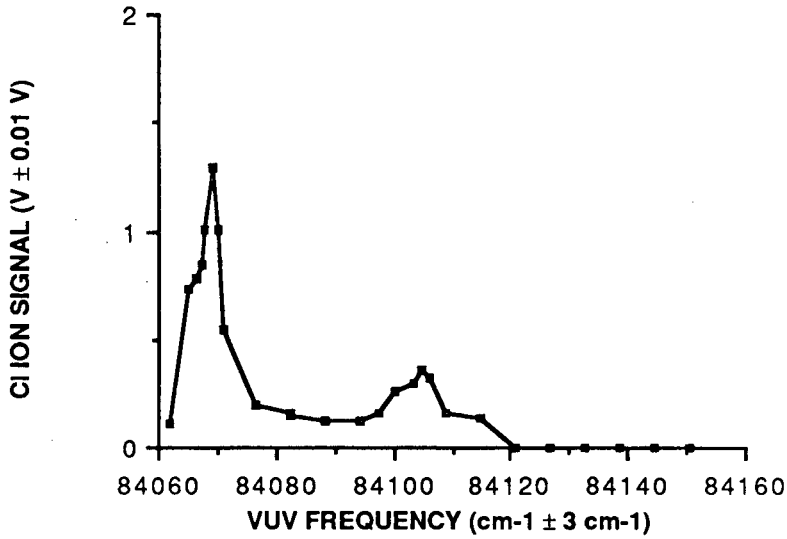
CI ION SIGNAL (V ± 0.01 V)
2
1
0
84060
84080
84100
84120
84140
84160
VUV FREQUENCY (cm-1 ± 3 cm-1)

Figure 6

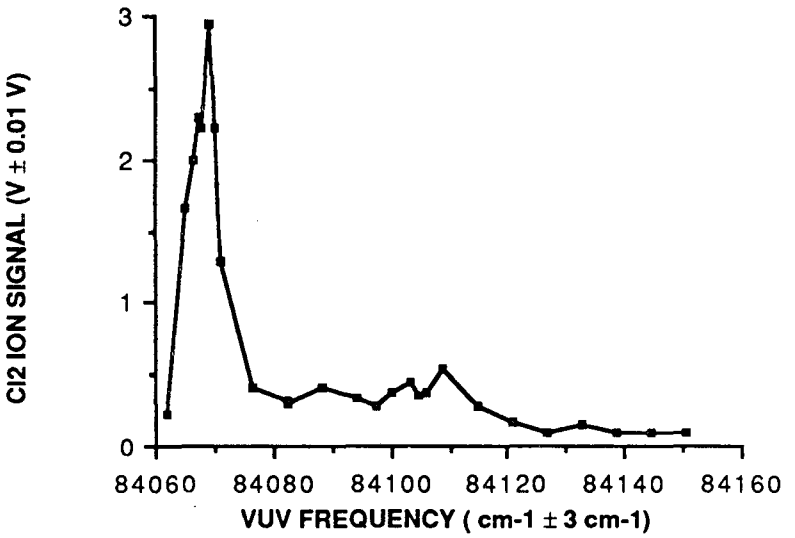
CI2 ION SIGNAL (V ± 0.01 V)
3
2
1
0
84060
84080
84100
84120
84140
84160
VUV FREQUENCY (cm-1 ± 3 cm-1)

Figure 7

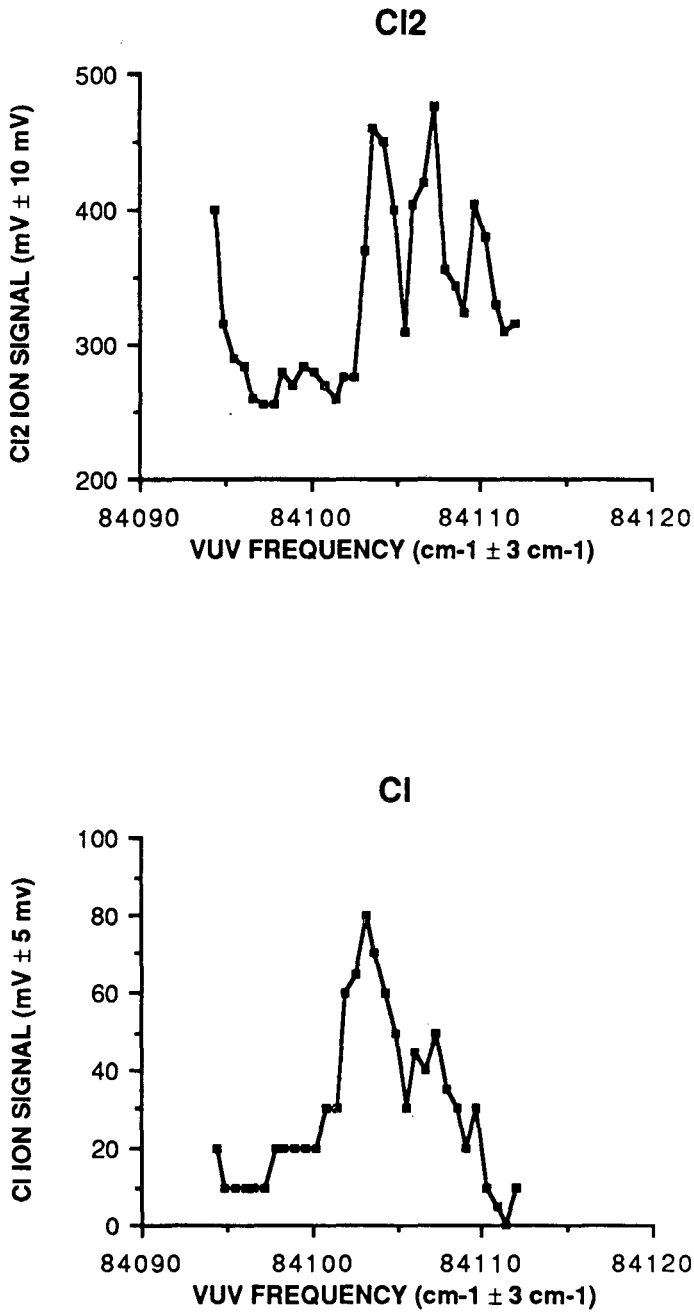
Cl2
Cl2 ION SIGNAL (mV ± 10 mV)
500
400
300
200
84090
84100
84110
84120
VUV FREQUENCY (cm-1 ± 3 cm-1)
Cl
Cl ION SIGNAL (mV ± 5 mv)
100
80
60
40
20
0
84090
84100
84110
84120
VUV FREQUENCY (cm-1 ± 3 cm-1)

Figure 8

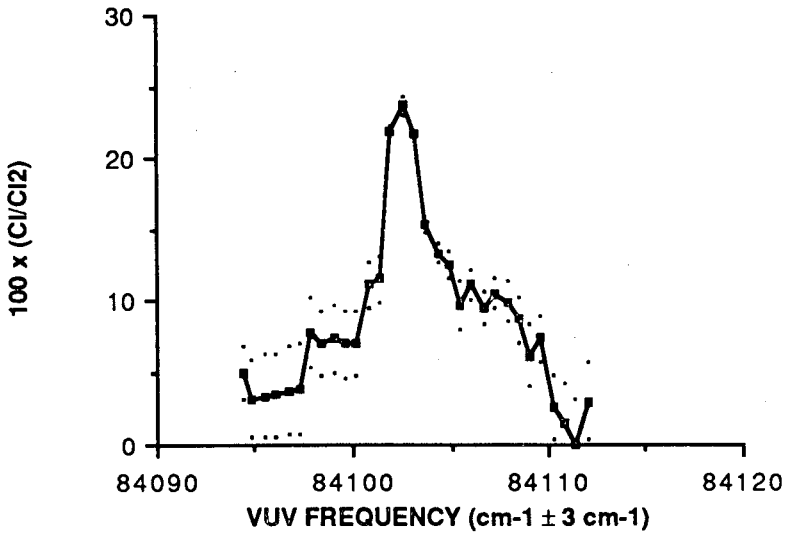
30
20
10
0
100 x (Cl/Cl2)
84090
84100
84110
84120
VUV FREQUENCY (cm-1 ± 3 cm-1)

Figure 9

LAWRENCE BERKELEY LABORATORY
TECHNICAL INFORMATION DEPARTMENT
1 CYCLOTRON ROAD
BERKELEY, CALIFORNIA 94720